Chemosphere 276 (2021) 130188

Contents lists available at ScienceDirect

Chemosphere

journal homepage: www.elsevier.com/locate/chemosphere

Treatment of real wastewater by photoelectrochemical methods: An overview

G. Divyapriya [a], Seema Singh [b], Carlos A. Martínez-Huitle [c, **], Jaimy Scaria [d], Ansaf V. Karim [e], P.V. Nidheesh [d, *]

[a] Virginia Polytechnic Institute and State University, USA
[b] Omvati Devi Degree College, Bhalaswagaj, Haridwar, India
[c] Institute of Chemistry, Federal University of Rio Grande do Norte, Lagoa Nova, CEP 59078-970, Natal, RN, Brazil
[d] CSIR-National Environmental Engineering Research Institute, Nagpur, Maharashtra, India
[e] Environmental Science and Engineering Department, Indian Institute of Technology, Bombay, India

HIGHLIGHTS

- Photoelectrochemical methods, its mechanism and synergistic effects are reviewed.
- Real effluents treatment by photoelectrochemical methods are discussed.
- Cost and energy analysis are compared.
- Photoelectrochemical approaches for treating soil washing effluents are deliberated.

ARTICLE INFO

Article history:
Received 10 December 2020
Received in revised form
24 February 2021
Accepted 3 March 2021
Available online 9 March 2021

Handling Editor: Derek Muir

Keywords:
Photoelectrochemical process
Real wastewater treatment
Photocatalysis
Advanced oxidation processes
Electrochemical treatment

ABSTRACT

An inadequate and inefficient performance ability of conventional methods to remove persistent organic pollutants urges the need of alternative or complementary advanced wastewater treatments methods to ensure the safer reuse of reclaimed water. Photoelectrochemical methods are emerging as promising options among other advanced oxidation processes because of the higher treatment efficiency achieved due to the synergistic effects of combined photochemical and electrolysis reactions. Synergistic effects of integrated photochemical, electrochemical and photoelectrochemical processes not only increase the hydroxyl radical production; an enhancement on the mineralization ability through various side reactions is also achieved. In this review, fundamental reaction mechanisms of different photoelectrochemical methods including photoelectrocatalysis, photo/solar electro-Fenton, photo anodic oxidation, photoelectroperoxone and photocatalytic fuel cell are discussed. Various integrated photochemical, electrochemical and photoelectrochemical processes and their synergistic effects are elaborated. Different reactor configurations along with the positioning of electrodes, photocatalysts and light source of the individual/combined photoelectrochemical treatment systems are discussed. Modified photoanode and cathode materials used in the photoelectrochemical reactors and their performance ability is presented. Photoelectrochemical treatment of real wastewater such as landfill leachate, oil mill, pharmaceutical, textile, and tannery wastewater are reviewed. Hydrogen production efficiency in the photoelectrochemical process is further elaborated. Cost and energy involved in these processes are briefed, but the applicability of photocatalytic fuel cells to reduce the electrical dependence is also summarised. Finally, the use of photoelectrochemical approaches as an alternative for treating soil washing effluents is currently discussed.

1. Introduction

Reuse of treated wastewater is mandated to address the increasing global water demand for cleaning water. Regulations for the reuse and discharge of effluents are strictly imposed on

* Corresponding author.
** Corresponding author.
E-mail addresses: carlosmh@quimica.ufrn.br (C.A. Martínez-Huitle), nidheeshpv129@gmail.com, pv_nidheesh@neeri.res.in (P.V. Nidheesh).

https://doi.org/10.1016/j.chemosphere.2021.130188
0045-6535/

municipal and industrial wastewater treatment plants. Various physical, chemical, and biological treatment processes are being carried out to remove organic and inorganic contaminants. Most of the places, the conventional biological treatment process is performed to remove organic contaminants. Due to the complexity and recalcitrant in nature, removal of persistent organic pollutants (POPs) through conventional treatment processes is often ineffective and inadequate. Advanced oxidation processes (AOPs) produce highly active and reactive hydroxyl radicals (•OH) ($E^{\circ} = 2.8$ V/SHE) that can accelerate the mineralization of POPs (Babu et al., 2019; Martínez-Huitle and Ferro, 2006; Nidheesh, 2017). AOPs that are widely studied for the treatment of various wastewater are Fenton, photocatalysis, ozonation, and wet oxidation. However, these processes have exhibited some drawbacks related to an effective implementation or concerning to incomplete removal of few POPs. It urges the need for the innovative advanced treatment processes that can be efficient, eco-friendly, versatile and techno-economical feasible.

Electrochemical based AOPs (EAOPs) are considered as promising next generation alternative since high treatability of the complex wastewater can be achieved with easiness, the process efficiency can be easily controlled through automation and the technology can be compact, occupying less space (Brillas et al., 2009; Martínez-Huitle and Panizza, 2018; Nidheesh et al., 2018a, b). EAOPs involve the *in-situ* production of •OH radicals through external power supply (Martínez-Huitle et al., 2005; Solano et al., 2016). Most widely studied EAOPs are anodic reactions based anodic oxidation (AO) (Martínez-Huitle et al., 2008; Nava et al., 2008; Santos et al., 2015) and cathodic reactions based electro-Fenton (EF) processes (Dos Santos et al., 2016; Nidheesh et al., 2013, 2019). Recently, innovative EAOPs emerged as efficient electrochemical technologies, which are photo-EF (PEF), solar PEF (PEF), photoelectrocatalysis (PEC), electro-peroxone (EP), photoelectro-peroxone (PEP) etc. Combination of photochemical and electrolysis processes not only provides the advantage of synergistic effects, but it also minimizes the disadvantage of the individual processes (Ganiyu et al., 2018). Based on the existing literature, which will be summarised and discussed in this review, the treatment efficiency of the photoelectrochemical processes is reported to be high, especially for the real wastewater. Thus, the fundamental reaction mechanisms, synergistic effects of the individual and integrated photoelectrochemical methods, various reactor configurations and modified electrodes studied, the treatability of different real wastewater including landfill leachate, oil mill, pharmaceutical, textile and tannery industries, hydrogen production in the process, cost and energy consumption are discussed in detail in this review.

2. Photoelectrochemical methods

In this section, fundamental reaction mechanisms involved in the various photoelectrochemical processes such as PEC, PEF, SPEF, photoanodic oxidation (PAO), PEP and PFC on the oxidation of contaminants owing to the synergistic effects that are exhibited between the photochemical and electrochemical reactions within the treatment unit.

2.1. Photoelectrocatalysis

Photoelectrocatalysis (PEC) process inherits the advantage of photocatalysis while improving the radical production efficiency with the combination of electrolytic reactions (Bessegato et al., 2015; Mousset and Dionysiou, 2020). Photocatalysis is one of the extensively investigated AOPs for mineralising the wide range of contaminants (Hoffmann et al., 1995). Upon the irradiation of the UV/vis light, semiconductor based photocatalysts such as titanium dioxide (TiO_2), zinc oxide (ZnO), tungsten trioxide (WO_3), and bismuth vanadate ($BiVO_4$) produces the reactive oxygen species ($•OH/O_2^{•-}$) (Peleyeju and Arotiba, 2018). As the light energy (hυ) higher than the bandgap energy is irradiated on the semiconductor photocatalyst, the electron is excited to the conduction band (e^-_{cb}) leaving behind the positive vacancy hole in the valance band (h^+_{vb}) which can produce •OH radical through the oxidation of H_2O/OH^- (Eq. (1–3)) (Carraway et al., 1994). However, the radical production capacity of the photocatalyst is decreased due to the rapid recombination of this light induced electron-hole (e^-_{cb}/h^+_{vb}) pair because the lifetime of these charge pairs are in the order of nanoseconds (Hoffmann et al., 1995). The recombination rate of the e^-_{cb}/h^+_{vb} pair can be altered through the external applied potential. In the photoelectrocatalysis process, the photocatalyst is coated on the conductive supporting matrix (called as photoanode) (Esquivel et al., 2009). As the photoexcited electrons are produced upon the irradiation of light, the external applied positive potential to the photoanode forces the transfer the electrons to the cathode. This phenomenon favours the h^+_{vb} to produce more radicals through the reaction with H_2O/OH^-.

$$\text{Photocatalyst} + h\upsilon \rightarrow e^-_{cb} + h^+_{vb} \quad (1)$$

$$h^+_{vb} + H_2O \rightarrow HO^{\bullet} + H^+ \quad (2)$$

$$h^+_{vb} + OH^- \rightarrow HO^{\bullet} \quad (3)$$

$$h^+_{vb} + R \rightarrow R^+_{ox} \quad (4)$$

$$e^-_{cb} + O_2 \rightarrow O_2^{-\bullet} \quad (5)$$

The degradation efficiency of the process could also be further increased through the direct oxidation of the organic contaminants (R) upon the direct contact to the light induced h^+_{vb} as represented in the Eq. (4). Further superoxide anion can also be produced as a side reaction between the electroexcited electrons and the oxygen molecules (Eq. (5)). Various photocatalysts are studied as photoanodes in photoelectrocatalysis processes such as TiO_2 (Esquivel et al., 2009; Shi et al., 2019), C, N, S doped TiO_2 (Li et al., 2015a; Peleyeju and Arotiba, 2018), electrochemically self-organised TiO_2 nanotubes (Vacca et al., 2020), ZnO, Sn_x-W(100-x)-oxide (Ghasemian and Omanovic, 2017), WO_3 (Longobucco et al., 2017; Mohite et al., 2016), $BiVO_4$ (Tolod et al., 2017), $Fe_2O_3/BiVO_4$ (Xia et al., 2017) etc. These photocatalysts are coated as films onto the conductive substrate materials such as titanium (Vacca et al., 2020), indium tin oxide (Wang et al., 2017), fluorine doped tin oxide (Wang et al., 2012), tungsten (Longobucco et al., 2017), optical fiber substrate (Shi et al., 2019), etc. through sol–gel and spin-coating methods, chemical vapour deposition, magnetron sputtering and electrochemical deposition technique. It is important to form a stable and active photocatalyst layer onto the conductive substrate material during the fabrication of photoanode. Ti and carbon-based materials are commonly used substrate materials (Bessegato et al., 2015; Garcia-Segura and Brillas, 2017). However, transparent supporting materials having high light transparency, high mechanical strength, and low surface resistivity such as FTO and ITO glasses facilitate the transmission of UV light and maximizes the utilization of incident photons (Guo et al., 2015). Hence, the transparent materials are the most popular choice among other substrates in the fabrication of photoanodes (Guo et al., 2015; Xu et al., 2020).

2.2. Photoelectro-Fenton and solar photoelectro-Fenton

Electro-Fenton based processes have been gaining much attentions owing to the environmentally-friendly, economical approach for the complete removal of recalcitrant organic contaminants (Nidheesh and Gandhimathi, 2012, 2014; Oturan et al., 2018). Electro-Fenton process experiments conducted under the irradiation of artificial UV–Vis light and natural sun light is called as photoelectro-Fenton (PEF) and solar photoelectron-Fenton (SPEF) processes, respectively (Coria et al., 2018). These processes were proposed and comprehensively studied by Oturan's and Brillas' groups (Boye et al., 2003; Brillas et al, 1998, 2009; Flox et al., 2007; Salazar et al., 2011a). Electro-Fenton process involves the *in-situ* generation of Fenton's reagent H_2O_2 and Fe^{2+} ions to produce •OH radicals through external power supply (Eq. (6)) (Baiju et al., 2018; Jacqueline George et al., 2016; Popat et al., 2019). Hydrogen peroxide is continuously electrogenerated at cathode via two electron oxygen reduction reactions (ORR) in acidic solution (Eq. (7)) (Nidheesh and Gandhimathi, 2014; Nidheesh et al., 2014; Sruthi et al., 2018).

$$Fe^{2+} + H_2O_2 \rightarrow Fe^{3+} + HO^- + HO^\bullet \quad (6)$$

$$O_2 + 2H^+ + 2e^- \rightarrow H_2O_2 \quad (7)$$

Upon the reaction between the electrogenerated H_2O_2 and Fe^{2+} ions, Fe^{3+} species are also produced that need to be regenerated to Fe^{2+} form once again to carry out the Fenton's reaction. Since the reactions are carried out at the optimum pH of 3.0, Fe^{3+} species are predominantly existing in $Fe(OH)^{2+}$ form which is electrochemically reduced to Fe^{2+} for further reactions (Eq. (8) and (9)). Series of other reactions are also occurring simultaneously as represented in the Eq. (10–12) (Brillas et al., 2009; Sirés and Brillas, 2021).

$$Fe^{3+} + H_2O \rightarrow Fe(OH)^{2+} + H^+ \quad (8)$$

$$Fe(OH)^{2+} + e^- \rightarrow Fe^{2+} + OH^- \quad (9)$$

$$Fe^{3+} + H_2O_2 \rightarrow Fe^{2+} + HO_2^\bullet + H^+ \quad (10)$$

$$Fe^{3+} + HO_2^\bullet \rightarrow Fe^{2+} + O_2 + H^+ \quad (11)$$

$$Fe^{3+} + R^\bullet \rightarrow Fe^{2+} + R^+ \quad (12)$$

In general, carbon-based materials are used as cathode to produce H_2O_2 via two electron ORR since it is characterised to exhibit high hydrogen over potential and low H_2O_2 decomposition ability (Nidheesh and Gandhimathi, 2012; Nidheesh et al., 2018a, b; Sirés et al., 2014). Three-dimensional porous structured high surface carbon cathodes such as carbon/graphite felt, carbon foam and carbon sponge can effectively absorb a high amount of oxygen molecules and subsequently convert them into H_2O_2 (Brillas et al., 2009; Ganiyu et al., 2021a; Nidheesh et al., 2018a, b; Wang et al., 2008). Other carbon electrodes that are used in the electro-Fenton process include nanocarbon modified carbon felt/carbon cloth (Divyapriya et al., 2018; Divyapriya and Nidheesh, 2020), carbon nanotubes (Hasanzadeh et al., 2018), reticulated vitreous carbon (El-Desoky et al., 2010), activated carbon fiber (Jiao et al., 2020), gas diffusion electrodes (Brillas, 2014; Valim et al., 2013), graphite (George et al., 2014; Venu et al., 2016), graphite felt (Nidheesh et al., 2020; Popat et al., 2019) etc. In the PEF and SPEF processes, the degradation rates of contaminants are further enhanced through the additional conversion of ferric hydroxide complex ($Fe(OH)^{2+}$) resulting in the regeneration of Fe^{2+} catalysed by the irradiated artificial UVA (315–400 nm)/UVB (280–315 nm)/UVC (<280 nm) lamp or sun light, as given in the Eq. (13). Moreover, the direct photolysis of the metal-ligand complexes formed between Fe^{3+} and organics such as Fe-carboxylate complexes that are resistant to •OH along with the regeneration of Fe^{2+} species as given in the Eq. (14) (Brillas, 2020; Liu et al., 2019).

$$Fe(OH)^{2+} + h\nu \rightarrow Fe^{2+} + HO^\bullet \quad (13)$$

$$Fe(OOCR)^{2+} + h\nu \rightarrow Fe^{2+} + CO_2 + R^\bullet \quad (14)$$

These photoreduction and photolysis reactions can effectively occur when the source light is emitted near to the wavelength that the reactants complexes can absorb. Further, the irradiation of UVC can decompose H_2O_2 to produce more •OH through the homolytic cleavage of the peroxide bond, as given in the Eq. (15).

$$H_2O_2 + h\nu \rightarrow 2HO^\bullet \quad (15)$$

Most of the PEF studies reported the use of the irradiation of UVA light. However, additional artificial irradiation could result in the increased cost of operation. Nevertheless, this disadvantage can be avoided through the usage of natural renewable solar energy where the reactant solution is directly exposed to the sun light. Further, better treatment efficiency can be achieved in homogenous SPEF process with the photons from sunlight ($\lambda > 300$ nm) compared to the low intensity artificial lamps (UVA with $\lambda = 315–400$ nm) due to the great UV input with additional photolysis reactions mediated by light adsorption at $\lambda > 400$ nm such as the decarboxylation of Fe(III)-carboxylate species (Brillas, 2020; Moreira et al., 2017).

2.3. Photoanodic oxidation

Anodic oxidation integrated with the photolysis is called as photo assisted anodic oxidation process. Anodic oxidation is the widely popular EAOPs that involve the production of radical species while oxidizing the water molecules at the anode surface (Eq. (16)) or directly oxidises the organic contaminant through direct electron transfer (DET) mechanism (Eq. (17) (Martínez-Huitle and Panizza, 2018).

$$H_2O \rightarrow HO^\bullet + H^+ + e^- \quad (16)$$

$$R \rightarrow (R^\bullet)^+ + e^- \quad (17)$$

Depending upon the properties of anode material, the hydroxyl radicals produced through water oxidation could be physiosorbed or chemisorbed. The standard oxygen evolution potential is 1.23 V/SHE. The 'active anodes' having the low oxygen evolution potential (<1.8 V/SHE) involve the partial and selective oxidation of organics through the production of chemisorbed radicals that include ruthenium dioxide (RuO_2: 1.4–1.7 V/SHE), iridium dioxide (IrO_2: 1.5–1.8 V/SHE), and platinum (Pt: 1.6–1.9 V/SHE). The chemisorbed radical (M(•OH) produced on the anode surface is transformed into its higher oxide/superoxide state (MO). Further MO/M act as redox mediator to oxidise the organic contaminant (R) into the intermediate product (RO) as represented in the Eq. (18–20). When the oxidation of water is not occurring (up to 2.0 V/SHE), the contaminant could be directly oxidised through DET mechanism depending on the property of electrode material (Brillas, 2021; Chaplin, 2014).

$$M(HO^\bullet) \rightarrow MO + H^+ + e^- \quad (18)$$

$$MO + R \rightarrow M + RO \quad (19)$$

$$MO \rightarrow M + 0.5O_2 \quad (20)$$

whereas 'non active anodes' having high oxygen evolution potential (>1.8 V/SHE) mineralises the organic contaminants through the production of physiosorbed hydroxyl radicals that include lead dioxide (PbO_2:1.8–2.0 V/SHE), tin dioxide (SnO_2: 2.0–2.2 V/SHE), sub-stoichiometric TiO_2 (1.7–2.6 V/SHE) and boron-doped diamond (BDD: 2.2–2.8 V). During the oxidation of contaminants through physiosorbed radicals, other unavoidable side reactions also occur (Eq. (21–23). Further, other oxidizing species such as H_2O_2 and O_3 is also produced along with the •OH (Eq. (24) and (25)) (Garcia-Segura et al., 2018; Martínez-Huitle et al., 2015; Moreira et al., 2017).

$$M + H_2O \rightarrow M(HO^{\bullet}) + H^+ + e^- \quad (21)$$

$$M(HO^{\bullet}) + H_2O \rightarrow M + O_2 + 3H^+ + 3e^- \quad (22)$$

$$2M(HO^{\bullet}) \rightarrow 2M + O_2 + 2H^+ + 2e^- \quad (23)$$

$$2M(HO^{\bullet}) \rightarrow 2MO + H_2O_2 \quad (24)$$

$$3H_2O \rightarrow O_3 + 6H^+ + 6e^- \quad (25)$$

Depending upon the existence of ions in the electrolyte medium like chloride, sulfate, carbonate, and phosphate; additional oxidizing species can be also produced owing to the electrochemical reactions {Formatting Citation}. Chloride ions present in the electrolyte can be directly converted into active chlorine species based on the anodic reaction as given in the Eq. (26). Further chlorine species disproportionate into HClO and Cl^- species (Eq. (27)) can also participate. Since the pKa value of HClO is 7.5, it establishes equilibrium with ClO^- species (Aravind et al., 2016) and the contaminants are oxidised by ClO^- species at the solution pH > 7.5 as represented in the Eqs. (28) and (29).

$$2Cl^- \rightarrow Cl_2 + 2e^- \quad (26)$$

$$Cl_2 + H_2O \leftrightarrow HClO + Cl^- + H^+ \quad (27)$$

$$HClO \leftrightarrow ClO^- + H^+ \quad (28)$$

$$ClO^- + Pollutants \rightarrow intermediates + Cl^- \quad (29)$$

In PAO, UV irradiation used in the anodic oxidation process can produce additional radicals through the indirect route in reaction to the reactive chlorine species as per the following Eqs. (30) and (31) (de Mello Florêncio et al., 2016).

$$ClO^- + h\nu \rightarrow O^{\bullet -} + Cl^- \quad (30)$$

$$O^{\bullet -} + H_2O \rightarrow HO^{\bullet} + OH^- \quad (31)$$

Persulfate ions can be also produced during the AO process which is mainly feasible with the non-active anodes such as BDD and PbO_2 (de Freitas Araújo et al., 2020; Escalona-Durán et al., 2020; Santos et al., 2018) and the persulfate ions can be further activated in the presence of UV irradiation (Eq. (32) and (33)) (Souza et al., 2016)

$$2SO_4^{2-} \rightarrow S_2O_8^{2-} + 2e^- \quad (32)$$

$$S_2O_8^{2-} + h\nu \rightarrow 2(SO_4^{2-})^{\bullet} \quad (33)$$

2.4. Photoelectro-peroxone

Photoelectro-peroxone (PEP) is the hybrid electrolysis, ozonation and UV induced photolysis process in which the progressive research studies are being reported on removing the persistent organic contaminants in recent years (Jaafarzadeh et al., 2017; Shen et al., 2017). PEP uses clean oxygen and electricity as the main resource to generate reactive oxygen species such as H_2O_2, and •OH. Further peroxone reagents (H_2O_2 and O_3) is activated by UV irradiation that does not require any catalyst addition. The unreacted H_2O_2, and O_3 (if any) can be easily decomposed to H_2O and O_2. Moreover, PEP eliminate the undesired production of by-products that may require further disposal or treatment. Thus, PEP is considered as one of the cleaner treatment processes (Frangos et al., 2016). H_2O_2 is electrogenerated through the two electrons ORR at the carbon-based cathode surface as represented in the Eq. (7) while the O_2 and O_3 mixer is continuously injected into the reaction mixture by the external ozone generator. Radical species are produced as per the reaction represented in the Eq. (34). Further decomposition of O_3 molecules through the electron transfer reaction can also produce additional radical species as represented in the Eqs. (35) and (36) (Ahmadi and Ghanbari, 2018; Frangos et al., 2016; Joy et al., 2020).

$$2O_3 + 2HO_2^- + H_2O \rightarrow 2HO^{\bullet} + 3O_2 + OH^- + HO_2^{-\bullet} \quad (34)$$

$$O_3 + e^- \rightarrow O_3^{-\bullet} \quad (35)$$

$$O_3^{-\bullet} + H_2O \rightarrow HO^{\bullet} + O_2 + OH^- \quad (36)$$

However, the reaction rate of O_3 with H_2O_2 decreases at the acidic condition. The presence of Fe^{2+}/Fe^{3+} ions in the wastewater could produce the metal organic complexes with the carboxylic acids intermediate products that reduce the further mineralization of the contaminants (Frangos et al., 2016). To enhance the radical production and the degradation kinetics, electro-peroxone process was combined with the UV induced photolysis. UV induces the photolysis decomposition of O_3 and H_2O_2 as well as the metal organic intermediate compounds as represented in the Eqs. (37) and (14) respectively (Ahmadi and Ghanbari, 2018; Frangos et al., 2016).

$$O_3 + H_2O_2 + h\nu \rightarrow 2HO^{\bullet} + H_2O \quad (37)$$

Moreover, the process does not produce any secondary contamination since the residual peroxone regents can be easily decomposed to H_2O and O_2.

2.5. Photocatalytic fuel cell

Photocatalytic fuel cell (PFC) is one of the sustainable process which involves the simultaneous treatment of organic contaminants and the energy recovery via photocatalytic reactions (Xu et al., 2019a; Zeng et al., 2018). PFC contains photoanode made up of photocatalyst where the oxidation of contaminants occurs under irradiation of UV light; while the photoexcited electrons are transferred to the photocathode where the oxygen reduction reactions occur through the external circuit accompanied by the electricity generation (Lee et al., 2016). Since the application of widely studied TiO_2 photocatalyst is restricted due to large band

gap energy ($E_g = 3.2$ eV) and the need of UV light irradiation, many visible light responsive photoanodes are developed in recent years for the broad solar spectrum absorption and improved energy generation such as CdS/TiO_2 (Li et al., 2015b), CdS/ZnS/TiO_2 (He et al., 2018), WO_3/W (Zeng et al., 2018), $BiVO_4$/WO_3 (Georgieva et al., 2012), $BiVO_4$/TiO_2 (Bai et al., 2016), Ag/AgCl/TiO_2 (Wang et al., 2015), etc. To improve the overall charge separation efficiency and the energy production, dual photoelectrode PFC systems are introduced that comprising of photoanode and photocathode in which the internal bias potential are developed. Photocathode materials include Cu_2O/Cu (Paracchino et al., 2011), ZnO/CuO (Bai et al., 2016), Pt-modified buried junction silicon (Zeng et al., 2018) etc. CuO is the p-type semiconductor having the low band gap energy (E_g = ~1.5 eV), hence it is highly preferred to be used in photocathode (Masudy-Panah et al., 2016; Patel et al., 2016). A few studies reported the combination of electro-Fenton reactions at the cathode along with the photoanode for improving degradation efficiency by using the carbon-based electrode such as Fe@Fe_2O_3/carbon felt (Xu et al., 2019a) and Pt-modified buried junction silicon (Zeng et al., 2018). PFC system has been performed in the conventional single chamber and dual chamber H-type cell (Lui et al., 2019; Macías-Sánchez et al., 2011). Membrane less micro-PFC process with lateral arrangement of the electrodes that can allow simultaneous illumination of light could be feasible process configuration for the practical application (Parmar et al., 2015; Xia et al., 2016).

3. Synergistic effects in photoelectrochemical methods

Integrating the individual photochemical, electrochemical and photoelectrochemical processes in a single treatment unit, it is the proven approach to improve the contaminant oxidation ability of the system compared to the individual processes owing to the increased radical generation capacity and the enhanced degradation kinetics (Ganiyu et al., 2021b). The enhancement in the treatment efficiency of the hybrid systems is achieved through the following synergistic effects:

(i) coupling of the processes complement the source of •OH radicals generation through the main reactions of individual processes,
(ii) the side reactions that are mediated by synergy between the individual processes supplement the additional •OH radicals generation sites as well as produce other oxidizing radical species,
(iii) combing photochemical and electrolysis enhancing the mineralization via the direct photolysis of complex intermediates such as metal-ligand complexes and carboxylic acid intermediates (Brillas et al., 2009; dos Santos et al., 2015; Oturan and Aaron, 2014).

Combined photolysis with the AO process (PAO) does not act as additional •OH radical source, while it can generate additional oxidizing species depending upon the anionic species supplemented in the electrolyte medium (Mousset et al., 2017). The contribution of homogeneous, heterogeneous •OH radicals and their synergy in the hybrid AO-EF treatment process is elucidated by Olvera-Vargas et al. (2021). In BDD-EF process, homogeneous •OH participate in the initial stage of degradation while heterogeneous BDD(•OH) involve in the later stage of treatment through electron transfer reactions (Olvera-Vargas et al., 2021). Enhancement in the mineralization efficiency of the photolysis coupled EF (PEF) process is achieved because of the formation of additional •OH radicals due to the photolysis of the metal-ligand complexes and direct photodecomposition of electrogenerated H_2O_2 (Brillas, 2020). When the photocatalysis is integrated with PEF or PAO processes, one extra •OH radical generation site is introduced. In the case of PEF/PC process, additional •OH radical can be also generated by the reactions between the electrogenerated H_2O_2 with superoxide produced in photocatalysis process (Eq. (38)) (Brillas et al., 2009).

$$H_2O_2 + O_2^{-\bullet} \rightarrow HO^{\bullet} + HO^{-} + O_2 \quad (38)$$

Likewise, coupling of anodic based PEC with the cathodic based PEF could result in similar reactions to PC (Mousset and Dionysiou, 2020). Nevertheless, the recombination rate of the photocatalyst is reduced in PEC resulting on the enhancement of the degradation kinetics (Orimolade et al., 2020). Further coupling of PEF and PAO in a single unit increases the •OH radical generation capacity of the system due to the obvious advantage of integrating anode and cathode based radical production reactions (Garza-Campos et al., 2014). Additional •OH radicals can be also produced as the side reaction between electrogenerated H_2O_2 and ozone molecule produced at the anode (Eq. (39)) (Merényi et al., 2010).

$$H_2O_2 + 2O_3 \rightarrow 2HO^{\bullet} + 3O_2 \quad (39)$$

Combination of three photoelectrochemical processes such as PEF/PAO/PEC and PEF/PAO/PC could result in the highest amount of •OH radical generation since the total active sites estimated in this coupled process is 8 (Mousset and Dionysiou, 2020). In the case of other hybrid processes such as PEF/PAO, PEF/PEC and PEF/PC, total •OH radical generation active sites are estimated to be 6 (Mousset and Dionysiou, 2020). When PEP is coupled to PC, subsequent side reactions (Eq. (40 – 42)) could contribute to extra •OH radical generation in addition to the other main reactions at acidic conditions (Li et al., 2020).

$$e_{cb}^{-} + O_3 \rightarrow O_3^{-\bullet} \quad (40)$$

$$O_3^{-\bullet} + H^{+} \rightarrow HO_3^{\bullet} \quad (41)$$

$$HO_3^{\bullet} \rightarrow HO^{\bullet} + O_2 \quad (42)$$

Similarly, integration of PEP and PAO increases the •OH radical generation since the radical generating active sites are increased. Introduction of Fe^{2+} ions to the PEP system could result in the production of extra •OH radical because of the iron catalysed decomposition of O_3 in addition to the Fenton reaction (Eq. (43)) (Bensalah and Bedoui, 2017).

$$Fe^{2+} + O_3 + H^{+} \rightarrow Fe^{3+} + HO^{\bullet} + H_2O \quad (43)$$

4. Integrated photoelectrochemical processes

The integrated photochemical, electrochemical and photoelectrochemical treatment processes that are discussed in this section include PEF/PC, PAO/PC, PEC/EF, PEC/PEF, PEF/PAO, PEF/PAO/PC, PEC/PAO/PEF, PEP/PEC and PEP/AO. These combined processes were studied for improving the removal efficiencies of different contaminants from synthetic and real wastewater under various reactor configurations and experimental conditions.

4.1. Hybrid PEF/PC, SPEF/SPC and PAO/PC processes

The coupling of the photoelectrochemical processes such as PEF and PAO with the PC process (PEF/PC and PAO/PC) introduces the additional •OH radical production site sourced through

photocatalytic reaction. In the integrated treatment system, photocatalysts are coated on to glass plates covering the walls of the electrolytic cell or immobilised on the substrate materials such as glass tube, glass beads, fiberglass, activated carbon, etc. that are placed within the photoelectrochemical reactor system (Garza-Campos et al., 2014; Iranifam et al., 2011). Many researchers have reported the combined PEF/PC and SPEF/SPC processes using TiO_2 and ZnO photocatalysts coated onto the glass substrate material through the artificial and natural light source (Garza-Campos et al., 2014; Iranifam et al., 2011; Khataee et al., 2012). The performance of PEF/PC to the individual processes was studied for the degradation of dyes by Khataee et al. (2012) and the performance efficiency of the processes were given in the following order: PEF/PC > PEF > EF > UV/TiO_2 > photolysis. Though the EF process accelerates the oxidation of the contaminants, but complete mineralization is difficult to achieve due to the formation of intermediate products that are hard to oxidise (Garza-Campos et al., 2016). Better mineralization efficiency was reported for the SPEF/SPC process than the EF, AO-H_2O_2, AO−H_2O_2−SPC since more radicals are produced during the photolysis and photodecomposition of the Fe(III) species and Fe(III)-carboxylate intermediate complexes and the fast removal of several intermediates formed during the degradation (Garza-Campos et al., 2016).

4.2. Hybrid PEC/EF, PEC/PEF and PEF/PAO processes

The integration of cathodic reactions-based EF, PEF, SPEF processes with the anodic reactions-based PEC, SPEC, PAO processes exploits the merits of individual treatments through the combined •OH radical generation ability and enhancement in the degradation kinetics due to the-other photochemical and electrochemical side reactions (Mousset and Dionysiou, 2020). Various photoanode materials were studied for the radical generation capacity along with the carbon-based cathodes in undivided and divided electrolysis cells. Xie and Li (2006) demonstrated the integrated PEC/PEF system containing TiO_2−Ti mesh photoanode for photoelectrocatalytic reactions and air-diffusion reticulated vitreous carbon cathode for the electrogeneration of H_2O_2 in PEF reactions. Though PEF process is pH sensitive (optimum pH 2.5−3.0), the combination of PEC with PEF exhibited less pH sensitive. Only 10% reduction in removal efficiency was observed from pH 3.0 to pH 9.0 with TiO_2−Ti photoanode and graphite felt cathode (Li et al., 2007). Esquivel and coworkers (Esquivel et al., 2009) studied the performance of TiO_2 modified optical fiber photoanode combined with the PEF process. The photoanode was prepared through the electrophoretic deposition of TiO_2 onto the optic fiber support that was modified by SnO_2:Sb film.

Visible light driven PEC coupled with EF process was demonstrated using Bi_2WO_6 coated FTO photoanode and Fe@Fe_2O_3 supported activated carbon fiber cathode by Ding and co-workers (Ding et al., 2012). TiO_2 nanotubes/Ti based photoanode assisted H_2O_2 generation on carbon felt cathode was studied for the simultaneous oxidation of two different organic contaminants in a two-chamber electrolytic cell (Ramírez et al., 2015). Photoanode was fabricated through electrochemical anodisation of Ti substrate followed by annealing. TiO_2 nanotubes annealed at 450 and 600 °C exhibited porous/organised structure with the anatase phase. Hernández and co-workers (Hernández et al., 2018) studied the performance of UVA driven PEC/PEF process to the sunlight driven SPEC/SPEF process using Au−TiO_2 photoanode and air diffusion cathode. Higher removal efficiency was observed at SPEC/SPEF process due to the greater generation of •OH radicals which resulted upon the irradiation of high-intensity broad-spectrum sunlight combined with the lesser recombination effect of charge carriers due to the additional trapping of some of the photoelectrons by Au dopant.

Interestingly, Xu et al. (2020) reported the electrochemically induced h^+_{vb} on FTO/TiO_2 anode with higher potentials than 2.2 V referred as dark PEC or anodic-breakdown entailing the generation of FTO-TiO_2(•OH) via oxidation of water. Under the irradiation of UV light, the enhancement in the dark PEC phenomenon is observed due to the formation of additional h^+_{vb} and •OH in which the dark PEC is responsible for the two-third mineralization of phenol. Further enhancement in the mineralization was achieved with the coupling of PEC-PEF processes. Wang and collaborators (Wang et al., 2018) examined the performance efficiency of PEF under the microwave discharge electrodeless lamp (MDEL) irradiation and compared it to the other process such as AO-H_2O_2 (electrogenerated H_2O_2), MDEL-AO-H_2O_2. MDEL-PEF process was found to be exhibiting better performance than the other coupled processes. Among the other UVC artificial lamps used in the photochemical studies, MDEL irradiation offers additional advantages of producing considerable portion of UVC along with the UVB, UVC, vacuum-ultraviolet (VUV) and other visible light wavelengths. VUV can produce additional •OH radicals through the direct photolysis of water molecules. At the wavelength of 185 nm, the production of •OH radicals from the homolysis (Eq. (44)) and ionisation (Eq. (45)) reaction exhibited the quantum yields (φ) of 0.33 and 0.045, respectively.

$$H_2O + h\nu(185\ nm) \rightarrow HO^\bullet + H^\bullet \phi = 0.33 \quad (44)$$

$$H_2O + h\nu(185\ nm) \rightarrow HO^\bullet + H^+ + e^-_{aq} \phi = 0.045 \quad (45)$$

4.3. Hybrid PEF/PAO/PC and PEC/PAO/PEF process

Among all of the other integrated photochemical and electrolysis processes, coupled PEF/PAO/PC and PEF/PAO/PEC processes exhibit highest •OH radical production sites which is estimated as 8 (Mousset and Dionysiou, 2020). Garza-Campos et al. (2014) studied the synergistic effects of integrated SPEF/AO/SPC process. BDD electrodes were used as both anode and cathode for the combined SPEF and AO processes. Anatase TiO_2 coated 5 mm diameter glass spheres were used as the catalyst for the SPC reaction. The schematic representation of the reactions involved in this integrated treatment process is given in Fig. 1a and b. Mousset et al. (2017) examined the performance of coupled PEF/PAO/PC process using carbon felt cathode, FTO anode and TiO_2 coated on the stirred glass reactor. FTO anode produced •OH species through AO process. The potential of FTO was evaluated as 2.1 V vs. SHE for the O_2 evolution reaction by linear scan voltammetry, which is high enough to generate •OH through the electrolysis of water. In comparison to the PEF/PAO process, an additional increase of 10% in the mineralization rate was observed with PEF/PAO/PC process.

4.4. Hybrid PEP/AO and PEP/PEC processes

Coupling of PEP process with AO and PEC can enhance the treatment efficiency since the additional radical production mechanisms are introduced. Bensalah and Bedoui (2017) studied the combined PEP and AO process for increasing the production of radicals using BDD anode, and carbon felt cathode. Fast mineralization of organic contaminants with improvement on the energy efficiency was achieved. While Shen et al. (2017) examined the performance enhancement of the coupled PEP with the Ti/RuO_2−IrO_2 anode mediated chlorine evolution process in which chlorine species act as the additional oxidising agent. Moreover, UV

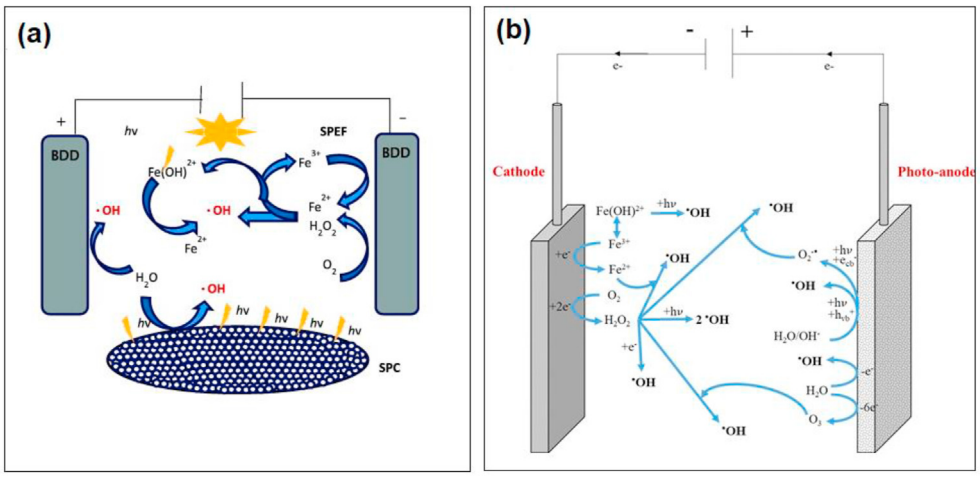

Fig. 1. Schematic representations of the reactions involved in the integrated (a) SPEF/AO/SPC Reprinted with permission from Ref (Garza-Campos et al., 2014). Copyright © 2013 Elsevier Ltd., and (b) PEC/PEF/PAO processes, Reprinted with permission from Ref (Mousset and Dionysiou, 2020). Copyright © 2020, Springer Nature Switzerland AG.

irradiation can also produce additional indirect •OH radicals in reaction to HClO and ClO^- species. PEC combined PEP process was reported by Li et al. (2020). Reduced graphene oxide/bismuth oxychloride (rGO/BiOCl) was used as photoanode, and the direct contact of organic contaminants to the electrogenerated holes could rapidly oxidise the contaminants in addition to radicals produced through PEP process.

5. Combination of photoelectrochemical reactors

The PEC systems are fundamentally composed of an electrolytic reactor with the photocatalyst, a light source to illuminate the photoanode and a power source or potentiostat to provide the electrical energy. However, a diverse range of PEC systems have been explained, with different cells and/or reactors such as stirred tank and flow reactors and positions of light source either inside or outside the reactor, which can be UV/Vis lamps such as UVA (λ_{max} from 320 to 400 nm), UVC (300 nm > λ_{max}) or a quartz window. In addition, Xe lamp can also be used to simulate the sunlight to allow the UV/solar irradiations on the anode surface. The reactor configuration can be differentiated through their shapes and the number of electrodes and compartments. The most general reactor is stirred tank reactor, while flow systems are as well utilized. One can subsequently work with (i) a divided or two-compartment cell, where a separator is used between anodic and cathodic solution and (ii) undivided cell or one-compartment cell. The latter arrangement is generally favored for avoiding the operating cost of a separator of the former one. Both divided and undivided cells are made up with two or three electrodes.

The two electrode system consists in the photoanode and cathode, giving a constant potential through the power source (Daghrir et al., 2013; Ding et al., 2014; Garcia-Segura et al., 2013; Garcia-Segura and Brillas, 2017; Hirakawa et al., 2009; Hosseini et al., 2020), while the reference electrode in a three-electrode system allows to control of the working electrode's potential. For example, Daghrir et al. (2013) reported the chlortetracycline hydrochloride oxidation in aqueous solution using the undivided two-electrode PEC tank reactor with a thin film Ti/TiO_2 photoanode. This reactor was made by acrylic material and a quartz window and the surface of the photocatalyst was illuminated with UVC light of $\lambda_{max} = 254$ nm. Apart from the photoanode, a parallel cathode with the same surface area was placed in the same chamber. Graphite and amorphous carbon, vitreous carbon, and stainless steel (SS) are frequently used as cathode materials. However, a limited number of studies have proposed the usability of divided reactors in the PEC process. Ding et al. (2014) proposed a comparative study on the dual performance of divided and undivided two-electrode PEC systems made by semi-circular quartz glass cylinders for 200 mL of Rhodamine B degradation, as shown Fig. 2a. The Bi_2WO_6/FTO film photoanode was prepared by the deposition of Bi_2WO_6 nanoplates on the surface of FTO glass and the composite cathode $Fe@Fe_2O_3$/ACF was prepared by the loading of $Fe@Fe_2O_3$ core−shell nanostructures on activated carbon fiber (ACF) support. A saturated KCl salt bridge was used to connect the anodic and cathodic chamber of the divided cell and the surface of photoelectrode was illuminated by 300 W tungsten halogen lamp with $\lambda > 420$ nm as a visible light source fixed outside the reactor.

An interesting result on undivided three-electrode PEC systems was reported (Ensaldo-Rentería et al., 2018) to carry out the experiments in a cylindrical quartz cell of three-electrode configuration; Ti/TiO_2-NT anode, carbon graphite cathode and saturated calomel electrode (SCE) as a reference electrode for the acid green 50 degradation. However, some studies reported the undivided three-electrode PEC system which is consisting of a quartz glass tank reactor, a potentiostat and a UVC light source (Su et al., 2008; Fu et al., 2009; Ensaldo-Rentería et al., 2018). It is observed that higher energetic light in these reactors can directly photocatalysed the organic pollutants. During this operation, UVC irradiation crossed the quartz glass wall without intensity loss and placed perpendicular to the photocatalyst surface. Additionally, some of the authors used Xe light source in similar electrode configuration (Zhang et al., 2020a). The Ti/B−TiO_2NTs and an inert Ni sheet act as the photoanode and cathode respectively, while SCE worked as a reference electrode (Su et al., 2008).

More recently, Yang et al. (2020) proposed a two electrode single-cell batch experiment for the degradation of perfluorooctanoic acid (PFOA) using a cylindrical quartz reactor. The graphene oxide titanium dioxide (GOP25)/fluorine-doped tin oxide (FTO) anode and SS cathode with an effective surface area of 6 cm^2 were employed at 50 mM NaCl concentration and a constant cell current density (j) of 16.7 mA cm^{-2}. The photoanode was irradiated by a 16W UVC lamp with $\lambda_{max} = 254$. Garcia-Segura et al. (2013) reported a modest study for the decolorisation and degradation of Acid Orange 7 dye by using the solar PEC system schematized in Fig. 2b. $ATiO_2$ photoanode with carbon-polytetrafluoroethylene (PTFE) air-diffusion cathode were used as electrodes and oxygen

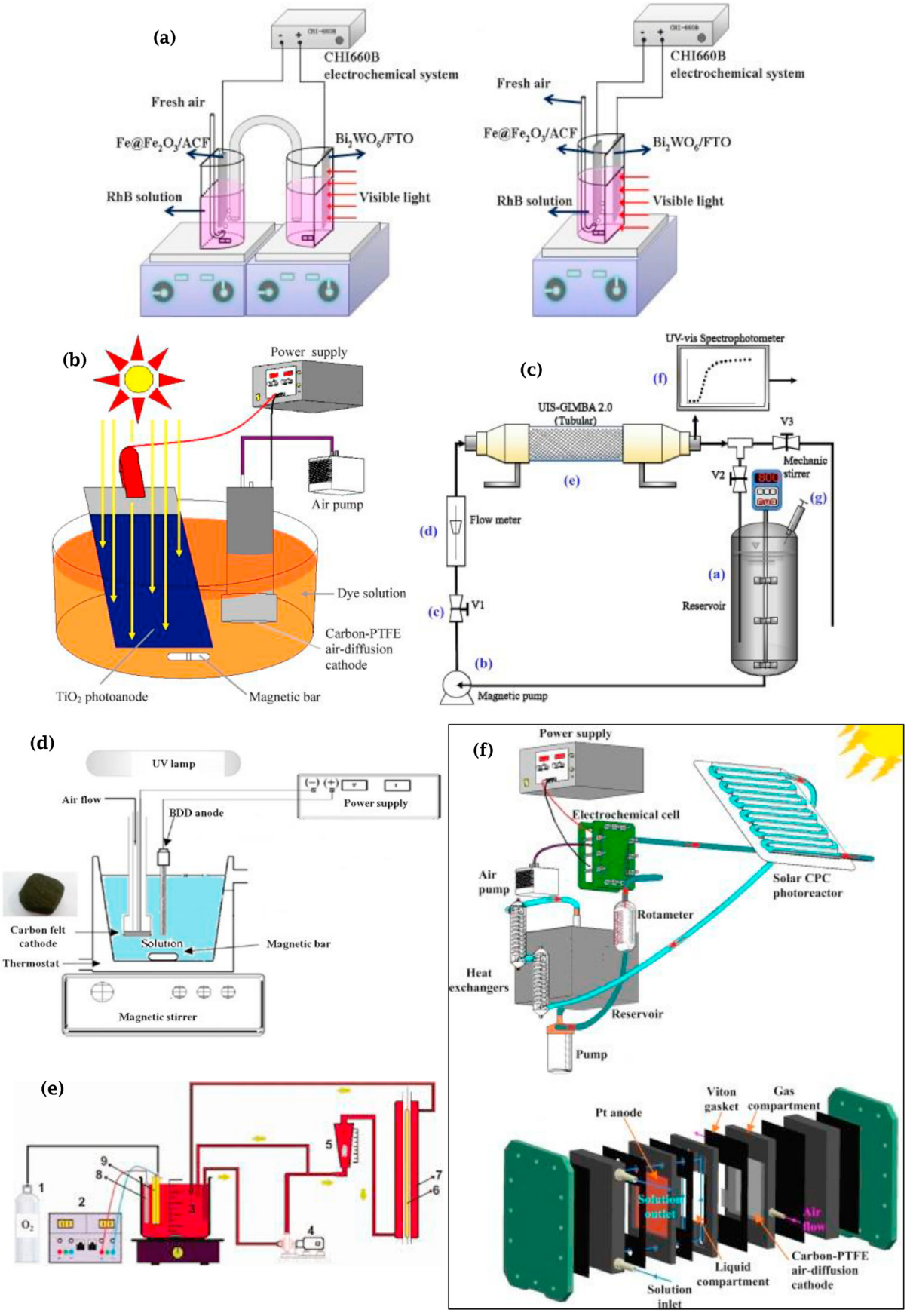

Fig. 2. Schematic presentation of experimental setups used in PEC & SPEC (a, b, c) and PEF & SPEF (d, e, f) treatments of organic pollutants: **(a)** a two-electrode divided (left) and undivided (right) cells in a batch stirred tank reactor with Bi_2WO_6/FTO photoanode and Fe@Fe_2O_3/ACF cathode connected with UVA lamp (Reprinted with permission from Ref

reduction produced the continuous H_2O_2, which can directly oxidised the organic pollutants and produce the more potent reactive oxidizing species (ROS) like •OH. At the optimum treatment conditions, almost complete color was removed in 120 min, while 40% mineralization was reached in 240 min.

On the other hand, three-electrode cells with flow PEC systems were also reported to degrade the different organic pollutants. Vidal et al. (2016) used undivided PEC system consisting of Ti/TiO_2NTs photoanode and Ti/RuO_x cathode connected over a glass end of UV light channel while Ag/AgCl (3 M KCl) acts as a reference electrode and connected with electrolyte exit near the photoanode to degrade 1.0 L of 0.25 $\times$ 10^{-3} M Methyl Orange dye solution in the presence of 0.1 mol L^{-1} Na_2SO_4 and the treatment temperature was controlled with water bath at 15 °C with the help of a centrifugal pump. In this study, a flow meter was used to regulate the flow rate between 20 and 100 L h^{-1} (de José Martín de Vidales et al., 2016). Moreover, Turolla et al. (2018) design a systematic methodology to optimise the scaled-up tubular PEC reactor (T-PECR). Similarly, Cardoso et al. (2016) declared the use of sunlight needed to design an additional competitive PEC system. More recently Jaramillo-Gutiérrez et al. (2020) proposed a new design of input/output distributors for T-PECR with external illumination and a concentric outer (Ti/TiO_2) and inner (nickel-plated SS) electrodes were used as photoanode and cathode, respectively schematized in Fig. 2c. The T-PECR length, the input/output distributor's geometry, and the inter-electrode gap were designed on the basis of convection-diffusion model and the laminar and turbulent regimes in the transitory regime and steady state, respectively. Although, two restrictions i.e., residence time distribution and mass transfer coefficients were considered for the perfect T-PECR design to reduce the inlet/outlet effects and therefore attain the completely developed velocity profiles which results enhance the homogeneous flow pattern in the T-PECR (Jaramillo-Gutiérrez et al., 2020). Similarly, most of the PEF studies have been carried out in stirred glass cubic or cylindrical divided and undivided tank reactors consisting either two or three electrodes covered with or without a thermostated jacket for water recirculation to maintain the solution temperature during the galvanostatic or potentiostatic mode of operation; usually,100–200 mL solution volume are employed, while 1.0 and 2.0 L volumes were infrequently used at bench scale in the laboratory (Brillas and Martínez-Huitle, 2015; Brillas, 2020; Brillas and Garcia-Segura, 2020).

PEF systems are irradiated with UV lamps and can be placed at different locations against the solution. Photo reactor configuration have significant effect on the degradation efficiency, particularly the source of irradiation. In conventional PEC reactors with annular geometry, the photoanode are immersed in the solution and light reaches the reactor after passing through the walls of the reactor and solution. This can reduce the degradation efficiency of organic compounds as significant radiation power is wasted due to absorption and uneven distribution of light (Xu et al., 2008). However, irradiating the system from outside increases the activated catalyst per unit volume of solution and photon distribution. It also eliminates the possibility of light loss by adsorption and scattering of the reactor medium (Ray, 1998). When comparing the photo-electrocatalytic reactors, slurry and packed-bed reactors with external light sources are more effective for practical implementation since it can reduce the energy cost by replacing the UV irradiation source with solar irradiation (Rajput et al., 2021). Fig. 2d shows a schematic presentation of undivided PEF reactor for which UVA lamp is on top of the solution (Bañuelos et al., 2016). For example, Thiam and Salazar (2019) achieved excellent mineralization ability with Pt and BDD during the PEF-UVA process because UV light-induced the removal mechanisms. Meanwhile, El-Ghenymy et al. (2015) reported the comparative studies on both divided and undivided PEF reactors and observed that the higher concentration of supporting electrolyte need to be employed in the divided cell due to higher E_{cell}. The rate of color removal was found to be higher in the divided cell since higher potential can be simply achieved by increasing current/potential in the power supply.

This phenomenon is responsible for increase the mass transport toward the anode, therefore supporting a faster reaction between M (•OH) and organics. Flores et al. (2017) observed that 80% of TOC decay of 4-hydroxyphenylacetic acid and real olive oil mill wastewater was achieved by using BDD/Air-diffusion electrodes (ADE) reactor like that of Fig. 2d by passing the 6 W UVA light at j of 100 mA cm^{-2}. These outcomes encourage the PEF process performance to the treatment of more real wastewater before discharge to water bodies. In addition, a majority of studies used undivided cells; however, a simple flow plants with a filter-press cell have also been used. Da Silva et al. (2014) and Nava et al. (2014) used a filter press reactor design in a simple reactor via the coupling with a reservoir and a pump. Later, a transparent quartz cell is suggested for absorbing most of the UVC photons produced via the lamp. Fig. 2e shows a cylindrical photoreactor in which external UV fluorescent is connected with a tank reactor (Khataee et al., 2013). In addition, some of the flow plants equipped with a tubular ceramic membrane with imbedded electrodes (Juang et al., 2013), a concentric annular cell (Peralta-Hernández et al., 2008) or a plug-flow cell (Carvalho et al., 2007) were rarely used.

The high operating cost of PEF process owing to UV lamp irradiation has been defeated by SPEF due to free and direct renewable sunlight irradiation. In principle, both processes utilized the same electrolytic reactor but the main difference is the sources of light irradiation. Brillas' group has reported SPEF method with three PEC systems: (i) a lab scale stirred tank reactor with BDD anode and ADC cathode under direct sunlight radiation instead of UV lamp (Moreira et al., 2013; Zhang et al., 2016), (ii) flow systems with BDD/ADC direct connected with solar radiation for the batch scale treatment of industrial effluent (Ruiz et al., 2011; Salazar et al., 2011b; Olvera-Vargas et al., 2015) and (iii) a pilot flow plant connected with Pt/ADE a filter-press and solar compound parabolic collector (CPC) photoreactor made-up of borosilicate tubes (see the schematic presentation in Fig. 2e) (Garcia-Segura et al., 2011; Garcia-Segura and Brillas, 2014). The CPC systems have significant light collecting properties. For example, Isarain-Chávez et al. (2011) study beta-blockers drug degradation in a solar CPC photoreactor connected with a series of 12 parallel borosilicate-glass tubes mounted in an aluminum frame on a tilted angle stand like site latitude to better collect the direct sunlight radiation, while some of the less efficient and simplest solar photoreactor were used in some works. These systems consist of a polycarbonate box made with a

(Ding et al., 2014). Copyright © 2014 Elsevier B.V. **(b)** Solar stirred tank with TiO_2 photoanode and air-diffusion cathode (ADC) (Reprinted with permission from Ref (Garcia-Segura et al., 2013). Copyright © 2012 Elsevier B.V. **(c)** Tubular PEC reactor (T-PECR) with liquid flow pipeline. (a) Recirculation tank with a mechanical stirrer, (b) centrifugal pump, (c) valve for flow regulation, (d) rotameter, (e) T-PECR, (f) UV–Vis spectrophotometer, and (g) tracer pulse injection, Reprinted with permission from Ref (Jaramillo-Gutiérrez et al., 2020). Copyright © 2019 Elsevier B.V. **(d)** Stirred tank reactor with a BDD/Carbon Felt-air diffusion arrangement (Reprinted with permission from Ref (Bañuelos et al., 2016). Copyright © 2016 Elsevier Ltd. **(e)** Recirculation flow plant with a stirred tank reactor: (1) oxygen cylinder, (2) power supply, (3) reservoir, (4) diaphragm pump, (5) rotameter, (6) UV-C lamp, (7) photoreactor, (8) anode, and (9) CNT-PTFE cathode (Reprinted with permission from Ref (Khataee et al., 2013). Copyright © 2012 American Institute of Chemical Engineers. **(f)** Solar pre-pilot flow plant with a filter-press electrolytic cell and a compound parabolic collector (CPC) photoreactor, Reprinted with permission from Ref (Garcia-Segura et al., 2011). Copyright © 2011 Elsevier B.V.

mirror at the bottom connected to the cell with an inclined angle similar to the site latitude (Ruiz et al., 2011; Brillas, 2020; Brillas and Garcia-Segura, 2020).

Some of the studies reported a comparison between the relative oxidation ability of PEF and SPEF using a stirred tank reactor by supply irradiation with 6 W UVA and direct sunlight (Antonin et al., 2015; Brillas, 2020; Brillas and Garcia-Segura, 2020). Although the decay rate is same for both processes since of the same amount of •OH radicals generation but a faster mineralization was attained with SPEF than PEF due to the higher sunlight UV irradiance (~30–35 W m^{-2}) than ~5 W m^{-2} of 6 W UVA light, which favours the quick photolysis by adsorbing the higher quantity photons. Moreira et al. (2013) designed a scale-up SPEF method from a 100 mL to 10 L undivided cell to filter-press pilot-scale flow plant and a photoreactor. No doubt the practicability of filter-press reactor was confirmed; however, the direct comparison between both PEF and SPEF reactors is not easy due to the different treatment conditions for example electrodes area/solution volume ratio, absorption of solar radiation, anode nature, irradiated volume/total volume ratio and anode nature. Pipi et al. (2014) observed that 100 mL pesticide quickly degraded in an undivided cell compared to 2.5 L flow plant during SPEF process because the ratio of electrode area/solution volume mainly accounted. Garcia-Segura and Brillas (2014) reported faster mineralization of 100 mL antibiotic chloramphenicol solution in an undivided stirred tank reactor (Fig. 2d) instead 10 L pilot-scale flow plant (Fig. 2f) during SPEF conditions because of less amount of irradiated volume/total volume ratio. Antonin et al. (2015) also reported a comparative study of SPEF in an undivided (Fig. 2d) and pilot-scale plant (Fig. 2f) during the treatment of Evans Blue diazo dye. After 60 and 5 min of treatment complete color was removed, while ~88% and more than 95% TOC removal were formed after 300 min at the pilot-scale plant and undivided cell, respectively. The main reason for this difference was attributed to the solution volume ratio and electrode area of both reactors.

6. Modified electrodes in photoelectrochemical processes

PEC process performance of pollutant remediation is directly related to the intrinsic photocatalytical properties of semiconductors metal oxides (MOs) with a suitable band gap (E_g) value selected as photoanodes (PAs) (Brillas and Martínez-Huitle, 2015; Garcia-Segura and Brillas, 2017; Sun et al., 2020). The photocatalytic performance of these metal oxides (MOs) mainly depends on the oxidation-reduction reactions that take place on the surface of PAs via the photogenerated electron/hole (e^-_{CB}/h^+_{VB}) pairs. The different semiconductor MOs are used in the PEC process of pollutants remediation for example, TiO_2 is an n-type semiconductor with three main crystalline phases, namely rutile (E_g = 3.02 eV), anatase (E_g = 3.23 eV) and brookite (E_g = 3.14 eV) (Georgieva et al., 2012; Brillas and Martínez-Huitle, 2015; Garcia-Segura and Brillas, 2017), the former phase is most thermodynamically stable and widely used as photoanode for environmental remediation. WO_3 is other n-type semiconductor with E_g values around 2.5–2.7 eV lower than those of TiO_2 (Fernández-Domene et al., 2019), whereas ZnO (E_g = 3.4 eV) is cheaper and extensively found in nature than above two with high PEC stability under natural sunlight irradiation (Hosseini et al., 2020). Other many pure MOs semiconductors such as hematite α-Fe_2O_3 (E_g = 2.2 eV) has been chosen as an alternate of these due to its higher chemical stability, low cost and high light absorbance in visible light (Qi et al., 2015; Meshram et al., 2019), whereas MnO with very low E_g = 1.3 eV has interesting PEC properties due to its interaction with polyaniline (E_g = 2.8 eV) that decreases the combination reaction of e^-_{CB}/h^+_{VB} (Yu et al., 2010). Additionally, SnO_2 semiconductor (E_g = 3.5–3.8 eV) is chemically and thermally stable therefore it is difficult to use as photocatalyst (PC) but Sb can be simply doped on pure non-conductive SnO_2 to significantly enhance its electrical conductivity and PC properties such as short lifetime and electrochemical stability (Qi et al., 2015; Subba Rao et al., 2017). Other semiconductor material like as β-PbO_2 (E_g = 1.4 eV) has also been used PC in alkaline medium (Gui et al., 2019; Li et al., 2006); however, it releases Pb^{+2} ions to the medium. In contrast, bismuth materials such as $BiPO_4$ (E_g = 3.8 eV) under UV illumination and Bi_2WO_6 (E_g = 2.8 eV), (Yao et al., 2019), $BiVO_4$ (E_g = 2.5 eV) (Liu et al., 2020) $Ag_3PO_4/BiVO_4$ (Cao et al., 2018) and $C_3N_4/Ag/AgCl/BiVO_4$ (Rather and Lo, 2020) under visible illumination have shown superb performance and excellent effectiveness for PEC treatment of organic pollutants.

To improve the PEC performance different modification approaches have been constructed including: (i) nanotubes (NTs) (Esbenshade et al., 2010), nanotube arrays (NTAs) (Ensaldo-Rentería et al., 2018), polyaniline (PANI)-modified nanotubular TiO_2 electrodes (NTs) (Mais et al., 2019) and nanorods (NRs) or nanobelts (NBs) structures (Chen et al., 2013), (ii) doping with metals such as Cr, Fe, Co, Ni, Cu and Zn (Brillas and Martínez-Huitle, 2015; Garcia-Segura and Brillas, 2017; Sun et al., 2020) or non-metals such as B, C, and N (Zhu et al., 2010; Chen et al., 2015a), (iii) composites synthesised with noble metals like Ag, Au, Pt and Pd (Rezaei et al., 2018; Zhang et al., 2020a), other MO_s such as Fe_3O_4, SnO_2 (Qi et al., 2015) Cu_2O (Koiki et al., 2020), and metal sulfides like Sb_2S_3 (Bessegato et al., 2014) and CdS (Hou et al., 2020), and carbonaceous materials such as graphene (Tayebi et al., 2019) and carbon quantum dots (Su et al., 2020) and (iv) new PAs materials like cubic double-perovskite $CaCu_3Ti_4O_{12}$ (Kushwaha et al., 2017) and $TiNbO_5$ (Zhang et al., 2012a).

Low E_{cell} or *j* values were applied to most of the modify PAs, due to their less stability towards electricity, whereas dimensionally stable anodes (DSAs) type TiO_2–RuO_2 electrodes shown higher stability and allowed the usability at higher *j* values. Substrates like as Ti and SS metals, fluor doped tin dioxide (FTO) and indium-tin oxide (ITO), among other have been extensively used in TiO_2 thin films preparation by using the several procedures such as sol-gel method, spray painting and thermal decomposition, magnetron sputtering, chemical vapour deposition (CVD), atomic layer deposition (ALD) and thermal spray coating technologies (shown in Table 1(a)). Since 2007, TiO_2NTs and TiO_2NBs are usually prepared from electrochemical and sonoelectro-chemical methods. In contrast, FTO/TiO_2 NR arrays are synthesised by a hydrothermal approach for PEC uses. The main advantage and disadvantages of these highly ordered and three-dimensional (3-D) nanostructures than thin-films electrodes is owing to their excellent surface properties, smaller recombination of e^-/h^+ pairs and diffusion length escape recombination that permits higher light absorption (Table 1(a)).

Fig. 3 shows the scanning electron microscopy (SEM) of various PAs. Fig. 3a–b shows granulate, compact and low porosity structure of typical TiO_2 NT synthesised by anodisation of Ti substrates and composed of uniform size crystalline one-dimensional NTAs (Liao et al., 2014; Ensaldo-Rentería et al., 2018). Using the similar approach, Ensaldo-Rentería et al. (2018) found calcinations from 600 to 800 °C increased the crystal size of anatase and rutile crystal structure, respectively; whereas, Liao et al. (2014) observed E_g values of crystalline anatase Ti/TiO_2NTAs (2.7 eV) much lower compared to granulate anatase (3.2 eV) (Fig. 3a–b), and that permitted an increased PEC performance using visible light offered by a 60 W luminescent lamps. Shang et al. (2011) was found indium tin oxide (ITO)/TiO_2/ITO enhances the PEC performance instead of an ITO/TiO_2 photoanode during the Rhodamine B dye degradation in 1.5 M NaCl at E_{cell} of 1.5V, since electrons can be quickly removed via the ITO/TiO_2 interfaces; as a result oxidant holes increased.

Table 1 (a)
Various synthesis methods for photo anodes at the optimum treatment conditions with their advantages and disadvantages during PEC process.

Synthesis techniques	Electrode types	Experimental conditions	Advantages	Disadvantages	References
UV-PEC					
Electrochemical anodisation	Ti/TiO_2-NT	Conc.: 17×10^{-6} mol L^{-1}; pH_{sol}: 1.0; 0.05 mol L^{-1} Na_2SO_4; time: 6 h	Photocatalytic reactivity of nanotube was influenced via applied potential and annealing temperature at fixed pH of solution.	TiO_2 NTs coating layer passivates the electrode surface.	Ensaldo-Rentería et al. (2018)
Electrochemical synthesis process	F−$BiVO_4$@NiFe-LDH	Conc.: 20 mg L^{-1}; pH_o: 7.0; time: 6 h	Degradation rate of core-shell photoanode was 6 fold than pristine $BiVO_4$ photoelectrode.	Opposite migration paths can be reduced the recombination of e^-−h^+ pairs.	Liu et al. (2020)
Solvothermal combined with hydrothermal<	TiO_2/Bi_2WO_6/Au NRAs	Conc.: 10 mg L^{-1}; 0.5 M Na_2SO_4; time: 7 h	Au NP decorated heterostructure to improve the photocatalytic activity.	Au and Ag NPs effectively enhance PEC performance but cost issue and practical applicability are serious concern.	Yao et al. (2019)
Hydrothermal treatment	SnO_2-g-C_3N_4	0.2 M Na_2SO_4; time t: 1.5 h	Synergistic effect SnO_2-g-C_3N_4 eight times higher than that of SnO_2 nanostructures PAs.	SnO_2 nanostructures have a relatively low surface area.	Mohammad et al. (2019)
Thermal decomposition and electrodeposition	Ti/TiO_2 NTs/Ta_2O_5−PbO_2	Conc.: 30 mg L^{-1}; pH_o: 3.0; V_i: 50 mL; 0.2 M Na_2SO_4; time: 25 min	MMOs (e.g., SnO_2, PbO_2, IrO_2, TiO_2 etc.) coatings conquer the passivation problem.	TiO_2 NTs is a non-conductive coating and blocks e^- transfer reasoning extreme voltage in PEC.	Gui et al. (2019)
Electro-deposition method<	Cu_2O/TiO_2/NTAs	Conc.: 10 mg L^{-1}; pH_o: 3.0; V_i: 100 mL; 0.1 M Na_2SO_4; time: 4 h	The p-n heterojunction enhances the charge separation, resulting reduced recombination rate and increased pollutant degradation percentage.	Heterojunction mitigate the challenge of UV light irradiation of TiO_2 NTA for activation due to its wide band gap energy.	Koiki et al. (2020)
Electro-deposition method<	Ag_3PO_4/$BiVO_4$	Conc.: 5.0 mg L^{-1}; 10 mmol L^{-1} $NaClO_4$; time t: 2 h	Effective electrode for PEC systems at comparatively low bias potentials.	$BiVO_4$ electrodes have low separation efficiency of photogenerated e^-−h^+ pairs.	Cao et al. (2018)
Dip-coating method	TiO_2/Ni-MWCNTs	COD_i: 3150 mg L^{-1}; 0.5 mol L^{-1} NaCl; pH_o: 3.0; time: 2 h.	Synergistic effect of free Cl_2 and atomic state oxygen increased COD and color removal efficiency.	Separation of catalyst and low quantum efficiency are two technical limitations.	Fang et al. (2013)
Electro-deposition followed by dip coating<	SnO_2−Sb_2O_4-WO_3	Conc.: 50 mg L^{-1}; V_i: 50 mL, 0.1 M Na_2SO_4; pH_o: 3.0; time: 5 h.	Rationale behind choosing nano-WO_3 with MMO modification refines the crystal structure and enhances the photoactivity.	Nano-WO_3 into MMO matrix improved the average current efficiency of PEC.	Subba Rao et al. (2017)
Chemical bath deposition method	C−N co-doped TiO_2 NTA	Conc.: 5 mg L^{-1}; V_i: 50 mL; pH_o: 4.0; 0.1 M Na_2SO_4; time: 1 h.	Nonmetal-doped PAs was most effective due to its p states contribute to narrowing the band gap by mixing with O 2p state.	Electron−hole recombination character of semiconductors not only inhibited the quantum efficiency but decreased the oxidation capability.	Chen et al. (2015)
Radio-frequency sputtering technique	Ni-doped ZnO	Conc.: 5 mg L^{-1}; V_i: 100 mL; pH_o: 7.0; 0.75 g L^{-1}, NaCl; time: 1.5 h.	ZnO modified with Ni to decrease band gap for enhanced UVA effect.	Poor oxygen vacancy in ZnO sites and band gap between valence band and conduction band is higher.	Hosseini et al. (2020)
Hydrothermal and solvothermal method	CdTe/CdS/N-rGO	Conc.: 50 mg L^{-1}; V_i: 100 mL; 0.75 g L^{-1}, NaCl; time: 6 h.	Longer lifetime of photon-generated carrier and stronger intensity of photocurrent.	Prominent disadvantage of rGO absence of band gap limits it in electronic application.	Liu et al. (2018)
Hydrothermal method	SnO_2/α-Fe_2O_3	Conc.: 50 mg L^{-1}; V_i: 100 mL; pH_o: 6.0; 0.1 M Na_2SO_4; time: 1 h.	Generation of photoinduced charge carriers increased with decreasing in charge transfer resistance as a result excellent PEC properties.	In absence of SnO_2, the stability of Fe_2O_3 in aqueous solutions is very poor.	Qi et al. (2015)
Solar-PEC					
Hydrothermal method	CoO_x modified Zr^{4+}doped Fe_2O_3 nanorods	Conc.: 10 μM; V_i: 70 mL; pH_o: 13.6; 0.1 M Na_2SO_4; time: 7 h.	Synergistic effect between CoO_x co-catalyst and tetravalent doping results enhanced the degradation efficiency.	Hetero structures undergo surface recombination matters of the photogenerated charge carriers.	Meshram et al. (2019)
Hydrothermal method followed by electrophoretic deposition	TiO_2/Pt−C_3N_4 NTs	Conc.: 1.0 mmol L^{-1}; V_i: 20 mL; 0.1 M Na_2SO_4; time: 2 h.	Pt−C_3N_4 modified PAs reduce the band gap energy and improve its ability of light absorption in the visible region.	Pure bulk g−C_3N_4 has fast recombination of e^-−h^+ pair, low oxidation ability and specific surface area.	Rezaei et al. (2018)
Spray pyrolysis method<	WO_3/TiO_2	Conc.: 10 mmol L^{-1}; V_i: 500 mL; 0.5 mol L^{-1} Na_2SO_4; time: 30 min.	No mixed phase formation, high crystallinity, large surface area, strong optical absorption in the visible range of solar spectrum.	TiO_2 absorbs only 4% photons as a result decrease the effectiveness of TiO_2 under solar irradiation.	Hunge et al. (2018)

Multi-walled carbon nano-tubes (MWCNTs).

Additionally, presence of Cl^- produced active chlorine species (Cl_2/HClO/ClO^-) act as additional oxidising agent by the photocatalytic reactions (Eqs. (46) and (47)).

$$TiO_2(h^+_{VB}) + Cl^- \rightarrow TiO_2 + Cl^{\bullet} \quad (46)$$

$$Cl^- + HO^{\bullet} \rightarrow Cl^{\bullet} + OH^- \quad (47)$$

Doping with noble metals (e.g., Au, Ag, Pd, Pt) onto TiO_2 and other semiconductor MOs had also extremely improved the charge separation efficiency by trap the e^- CB, and help in electrons transfer (Rezaei et al., 2018; Zhang et al., 2020b). In addition,

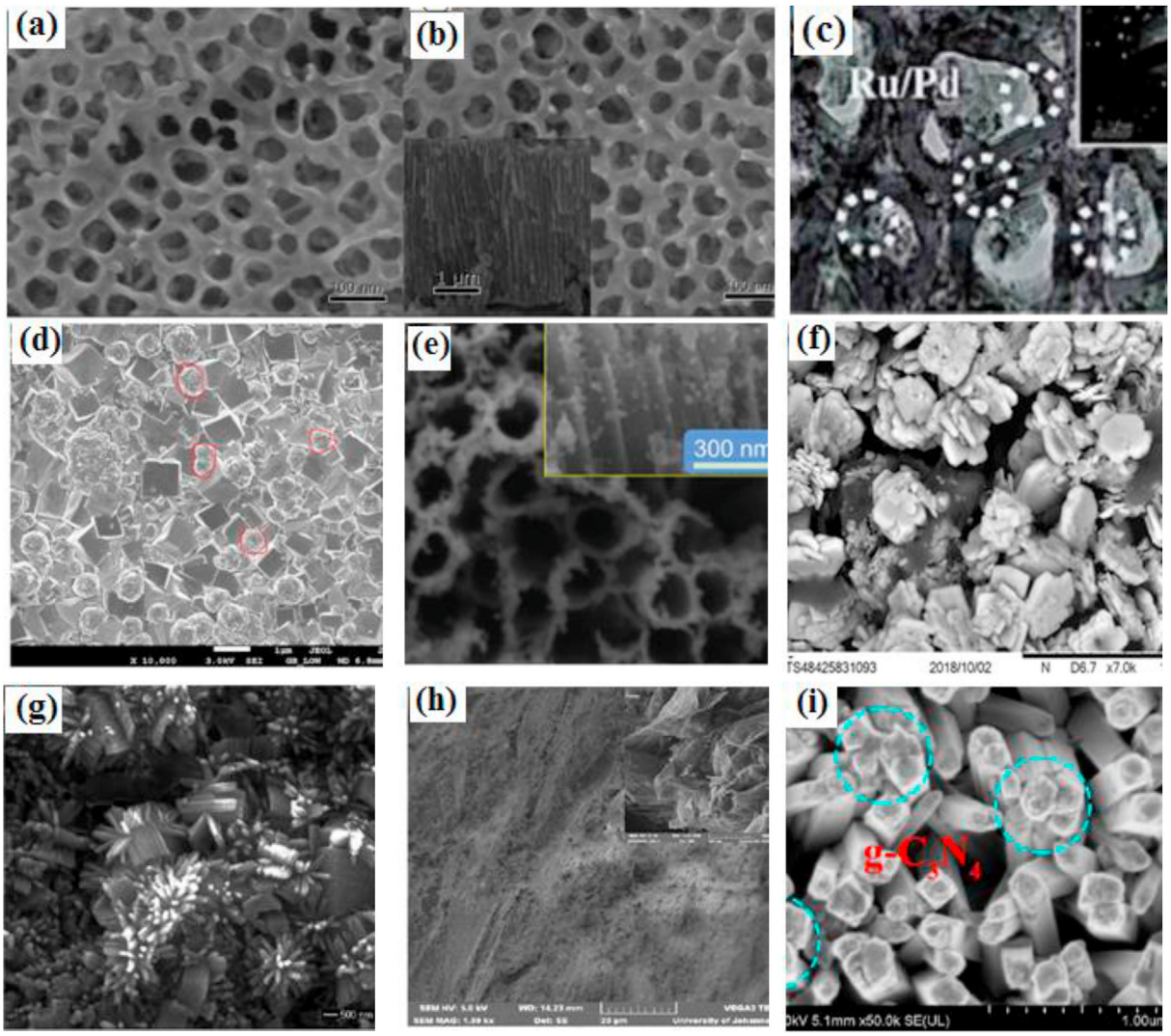

Fig. 3. Typical SEM images of various PAs prepared different methods (a–b), Reprinted with permission from Ref (Liao et al., 2014). Copyright © 2014 Elsevier Ltd. (c) Ru–Pd BQDs/TiO_2 NTA Reprinted with permission from Ref (Fan et al., 2018). Copyright © 2018 Elsevier B.V. (d) TiO_2 NTA/Cu_2O heterojunctions, Reprinted with permission from Ref (Koiki et al., 2020). Copyright © 2020 Elsevier Ltd., (e) Bi_2O_3/C@TiO_2 NTAs interface, Reprinted with permission from Ref (Pang et al., 2019). Copyright © 2019 Elsevier B.V., (f) CAB-1 Reprinted with permission from Ref (Rather and Lo, 2020). Copyright © 2019 Elsevier Ltd., (g) SnO_2/Fe_2O_3 Reprinted with permission from Ref (Qi et al., 2015). Copyright © 2015 Elsevier B.V., (h) Exfoliated graphite (EG)/TiO_2 Reprinted with permission from Ref (Ama and Arotiba, 2017). Copyright © 2017 Elsevier B.V., and (i) TiO_2/g-C_3N_4/CQDs nanorod arrays (TCNC NRAs) Reprinted with permission from Ref (Su et al., 2020). Copyright © 2020 Elsevier Ltd.

Schottky type junctions with n-type TiO_2 could facilitate the interfacial transfer of electrons from CB of TiO_2 to the VB of noble metals (Fan et al., 2018; Rezaei et al., 2018; Zhang et al., 2020a).

Despite the benefits of noble metals doped semiconductor MOs, non-noble metals and MOs doped semiconductor MOs comes into practical application since of the cost issue and practical applicability of the first one. For example, Koiki et al. (2020) synthesised p-n heterojunction photoanode via the electrodeposition of cubic like Cu_2O on anodised TiO_2 NTAs (Table 1(a)). Fig. 3d shows Cu_2O possess high reflectivity and more pronounced morphology; however, red mark circled on Cu_2O cubes represents the remaining TiO_2. The PEC of TiO_2 NTA/Cu_2O was examined in ciprofloxacin (CF) degradation. More than 73% CP was removed after 4 h because photogenerated holes played major role in CP oxidation than •OH radicals as shown in Fig. 4a and reactions (Eqs. (48)–(50)).

$$TiO_2NTA \Big/ Cu_2O + h\upsilon \rightarrow \frac{TiO_2NTA}{Cu_2O}(e^- + h^+) \quad (48)$$

$$h^+ + H_2O \rightarrow H^+ + HO^- \quad (49)$$

$$e^- + O_2 \rightarrow O_2^{\bullet -} \quad (50)$$

Moreover, different Bi-based novel visible light-driven (VLD) semiconductors with narrow band gaps to increase the response range of the solar energy in PEC have been discovered such as $BiVO_4$ (Liu et al., 2020), 3D Bi_2S_3/TiO_2 NTAs (Guo et al., 2019), TiO_2/Bi_2WO_6 (Yao et al., 2019), Bi_2O_3/C@TiO_2 NTAs (Pang et al., 2019) and Bi/Bi_2MoO_6 co-sensitized TiO_2 NTAs (Cao et al., 2020). Pang et al. (2019) reported a novel Z-scheme heterostructure system. Fig. 3e shows a highly-ordered and uniform tubular structure of Bi_2O_3/C@TiO_2 NTAs which is prepared by introducing the metal oxides (Bi_2O_3) nanocrystals with uniform size (2–3 nm) on the carbon bridged TiO_2 NTAs. In this scheme, carbon played both roles i.e.,

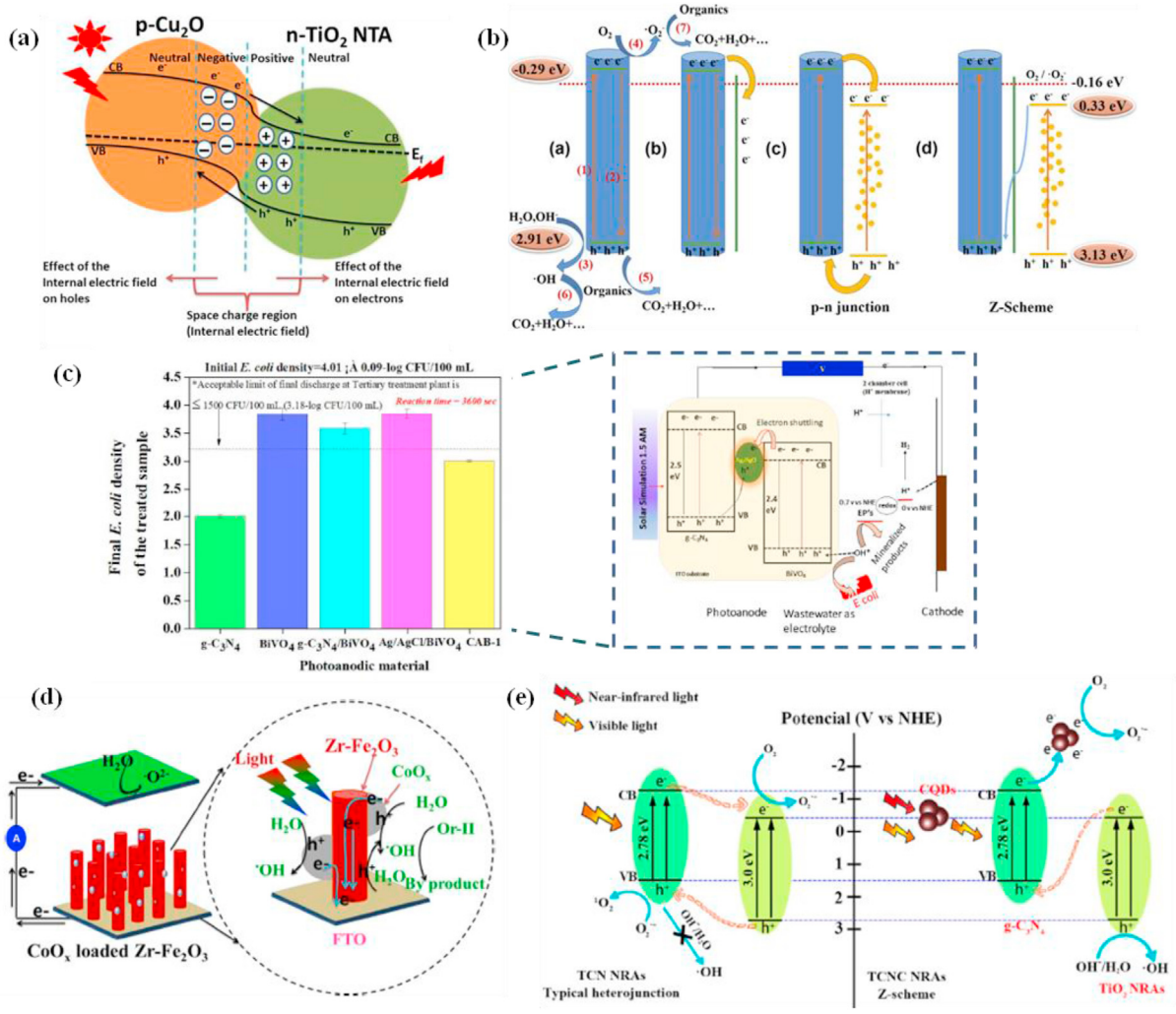

Fig. 4. Schematic presentation of transferring the photogenerated e^-/h^+ in various interfaces (a) TiO_2NTA/Cu_2O Reprinted with permission from Ref (Koiki et al., 2020). Copyright © 2020 Elsevier Ltd., (b) proposed mechanism of TiO_2 (a), C@TiO_2 (b), Bi_2O_3/TiO_2 (c) and Bi_2O_3/C@TiO_2 (d) NTAs, Reprinted with permission from Ref (Pang et al., 2019). Copyright © 2019 Elsevier B.V., (c) PEC disinfection ability of CAB-1 PA in fresh sewage and schematic presentation of pollutant degradation, H_2 evaluation and disinfection, Reprinted with permission from Ref (Rather and Lo, 2020). Copyright © 2019 Elsevier Ltd., (d) PEC performance for Orange-II degradation over CoO_x modified Zr−Fe_2O_3 Reprinted with permission from Ref (Meshram et al., 2019). Copyright © 2019 Taiwan Institute of Chemical Engineers. Published by Elsevier B.V., (e) e^-/h^+ separation and transport at the TCN NRAs and TCNC NRAs Pas, Reprinted with permission from Ref (Su et al., 2020). Copyright © 2020 Elsevier Ltd. (For interpretation of the references to color in this figure legend, the reader is referred to the Web version of this article.)

system integration and electron trapping with high efficiency. The TiO_2NTAs possesses different PEC mechanisms such as light absorption, charge separation and transfer, and surface reactions during novel Z-scheme heterostructure system. Fig. 4b shows that photogenerated e^-/h^+ pairs are generated under UV illumination but refraining of e^-/h^+ pairs recombination in the charge transfer (CT) process cannot be formed with TiO_2. For C@TiO_2, the carbon layer helps in electron trapping from CB of TiO_2 to carbon layer. The CT of photogenerated e^-/h^+ pairs occurs due to the difference of CBs and VBs between Bi_2O_3 and TiO_2 in Bi_2O_3/TiO_2 NTAs. The p-n junction formed by the transfer of photo-generated holes and electrons from VB of Bi_2O_3 to the TiO_2 and CB of TiO_2 to the Bi_2O_3, respectively. Fig. 4b shows the Z-scheme system of Bi_2O_3/TiO_2 NTAs introduced by carbon layer which is more favorable for CT from Bi_2O_3 to TiO_2 and enhanced the PEC performance.

Recently, Ag-based semiconductor PAs, particularly silver phosphate (Ag_3PO_4) and silver chloride couple with $BiVO_4$, reduced grapheme oxide (rGO); carbon nitride (g-C3N4) have attained specific attention (Cao et al., 2018; Rather and Lo, 2020). For example, Cao et al. (2018) used Ag_3PO_4/$BiVO_4$ on FTO for 5 mg L^{-1} norfloxacin degradation and apparent rate constant was estimated about 2.83×10^{-4} min^{-1} and 7.94×10^{-4} min^{-1} for $BiVO_4$ and Ag_3PO_4/$BiVO_4$, respectively, within 90 min; whereas, Rather and Lo (2020) discovered flower shaped g-C_3N_4/Ag/AgCl/$BiVO_4$ (CAB-1) microstructures (size range between 3 and 5 μm) (Fig. 3f) 3-D electrode configuration for emerging pollutant removal. Fig. 4c shows CAB-1 follows a Z-schematic approach during PEC. The small E_g of $BiVO_4$ (2.40 eV) and g-C_3N_4 (2.50 eV) enable to activate under the solar- PEC, while CT ability of CAB-1 increased due to the generation of e^-/h^+ pairs as charge carriers. The electrons excited from CB of g-C_3N_4 than $BiVO_4$ and these electrons were transferred towards Pt cathode. At the same time, h^+ in the VB of $BiVO_4$ has enough potential to oxidise the pollutant. The Ag/AgCl helps to make the CAB-1 an active Z-schematic heterojunction by the annihilation of e^- and h^+ from CB of $BiVO_4$ and g-C_3N_4, respectively.

In comparison of TiO_2, ZnO also appeared as a promising PAs since to its lower cost and higher absorption efficiency. For example, Hosseini and collaborators (2020) tested Ni-doped ZnO in

ciprofloxacin (CIP) degradation (Table 1(a)). In addition, strong optical properties of stratified WO_3/TiO_2 under sunlight illumination were tested for 94% Reactive Red 152 and 98% Rhodamine B dyes degradation within 40 and 30 min, respectively (Hunge et al., 2018); whereas Oliveira et al. (2015) tested the excellent performance of this anode during the 10 mg L^{-1} 17-α-ethinylestradiol irradiation under 4 h solar illumination.

More interestingly, among semiconductors MOs, hematite (α-Fe_2O_3) nanostructured has emerged as an effective catalyst for persistent pollutant degradation since of its high chemical stability, suitable band gap energy and excellent environmental compatibility. Moreover, α-Fe_2O_3 suffers with several disadvantages such as low carrier mobility, low absorption coefficient (<1 $cm^2 V^{-1} s^{-1}$), shorter excited state lifetime (~10 ps) and short hole diffusion length (2–4 nm) (Meshram et al., 2019). Therefore, many doping approaches have been recently proposed to overcome the limitations of α-Fe_2O_3 (Qi et al., 2015; Meshram et al., 2019). Meshram et al. (2019) proposed the CoO_x surface modification and tetravalent ions dopants (Ti^{4+}, Si^{4+}, Sn^{4+}, and Zr^{4+}) on hematite nanorod array (HNRAs) during PEC of Orange- II dye degradation. Amongst four tetravalent Zr^{4+} doped HNRAs (Zr–HNRAs) can considerably improve the performance, while Zr–Fe_2O_3 PAs further modified with CoO_x to enhance the photo-activity, higher than 93% dye removal was formed under sun illumination within 270 min due to the effective CT leads to •OH radicals formation (Fig. 4d).

The integral treatment system including photoelectro catalytic oxidation and electro catalytic oxidation has been reported for SnO_2 modified Fe_2O_3 (SnO_2/Fe_2O_3) (Qi et al., 2015), TiO_2 (TiO_2/Fe_2O_3) (Hu et al., 2011) and SnO_2–Sb_2O_4 mixed metal oxides (MMOs) modified nano-WO_3 (SnO_2–Sb_2O_4-WO_3) composites by assembling of Sb–SnO_2 film on TiO_2NTs (Subba Rao et al., 2017) for enhancing the photoactivity of bicomposites owing to strong hetero-junction between Fe_2O_3, TiO_2, WO_3 and other n-type MOs semiconductors. For example, Qi et al. (2015) developed a rod-like shape with a hexagonal snow flake structure of SnO_2 modified Fe_2O_3 composite SnO_2/Fe_2O_3 electrodes (Fig. 3g) for removing the 84.87% Methylene Blue (MB) during PEC than 76% of MB by EO due to increased additional vacancies in VB of Fe_2O_3 and SnO_2 which could oxidise the H_2O and OH^- to strong oxidant •OH in aqueous medium. Subba Rao et al. (2017) prepared SnO_2–Sb_2O_4 a mixed metal oxides (MMOs) and nano-WO_3 modify SnO_2–Sb_2O_4-WO_3 (MMO-WO_3) PA with excellent oxygen evolution potential (OEP) and accelerated service life about 2.21 V and 1.7 times, respectively.

In sight of remarkable electronic mobility and chemical stability, larger surface area, strong π-π interaction, as well as hydrophobic and hydrophilic interaction, and other weak interaction, graphene with heterojunction construction and E_g of 2.1–4.3 eV has been highly applicable in PEC of pollutant remediation. In this regard, n-type semiconductors decorating graphene-based materials have been synthesised which mainly profited from their electrons shuttling ability or the formation of heterojunction and exceptional storing (Ama and Arotiba, 2017; Tayebi et al., 2019; Carreño-Lizcano et al., 2020). Fig. 4h shows the image of exfoliated graphite (EG)/TiO_2NPs composite electrode for 0.1×10^{-4} M MB dye degradation in 0.1 M Na_2SO_4 under visible light irradiation (Ama and Arotiba, 2017). About 85% of MB dye was removed within 240 min. Moreover, g-C_3N_4 (Rezaei et al., 2018; Mohammad et al., 2019) with low E_g of ~2.7 eV and higher delocalised conjugated p structures, it acts as an excellent photocatalyst by utilizing sunlight within the visible region, however high e^-/h^+ pairs recombination rate of pure g-C_3N_4 diminishes its PEC properties. Recently, Su et al. (2020) developed zero-dimensional carbon quantum dots (CQDs) nanostructures for the decoration of TiO_2/g-C_3N_4 (TCN) film electrode. Fig. 3i shows the morphology of TiO_2/g-C_3N_4/CQDs nanorod arrays (TCNC NRAs). The narrower E_g of ~2.47 eV and longer lifetime of photogenerated e^-/h^+ pairs recombination of TCNCNRAs recommended excellent PEC performance in visible light irradiation of 1,4-dioxane (1,4-D) at j of 0.16 mA cm^{-2}, the removal rate is 1.5 times of TCN NRAs electrode. Fig. 4e shows the excellent photocatalytic activity of TCNC NRAs could be attributed to the increase of CT mechanism and charge separation from classical heterojunction to Z-scheme, which may change the main reactive species from $O_2^{\bullet -}$ to •OH and enhance the active species generation.

7. Application in real field wastewater treatment

7.1. Landfill leachate

Leachates of a landfill are generated through the physicochemical and biological decomposition of the solid wastes, as well as through the precipitation and percolation through the wastes (Panizza et al., 2010). The possibility of these leachates to percolate and contaminate the groundwater is a serious issue associated with landfill management. The landfill leachate characteristics depend on factors like the age of the landfill, seasonal factors, and the origin of waste (Ye et al., 2016). In general, landfill leachates possess a large concentration of organic pollutants, inorganic salts, heavy metals, ammonia nitrogen etc. (Pellenz et al., 2020). Specifically, young landfills (<5 years old) liberates leachates of majorly biodegradable organics BOD/COD ratio (>0.3) and COD>10,000 mg L^{-1}; whereas old landfills (>10 years) liberate leachates of majorly refractory organics like humic acid, fulvic acid with BOD/COD ratio (<0.1), alkaline pH, and low COD (<4000 mg L^{-1}) (Renou et al., 2008; Tauchert et al., 2006). Thus, the conventional treatment techniques such as biological oxidation processes fail to deal with leachates, especially which are from the old landfills (Ye et al., 2016).

Tauchert et al. (2006) considered aged landfill leachates of highly recalcitrant nature (BOD/COD ratio of 0.004, pH 8, and low COD of 5500 mg L^{-1}) for the photoelectrochemical study. They compared photolysis, heterogeneous photocatalysis, electrolysis, and photoelectrolysis using a photoelectrochemical reactor having DSA and 125 W UV mercury lamp. The degradation efficiency is due to the indirect electrochemical oxidation aided by •OH, H_2O_2 and chlorine species, which were further photochemically transformed into more active radical forms. They found that the dark coloration of landfill leachate was the restraining factor in photoelectrochemical process, which urges the need of some coagulative techniques before electrochemical advanced oxidation processes (EAOPs) for achieving recommendable removal efficiency.

Electrocoagulation (EC) can be adopted as a suitable pretreatment to EAOPs, whereby the color and some extend of COD removal is possible. A series of EC, electrooxidation (EO) and UV based $CuFe_2O_4$ AOP removed 95.6% of COD, 91.6% of BOD, 90.5% of TOC, and 99.8% of ammonia (NH_4–N), respectively. Table S1 shows the quality of the effluent after each process. Biodegradation test and phytotoxicity analysis confirmed the practicality of the treatment procedure (Ghanbari et al., 2020).

PEF was also found to be effective for landfill leachate treatment (Pellenz et al., 2020). A statistical experimental design methodology was adopted by Zhang et al. (2012b) for studying the PEF treatment of landfill leachate. Primary characteristics of landfill leachate such as pH, COD, ammonia-nitrogen, and chloride were found as 8.10, 2747 mg L^{-1}, 3348 mg L^{-1}, 3583 mg L^{-1}, respectively. Nearly 90% of color and 75% of COD removals were obtained in 90 min when using UV light of λ_{max} = 254 nm, the parallel arrangement of Ti/RuO_2–IrO_2 anode and stainless-steel cathode, H_2O_2: 153.2 mM and Fe^{2+}: 39 mM.

Although photo-EAOPs are giving exceptional degradation efficiency, adopting a single technique cannot be a complete solution,

especially for lowering acute toxicity, and cytotoxicity caused by the by-products of treatment (Klauck et al., 2017). These individual photo-EAOPs are suitable tools to enhance the biodegradability of the landfill leachates; thus can be followed by biodegradation for further detoxification. Pellenz et al. (2020) employed PEF as a pre-treatment to biological oxidation in landfill leachate treatment. Combined effects of electro Fenton and photo-Fenton achieved in a PEF reactor composed of boron-doped diamond (BDD) soft iron anodes under 0.9 A current intensity, 300 mg L^{-1} H_2O_2, and system flow rate of 0.6 L min^{-1}. A 15 min PEF followed by a 72 h activated sludge process removed 77.9% of COD, as well as a significant lowering of genotoxicity (*Allium cepa*). The combination of PEF and biological oxidation was also investigated by Seibert et al. (2019). They found the lesser amount of by-products formation in the sequential 45 min PEF followed by 24 h bio oxidation.

Meanwhile, the suitability of photo assisted electrolysis as a post-treatment to biological treatment was evaluated by Ye et al. (2016). In their study, the leachate after a two-stage anaerobic-aerobic sequencing batch reactor was tested for COD and NH_3—N removal in a DSA based electrolysis reactor equipped with a 10 W UV lamp. The indirect oxidation based on *in situ* electrogenerated active chlorine and radical species mediated the degradation process. At a pH 5.0, *j* of 60 mA cm^{-2}, nearly 87% of NH_3—N and 77% of COD were removed without the addition of electrolyte. The total energy consumption and current efficiency for 8 h treatment were 216.5 (kW h/kg COD) and 17.5%, respectively. During the process, most of the NH_3—N was converted into N_2 as well as a little NO_2^-, NO_3^- and chloramines remained in the solution. Effective Cl^-/Cl_2 recycling enables the lowered concentration of both active chlorine and chloride ions in the system. Zhao et al. (2010) studied a biologically pre-treated landfill leachate under similar photo-electrochemical reaction conditions in a pilot scale continuous flow reactor of 6.5 L capacity. After 2.5 h, 41.6% of TOC, 74.1% of COD, and 94.5% of ammonium removal were observed by applying 67.1 mA cm^{-2}. The UV lamp influenced the effective mineralization of the organic contaminants into small molecular acids, while reduction of pollutants such as metal ions was primarily due to indirect oxidation.

7.2. Oil mill wastewater

Vegetable oil industry effluents are usually dark colored acidic effluents possessing broad spectrum of organics and inorganics in their suspended and dissolved forms and turbidity causes poor light penetration and under-oxygenation; and thus highly toxic to the aquatic system in case released into water bodies without proper treatment (Flores et al., 2018; Verla et al., 2014). Based on the type of oil processed and the operating conditions, the amount and characteristics of organic load vary, and the COD values lie in the range 2000 mg L^{-1} – 30,000 mg L^{-1} (Pandey et al., 2003; Sharma and Simsek, 2019; Verla et al., 2014).

PEF showed exceptional performance among BDD anode/air-diffusion cathode based EAOPs for the overall treatment and the removal of 4- hydroxyphenylacetic acid from olive oil mill wastewater (Flores et al., 2017). About 80% of TOC reductions (in 540 min) and better biodegradability were achieved for the PEF treatment of real oil mill wastewater, and the treatment efficiency follows the order; PEF > EF > AO-H_2O_2. The quick mineralization of photoactive by-products in PEF towards UV-A might be the reason behind the effectiveness of the system towards real wastewater treatment (Flores et al., 2017). A further improvement in removal was achieved by adopting EC pre-treatment to PEF. A 20 min Fe EC at 3 mA cm^{-2} reduced 40% of TOC, followed by PEF at pH 3.0, 0.5 mM Fe^{2+}, 25 mA cm^{-2} resulted in 97.1% of TOC removal after 600 min (Flores et al., 2018).

7.3. Pharmaceutical wastewater

The pharmaceutical effluents are composed of large varieties of compounds such as synthetic or natural organics, inorganics, catalysts, and solvents (Panizza, 2018). The high concentration of xenobiotics, solids, and active antibiotics residues makes the pharmaceutical wastewater become highly toxic and possess high COD and BOD values as well as very low biodegradability ratio (Lalwani et al., 2020). So the conventional treatments techniques are not suitable in order to avoid the negative impacts on human and other animals, which is clear from the emergence of antibiotics resistant bacteria and genes (Xu et al., 2019b). Thus, some highly advanced treatment processes are necessary to deal with pharmaceutical effluents.

The removal of trimethoprim (TMP) from municipal wastewater was evaluated using various AOPs and EAOPs like UVC, AO, H_2O_2/UVC, AO- H_2O_2/UVC, AO with electrogenerated H_2O_2 (AO-H_2O_2), PEF-UVA, and PEF-UVC. Among the processes, the TMP removal efficiency was highest in PEF-UVA, and the UVC was inefficient to cause H_2O_2 photolysis (Moreira et al., 2016). The improvement on the COD reduction in pharmaceutical industry wastewater through UVA irradiation in PEF than simple EF process was also proved by Behfar and Davarnejad (2019).

A single reactor based electrochemical photocatalysis was employed by Fang et al. (2013) for the discoloration and organic matter removal, in terms of COD, of a pharmaceutical effluent. The photoreactor system composed of nano-TiO_2 coated Ni photoanode, and multi-walled carbon nanotubes (MWCNTs) air cathode under 250W high-pressure mercury lamp irradiation. The raw effluent having 3150 mg L^{-1} COD upon 2 h treatment removed 93.5% of COD and 78.5% of color. The Cl^- depletion was found to be a major factor behind the removal. Thus an increase in NaCl concentration and applied bias voltage resulted in an increase in COD and color removal due to the active chlorine species produced. In another study, a synergistic effect, as well as cost effective combination of UV photolysis and conductive diamond electrochemical oxidation, was found suitable for the treatment of pharmaceutical industry effluents (Martín de Vidales et al., 2017).

The adoption of a single technique sometimes is not adequate to remove the resistant organic compounds from water. Başaran Dindaş et al. (2020) evaluated the various combinations of EC, EF and photocatalysis for treating pharmaceutical wastewater. Among the combinations, 1 h EF using 5 mA cm^{-2} followed by 4 h photocatalysis using 1.5 g L^{-1} of TiO_2 found to be preferable as 64.0% of TOC, 70.2% of COD, and 97.8% of BOD_5 removed during the process. During EF, organic compounds were degraded to small but resistant molecules, which on undergoing photocatalytic treatment got degraded (Başaran Dindaş et al., 2020).

7.4. Textile wastewater

The textile wastewater has complex characteristics as it contains different kinds of dyes, salts, pesticides, surfactants, fabric softeners, polishing and coating agents, and coupling agents and possess varied composition from one batch to another (Alves et al., 2014; GilPavas and Correa-Sánchez, 2019). Consequently, the conventional treatment techniques are not feasible.

In EAOPs, the presence of chloride ions can result in the formation of toxic organochlorine degradation by-products. Alves et al. found a lowering of chlorine containing by-products by 65% in photoassisted EAOP compared to the simple electrochemical method (Alves et al., 2014). In another study, when UV incorporated into the electrochemical reaction system possessing $Ti/Ru_{0.3}Ti_{0.7}O_2$ anode, the simultaneous formation and destruction of organochlorine products resulted in an enhancement on the TOC and COD

removals by 13% and 30%, respectively, within 90 min (de Mello Florêncio et al., 2016). Similarly, Moraes et al. (2007) designed an 18 L pilot-scale tubular flow reactor with TiO_2/RuO_2 electrode for the electrochemical and photoelectrochemical treatment of textile effluent. One order of magnitude improvement in TOC and COD removal is found using photo-irradiation.

A solar based photoreactor having monopolar arrangement of BDD/Ti electrodes was developed by GilPavas et al. (2018) for treating dyeing wastewater. They found that a real indigo dyeing effluent on undergoing 15 min of treatment, reduced 83% of COD together with enhanced biodegradability index (BOD_5/COD) to more than 0.4 under the optimum condition (pH = 4, j = 40 mA cm^{-2}, and Fe^{2+} = 0.3 mM). The presence of Cu^{2+} along with Fe^{2+} in solar PEF using BDD anode and air-diffusion cathode can be helpful to achieve a fast and complete decolorization and mineralization by promoting the photolysis of the Fe(III) complexes under solar irradiation and/or aiding in mineralization through easy oxidation of Cu(II)-intermediates complexes (Salazar et al., 2012).

As electrochemically stable cellulose in real textile effluents can hinder the activity of EAOPs, adoption of biological removal of cellulose is effective. Photo assisted indirect electrochemical oxidation carried out in a biologically treated textile effluent by using $Ti/IrO_2–RuO_2–TiO_2$ and Ti electrodes by applying 20 mA cm^{-2} and UV–visible light of 280–800 nm, removed 98% of color and 68% of COD. In the absence of photo-irradiation, no COD removal is observed, which indicates the importance of oxychloride (•OCl) radicals in photoassisted electro-oxidation (Aravind et al., 2016). Manenti et al. (2014) adopted sequential EC, PF, and activated sludge process for the treatment of real effluent (COD: 1200 mg L^{-1}) from a textile industry in Portugal. The iron-organic complex formation and associated low radical formation in PF treatment of textile effluent can be overcome by EC pre-treatment. When EC followed by PF, nearly 65% of COD removal and significant biodegradability improvement is achieved, which on undergoing activated sludge process makes the COD level below the permissible level in Portuguese (150 mg L^{-1}). A hybrid approach including EC, adsorption, followed by PF oxidation was developed by Berner et al. (Bener et al., 2020) for textile effluent to meet irrigation water standard. The treatment consists of Al EC, activated carbon adsorption and $BiNiO_3$-activated carbon catalysts based PF process. After treatment, 49% of COD (18–20% by EC, 8–10% by adsorption and 24% by PF), 87% of TOC (nearly 35% by EC, 40–45% by adsorption and 8% by PF), and around 90% of color (50–55% by EC, 35–40% by adsorption and nearly 2% PF) were synergistically removed.

7.5. Tannery wastewater

The tanning industry, as a wholly wet process, consumes a tremendous amount of water and liberates nearly 30–35 L of wastewater per kg of skin/hide processed (Bharagava and Mishra, 2018). The effluents released during the transformation of raw or semi-pickled skins to commercial materials, composed of acids/bases, chromium salts, solvents, tannins, dyes, sulphides, and many others (Lofrano et al., 2013). This complex mixture contains a high concentration of both organic and inorganic compounds in the range of COD: 1–58 g L^{-1}, Cr^{6+}: 0.01–4.24 mg L^{-1}, Cr^{3+}: 0–4.1 g L^{-1}, total dissolved solids: 22–67 g L^{-1}, sulphides: 0.025–3.3 g L^{-1} (Bharagava and Mishra, 2018; Borba et al., 2018).

The oxidative degradation of tannery effluents through photo assisted EAOPs were studied by many researchers. The importance of photo-irradiation in electrolytic treatment of tannery effluent was determined by Selvaraj et al. (2020) using an electrochemical cell of titanium cathode and $Ti/IrO_2–RuO_2–TiO_2$ anode. Under UV illumination of λ_{max}: 254 nm, they found 100% sulfide, 92% of COD and 70% TOC elimination, whereas in the absence of UV irradiation, the treatment is found not effective. Isarain-Chavez et al. (2014) investigated the treatment of tannery wastewater by a BDD based PEF process. During the process, oxidation ability of BDD, •OH as well as the UVA light in PEF contributed to the effective mineralization of organic pollutants in the tannery wastewater. Photo peroxi electrocoagulation conducted in batch mode in a reactor equipped with iron plates electrodes, with solar irradiation found that due to electrochemical and Fenton associated phenomena, 80% of COD, 95% of color, 98% of turbidity, 88% of total suspended solids, 96% of total fixed solids and 83% of total volatile solids were removed within 120 min (Borba et al., 2018). Although, excellent efficiency is obtainable in organic matter elimination, the authors suggesting the necessity of adopting some integrated techniques for attaining effluent discharging quality.

Thus, along with COD removal, Cr^{6+} reduction, as well as sulphide oxidation are important criteria for choosing the proper treatment technique for tannery effluent. Moradi and Moussavi (2019) adopted photolysis under vacuum UV (VUV) as a suitable technique for achieving it. They overcome the major rate limiting

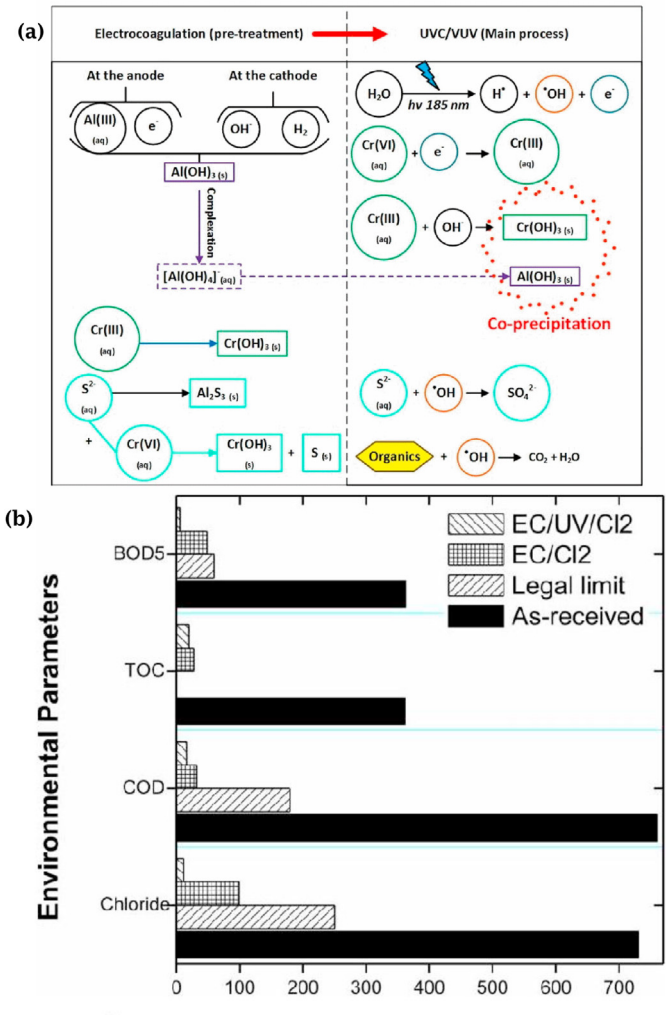

Fig. 5. (a) Reaction mechanism in EC-UVC/VUV Reprinted with permission from Ref (Moradi and Moussavi, 2019). Copyright © 2018 Elsevier B.V.; **(b)** comparison of the effluents from electrolysis (EC/Cl_2) and photo assisted electrolysis ($EC/UV/Cl_2$), where BOD, COD, TOC, and chloride units are in mg L^{-1} Reproduced from Ref (Pereira De Sousa et al., 2019). with permission from the copyright holders, IWA Publishing.

factor of photo asssisted mechanisms, i.e., the hindrance due to high turbidity and suspended solids by following Al EC prior to photolysis. Thus the combined effect of 20 min EC followed by 40 min photolysis EC and photolysis removed 99% COD and 100% chromium from the tannery effluent having 20,600 mg L^{-1} COD, and 30.11 mg L^{-1} total chromium (Moradi and Moussavi, 2019). As from Fig. 5a, UVC/VUV process involves a multilateral system of advanced oxidation-reduction mechanism involving the direct photolysis of organic pollutants as well as the indirect oxidation-reduction through reactive oxygen species, and photo-generated electron. The Cr^{6+} reduction in the photoreactor was followed by total chromium removal by co-precipitation with the EC originated $Al(OH)_3$. In a similar study, the coupling of EC with PF was investigated by Módenes et al. (2012) where PF was chosen as a pre-treatment to EC, to lower sludge production along with COD reduction. After 540 min of PF process using 15 g L^{-1} H_2O_2 and 0.4 g L^{-1} Fe^{2+}, followed by 15 min EC applying 68 mA cm^{-2}, pH 8.3 was found as optimal condition with almost complete removal of COD and chromium as well as lower cost requirement than the traditional treatment techniques prevailing in tannery industries.

7.6. Other wastewater

Pulp and paper effluent was treated by EC followed by UV/sulfate radical based AOP (Jaafarzadeh et al., 2016). Although sole EC process removed about 61% of COD, it failed to achieve the effluent discharge quality due to the lack of biodegradability. The authors found that when EC combined with UV/sulfate radical based AOP, a shift obtained from partial oxidation to total oxidation. This was reflected in the biodegradability enhancement (Jaafarzadeh et al., 2016).

A sequential implementation of up-flow anaerobic sludge blanket (UASB) followed by SPEF process removed more than 91% of total COD from slaughterhouse wastewater (Vidal et al., 2019). The limitations found in UASB systems regarding turbidity removal and mineralization were overcome to a great extend through the solar PEF system (Vidal et al., 2019). The effectiveness of solar PEF in achieving fast mineralization than other EAOPs such as EO and EF was proven by another study (Vidal et al., 2016). They adopted a 3 h solar PEF as a post-treatment to the UASB treatment of slaughterhouse effluent and obtained 99% of COD removal.

Polyaniline wastewater was treated using the PEF coupled with heterogeneous photocatalysis (Ou et al., 2019). In a photoreactor having inner wall lined by black TiO_2, visible light irradiation using Xe lamp, and having IrO_2/Ti (anode), graphite felt (cathode), removed about 85% of TOC and 96.4% of COD of polyaniline wastewater within 360 min. Under the same reaction time, the efficiency of various electrochemical process found to be in the following order: PEF/black TiO_2 > PEF > EF > visible light/black TiO_2/AO- H_2O_2 > AO-H_2O_2 > visible light/TiO_2, which reveals the superiority of coupled PEF/visible light TiO_2 photocatalysis in fast mineralization through more radical generation (Ou et al., 2019).

Wang et al. (2017) developed a photoelectrochemical cell (PEC) having a Pt cathode and a photoanode (by depositing a layer of polymer capped TiO_2 on ITO glass) for the recovery and removal of the metal ions, as well as for the production of electricity from lead-acid battery industry wastewater. The effluent having SO_4^{2-} of 260 mg L^{-1} and Pb 25 mg L^{-1}, when undergone treatment for 90 min, complete removal of both SO_4^{2-} and Pb^{2+} along with a pH increase to 6.4 from 2.3 was achieved, suggesting the potential use for the treatment of wastewater. The better performance, even after the ninth cycle and the satisfactory performance in the presence of suspended solids, suggested the industrial applicability of this technology.

The importance of UV in electro-oxidation was evaluated for the treatment of dairy wastewater based on removal and cost effectiveness. They found that post-treated effluent possesses all the examined environmental parameters values lies below effluent discharge standards, together with energy per order (EEO) values lower by 0.33 kWh m^{-3} $order^{-1}$ than simple electro-oxidation. The experimental conditions include Ti/$Ru_{0.3}Ti_{0.7}O_2$ mesh, UV lamp of λ_{max} = 254 nm, provided better removal efficiency and biodegradability to the dairy wastewater (Fig. 5b) (Pereira De Sousa et al., 2019).

A wastewater treatment plant (WWTP) effluent spiked with synthetic food azo dyes treated by solar PEF (SPEF) treatment in a 2.5 L plant having BDD/air-diffusion cell coupled with solar irradiation. The SPEF process helped the photodegradation of Fe(III)-oxalate complexes and other byproducts. Significant degradation, in terms of dissolved organic carbon (DOC) removal, was found in a complex effluent matrix containing sulfate, perchlorate, and nitrate ions. The formation of chloroderivatives as degradation byproducts found to decelerate the removal process; thus sulfate medium is preferred than chloride ones. Lower specific energy consumption and greater current efficiency make the sulfate medium more attractive (Thiam et al., 2015).

The photo-irradiated electrolytic degradation of atrazine manufacturing effluent was carried out using DSA and Ti cathode in a 20 L tubular flow reactor. During the process, both direct electrochemical process and indirect anodic oxidation pathways assisted for removing both atrazine and its by-products (simazine, hydroxy-triazine and propazine) at high degradation rate (Aquino et al., 2017). Table 1(b) summarizes the different studies available for photoelectrochemical treatment of real wastewaters.

8. Application of photoelectrochemical process for hydrogen production from wastewater

The worldwide demand for sustainable energy is on the continuous rise as the global warming caused by the misuse of fossil fuels has caused severe problems to living organisms, setting off a considerable exertion toward inexhaustible and sustainable energy sources (Ma et al., 2018). To satisfy the increasing energy demands, an economical and sustainable source of production is required to meet the limited resources available for energy production. Hydrogen is the most intensively studied clean energy carrier for the future due to its higher efficiency and clean burning with water vapour as the only byproduct (Lu et al., 2014). It possesses a higher specific energy density than other conventional fuels and has a potentially low environmental impact with high recycling capability (Ishihara et al., 2010). Several methods are available for the production of H_2 such as the burning of fossil fuels, high-temperature water dissociation, electrolysis, thermochemical water splitting photolysis etc. (Dincer and Acar, 2015). However, hydrogen production by burning fossil fuel derivatives is energy-intensive and releases CO_2 into the atmosphere while thermochemical water splitting and electrolysis processes are expensive. Also, it is necessary to reduce the dependence on fossil fuels for H_2 production and use renewable sources such as biomass derivatives, photovoltaic, wind, etc. to achieve clean reactions without any CO_2 emission (Ganiyu et al., 2020; Ganiyu and Martínez-Huitle, 2020; Lu et al., 2014; Sathre et al., 2014). Photoelectrochemical (PEC) water splitting process is successfully used for the generation of H_2 and is a promising technology to produce renewable energy with oxygen as a byproduct (Chehade et al., 2020; Chen et al., 2010). Besides, the sustainable photoelectrochemical processes rely on cheaper external energy sources provided by solar irradiation, wind energy, biomass etc.

PEC process is also efficient in removing organic pollutants present in wastewater (Goulart et al., 2019; Xie et al., 2016). The

Table 1(b)
Studies on the photoelectrochemical treatment of real wastewater.

Wastewater type	Treatment process	Electrode materials	Optimized experimental conditions	Efficiency	Highlights of the study	References
Landfill leachate	PEF	$Ti/RuO_2–IrO_2$ anode and stainless steel cathode	UV light of λ_{max} 254 nm, H_2O_2 153.2 mmol L^{-1} and 39 mmol L^{-1} Fe^{2+}	≈90% of color and 75% of COD removal in 90 min	• Developed response surface methodology models	Zhang et al. (2012)
Landfill leachate	PEF	boron-doped diamond (BDD) anode	0.9 A current intensity, 300 mg L^{-1} H_2O_2, and system flow rate of 0.6 L min^{-1}	15 min PEF followed by 72 h activated sludge biological oxidation removed 77.9% of COD, 71.5% of total carbon and 76.3% of color	• PEF as a pre-treatment to biological oxidation	Pellenz et al. (2020)
Landfill leachate	Photo assisted electrolysis	DSA anode	10 W UV lamp, pH 5.0, $j = 60$ mA cm^{-2}	≈87% of NH_3–N, and 77% of COD removal in 8 h.	• A post-treatment to biological treatment • The total energy consumption was 216.5 kW hkg^{-1} COD and current efficiency was 17.5%	Ye et al. (2016)
Landfill leachate	photo-electrochemical reaction	DSA anode	67.1 mA cm^{-2}	41.6% of TOC, 74.1% of COD, and 94.5% of ammonium removal in 2.5 h	• A post-treatment to biological treatment	Zhao et al. (2010)
Olive oil mill wastewater	PFE	BDD anode/air-diffusion cathode	A 5 W m^{-2} fluorescent black light blue tube of λ_{max} 360 nm, initial pH: 3, $j = 16.7$ mA cm^{-2}	About 80% of TOC reduction in 540 min	• The superiority of was due to the photolytic action of UVA radiation on photosensitive by-products.	Flores et al. (2017)
Trimethoprim (TMP) spiked in municipal wastewater	PEF	BDD anode	PEF-UVC, $j = 30$ mA cm^{-2}, pH 2.8	100% TMP removal in 15 min	• A high participation of BDD(•OH) on TMP degradation	Moreira et al. (2016)
Pharmaceutical effluent	PEC	nano-TiO_2 coated Ni photoanode, and multi-walled carbon nanotubes (MWCNTs) air cathode	250 W high-pressure mercury lamp irradiation applied bias voltage 10.0V, NaCl electrolyte concentration 0.5 mol L^{-1}, pH 3.0	93.5% of COD and 78.5% of color removal in 2 h	• UV light and power have a synergistic effect in photoelectrocatalytic degradation • The Cl^- ion depletion during photoelectrocatalytic oxidation enhances the removal	Fang et al. (2013)
Pharmaceutical wastewater	EF + photocatalysis	Iron electrodes	pH 3, $j = 5$ mA cm^{-2}, Fe:H_2O_2 molar ratio as 1:10	64.0% of TOC, 70.2% of COD, and 97.8% of BOD_5 removed by 1 h electroFenton followed by 4 h photocatalysis	• Energy consumptions was 1051.21 kW hkg^{-1} TOC • Sequential processes with advanced oxidation processes proved efficient degradation	Başaran Dindaş et al. (2020)
Textile effluent	Photo-assisted electrochemical degradation	$Ti/Ru_{0.3}Ti_{0.7}O_2$ anode	Current 1.5 A and NaCl 0.3 mol dm^{-3}	86% COD and 92% TOC in 300 min	• photolysis of reactive chlorine species to produce HO•	de Mello Florêncio et al. (2016)
Textile effluent	Photo-electrochemical treatment	TiO_2/RuO_2 electrode	$j = 80$ mA cm^{-2}, UV-C 4.6 mW cm^{-2}, initial pH 7.4	≈85% of color, 42% of TOC and 58% of COD removal in 90 min	• Energy consumption was 1.388KWhm^{-3}	Moraes et al. (2007)
Indigo dyeing effluent	SPEF	BDD/Ti electrodes	solar based, pH 4, $j = 40$ mA cm^{-2}, and Fe^{2+} 0.3 mmol L^{-1}	Elimination of 83% of COD, 70% TOC mineralization BOD_5/COD to more than 0.4 in 15 min of treatment	• SPEF as an efficient and economical alternative, as the operational costs were estimated as 1.56 USD m^{-3}	GilPavas et al. (2018)
Textile effluents	Photo assisted indirect electrochemical oxidation	$Ti/IrO_2–RuO_2–TiO_2$ and Ti electrodes	$j = 20$ mA cm^{-2}, UV–visible light of 280–800 nm	Removed 98% of color and 68% of COD in 30 min	• Post treatment to biologically treated effluent • oxy-chloride radicals involved	Aravind et al. (2016)
Tannery wastewater	photo assisted EAOPs	Titanium cathode and $Ti/IrO_2–RuO_2–TiO_2$ anode	$j = 25$ mA cm^{-2}, UV lamp of λ_{max}: 254 nm	Removal of 100% sulfide, 92% of COD and 70% TOC elimination in 3 h	• A green technology for the large-scale process for the efficient removal of sulfide and COD from tannery lime wastewater	Selvaraj et al. (2020)
Tannery wastewater<	Photo peroxi electrocoagulation	iron plates electrodes	Solar irradiation, 6 g H_2O_2 L^{-1}, pH 4, $j = 34.2$ mA cm^{-2}	80% of COD, 95% of color, 98% of turbidity were removed within 120 min	• The final characteristics are unsuitable for final discharge in terms of toxicity effect	Borba et al. (2018)
Tannery effluent	Solar photo Fenton followed by electrocoagulation (EC)	Aluminum electrodes for EC	Solar irradiation, 0.4 g L^{-1} [Fe^{2+}], 15 g L^{-1} of [H_2O_2], initial pH of 3	Nearly 100% COD removal in 540 min	• PhotoFenton was as a pre-treatment to EC • Least amount of sludge generation after 540 min of irradiation	Módenes et al. (2012)
Dairy wastewater	UV assisted electro-oxidation	$Ti/Ru_{0.3}Ti_{0.7}O_2$ mesh	Current 533.42 mA, UV lamp of λ_{max} 254 nm	97.80% COD, 94.62% TOC in 120 min	• Efficiency enhancement by the electrochemical production of free chlorine species.	Pereira De Sousa et al. (2019)

Table 1(b) (*continued*)

Wastewater type	Treatment process	Electrode materials	Optimized experimental conditions	Efficiency	Highlights of the study	References
Polyaniline wastewater	PEF coupled with heterogeneous photocatalysis	IrO_2/Ti anode, graphite felt cathode	pH 3.0, $j = 16$ mA cm^{-2}, 0.2 mmol L^{-1} [Fe^{2+}], O_2 flow rate 200 mL min^{-1}, T 25 °C	≈85% of TOC and 96.4% of COD within 360 min	• Energy per Order (EEO) values of 0.89 kWh m-3 order-1 • The black TiO_2 nanotubes exhibited good stability and photocatalytic performance	Ou et al. (2019)

mineralization of organic compounds by PEC process results in the formation of CO_2 and protons. During PEC degradation process, the molecular oxygen produced by electrochemical process acted as an electron acceptor for the electrons produced from photocatalysis. They generated an increased amount of active species resulting in significant pollutant degradation (Ama et al., 2018; Peerakiatkhajohn et al., 2021). To overcome the energy crisis and to achieve sustainable treatment, researchers studied simultaneous pollutant degradation and H_2 generation from wastewater. Organic rich wastewater is less abundant than water itself; however, it is an increasing concern worldwide. The organic pollutants in the wastewater contain a high level of chemical energy that can act as electron donors and promote the hydrogen production at cathodes (Baltrusaitis et al., 2014; Wu et al., 2017; Zhou et al., 2017). PEC cell consists of a photoactive semiconductor anode material where oxidation occurs, a counter cathode material (usually platinum), electrolyte and a membrane. Photoanode with a higher photocatalytic activity initiates the pollutant degradation whereas a photocathode with more negative than E° of H^+/H_2 of 0.0 V for hydrogen production.

Further, the efficiency of hydrogen production and pollutant degradation strongly depends upon the photoanode properties. TiO_2, WO_3, and α-Fe_2O_3 are commonly used as photoanodes for PEC process due to their easy availability, lower cost and environmental friendliness. Additionally, the efficiency of photoanode depends upon the bandgap of the material, smaller bandgap materials are easily activated, and faster charge transport takes place. Table 1(c) summarizes the different studies available for simultaneous pollutant removal and H_2 production. The ability of organic compounds or waste to act as sacrificial agents in water can improve the

Table 1(c)
Studies on H_2 production from wastewater using photoelectrochemical method.

Wastewater	Electrode material	Optimized Experimental Conditions	Highlights of the study	References
Dye wastewater	Ti/TiO_2/WO_3 electrodes Ag/AgCl - reference electrode Pt mesh - counter electrode	120 min experiments Applied voltage 1 V 125 W high-pressure mercury lamp	100% discoloration, 85% TOC removal and 45% H_2 generation efficiency Lower charge consumption observed for bicomponent anode with improved H_2 production	Guaraldo et al. (2016)
Oilfield- produced wastewater	TiO_2 films on AISI/SAE 304 SS-expanded meshes- anode Nickeled AISI/SAE 304 SS expanded meshes -cathode	Cell current of 32.44 mA 2 h experiment	H_2 production rate of 12.36 μmol h^{-1} 80% conversion of wastewater	(Gutierrez and Revero, 2016)
Dye wastewater	Tungsten doped TiO_2 nanotube arrays- anode Platinum plate- cathode	300 W Xe lamp Na_2SO_4 - supporting electrolyte	97% degradation of pollutant observed with 24.97 μmol h^{-1} H_2 production after 90 min	Gong et al. (2013)
Wastewater containing phenols and alkylbenzenes	TiO_2 NRs/FTO nanorods - anode Carbon-coated Cu_2O nanowires - cathode	3 cm^{-2} working area of electrodes No external potential Constant light intensity of 100 mW cm^{-2}	TOC removal 63.5%–93.6% with highest H_2 production of 81.52% H_2 production amount using phenol was maximum	Wu et al. (2017)
Wastewater containing a mixture of dyes and phenol	g-C_3N_4 loaded on reduced GO loaded over Ni foams- anode Platinum sheet - cathode	300W Xe lamp AC voltage - 4 mV	Synergistic effect of pollutant degradation and H_2 production Highest H_2 production at 5.8 μmol h^{-1} cm^{-2} rate	Zhao et al. (2019)
Wastewater containing phenol	WO_3 NFs - anode C–Cu_2O nanowire arrays - cathode	300 W Xe lamp (intensity of 100 mW cm^2), 2 cm^2 working area of electrodes	TOC removal of 82.12% H_2 production rate of 93.08 mmol cm^{-2}	Zhou et al. (2017)
Dye wastewater	Hematite anode with Mn^{2+} ions Platinum - cathode	Simulated sunlight (100 mW cm^{-2}) Current - 0.2 mA pH 2.5	Complete degradation of dye Three-fold higher photocurrent generated at the cathode confirms the production of H_2 in the system	Wang et al. (2019)
Sewage containing emerging contaminants from 3 locations	Anode- modified g-C_3N_4/Ag/AgCl/$BiVO_4$ heterojunction Cathode- Pt wire and thin films of MoS_2	Applied voltage −1.23 V 1.5 a.m. solar simulator of 150 W	Simultaneous H_2 production and pollutant degradation 118 μmol cm^{-2} of H_2 produced corresponding to a Faradic efficiency of 69.38%	Rather and Lo (2020)
Spent acids from galvanizing industry	TiO_2 coated SS – anode 3 SS mesh stacked and rotated 30° - cathode	Sunlight Applied AC voltage between 1 mV and 10 mV	Higher surface area of cathodes minimized the polarization effect H_2 at a rate of 3 mL min^{-1} under an applied voltage of 1.8 V	Chehade et al. (2020)
Humic acid	TiO_2- 1 wt% Au@TiO_2/Al_2O_3/Cu_2O- anode Pt plate - cathode	150 W Xe lamp ((100 mW cm^{-2}	87% degradation of pollutant Humic acid acted as hole scavenger and promoted H_2 production	Peerakiatkhajohn et al. (2021)

catalysts' photocatalytic performance by inhibiting charge recombination. In a study conducted by Raptis and coworkers (Raptis et al., 2017), the organic waste in water improved the performance of photoelectrochemical cell by acting as a sacrificial agent and enhanced the photocurrent produced by WO_3 photoanodes. H_2 production was only observed under visible light illumination and forward bias of 0.8V and 1.6V were applied with an average output of 0.36 mmol h^{-1}. Ethanol as fuel gave maximum H_2 production compared to glycerol and sorbitol as ethanol molecules were more extensive and produce a higher number of hydrogen ions per carbon atom.

In an ideal condition, the organic pollutant removal occurs at the anode by oxidation whereas the reduction of heavy metals and other inorganic species occurs at the cathode (Rather and Lo, 2020). In this regard, the selection of cathode materials with an active metal surface is also important as its potential for reduction of protons to spontaneous H_2 evolution is a critical parameter. Further the selection of cathodic materials depends upon the cost, chemical stability, environmental sustainability, H_2 conversion efficiency etc. (Saraswat et al., 2018). The most commonly used cathodic materials for PEC application are platinum, platinized glass, stainless steel, graphite, Cu_2O etc. (Baltrusaitis et al., 2014; Demir et al., 2019; Gutierrez and Revero, 2016; Ma et al., 2018; Wang et al., 2015). Moreover, several modifications of the cathode materials were studied to improve the performance of PEC system by improving the charge separation and alleviating photocorrosion.

A synergistic effect was observed for the photoelectrochemical processes using C—N co-doped TiO_2 nanotube arrays in which under the externally applied potential the pollutants are removed by electrochemical oxidation and H_2 generated simultaneously (Chen et al., 2015b). The photocatalysis process is promoted by the applied potential, which enhanced the charge separation and furthered the electrons gets transferred to the cathode. Zhao and co-workers (Zhao et al., 2019) studied the photoelectrocatalytic technique for simultaneous wastewater treatment and H_2 production using a hybrid porous graphitic carbon nitride (g-C_3N_4) loaded on reduced graphene oxide (rGO) (CNG) which is further loaded on Ni foams as photoanode. They have reported that the organic pollutants acted as the sacrificial agent and the photogenerated holes react with them, leaving behind the electrons to produce H_2 at the platinum cathode. Under visible light irradiation, 21.6% of Rhodamine dye was degraded corresponding to the highest H_2 production of 5.8 μmol h^{-1} cm^{-2} after 1 h of treatment. Further, the performance of the electrode remained stable for three cycles of experiment with constant H_2 evolution.

Various structural modifications including metal doping, sensitization with lower bandgap semiconductors, modification using catalyst etc. have been developed to improve the properties of photoanode materials (Guaraldo et al., 2016; Iervolino et al., 2017). For instance, A dye-sensitized photoelectrochemical cell with novel nanostructured plasmonic Ag/AgCl@chiral TiO_2 nanofibers as photoanode and urban wastewater containing an estrogen (17-β-ethynylestradiol) and heavy metal (Cu^{2+}) as the electrolyte was used for H_2 production (Wang et al., 2015). They have observed complete mineralization of pollutant with relatively higher solar energy conversion achieving 98% of electricity converted to H_2. The enhanced performance was attributed to the synergetic relationship between the TiO_2 chiral nanofibers and Ag nanoparticles in the photoanode which hindered the recombination enabling faster degradation of pollutants and subsequent H_2 production at the cathode. In another study, simultaneous pollutants degradation and H_2 production were achieved using an electrochromic titania nanotube arrays (Blue TNTs) as photoanode (Koo et al., 2017). The cathodic polarization of TNTs positively enhanced the electrical conductivity and the photocurrent was utilized by the photocathode to produce H_2. The surface modification of TNTs by electrochemical process improved the photoanode's overall properties and enhanced the visible light absorption and doubled the H_2 generation compared to that of intact TNTs. Another critical factor to be considered for the PEC process is the light source. The use of high power and renewable sources of energy is preferred as they can easily initiate the formation of electron-hole pairs at the photoanode. Sunlight as the potential source of irradiation for the PEC process can overcome the limitations of photocatalyst materials with continuous light energy input (Zhou et al., 2017).

9. Cost and energy consumption

Cost and energy consumption are one of the most challenging issues for all photoelectrolysis processes, including PEC and PEF, which needs higher energy consumption than the photocatalytic process alone. There are several factors which govern the overall cost of PEC during the degradation of organic compounds. For example, Daghrir et al. (2013) reported that the PEC technique for the decomposition of chlortetracycline (CTC) solutions is highly effective in terms of the estimated cost of chemicals plus energy consumption at the optimum conditions of 1 L of 0.025 mg L^{-1} CTC solution in 0.050 M Na_2SO_4 at pH ~6 under 6.9 mW cm^{-2} UVC irradiation and I of 0.39 A using a vitreous carbon (VC) cathode than amorphous carbon, graphite and SS. Under these optimum conditions, CTC was diminished up to 98% with high mineralization of 67.3% TOC and 69% of TN removal. An estimated cost of 4.52 US$ m^{-3} was tested with the same value of concentration for chemicals plus energy consumption because VC cathode has the superiority ability to produce the H_2O_2, which can be photolyzed sufficient •OH radicals with UVC light, and enhanced the CTC removal from the •OH generated.

The selection of efficient electrode materials for the PEC process improves the degradation efficiency of pollutants and reduces energy consumption (Olvera-Rodríguez et al., 2019). Aquino et al. (2017) studied the mineralization of actual atrazine effluents on the $Ti/Ti_{0.7}Ru_{0.3}O_2$ electrode. It was reported that UVC was found to increase the energy needed for the complete destruction of about 90% of atrazine effluents. During the PEC treatment, the energy consumption was found 20 $kWhm^{-3}$ at 9.0 $mAcm^{-2}$ and flow rate of 300 Lh^{-1} because at laminar flow rate treatment conditions, the atrazine efficiently removed with an almost complete reduction for the higher current densities. Further, modifying the electrode materials or using an electrode with inexpensive materials can reduce the overall treatment cost by reducing energy consumption (Rajput et al., 2021). The use of visible light active electrode materials and the inexhaustible solar irradiation as the light source for the PEC degradation process also reduces the overall cost of treatment. The low cost and durable heterojunction $BiVO_4/TiO_2$ nanotubes/FTO photoanode used for simultaneous wastewater treatment and electricity generation possess excellent visible light activity and higher photoconversion efficiency under solar irradiation (Bai et al., 2016). These electrode materials remain highly active under different wastewater conditions, making it more economical for organic pollutant removal.

The use of solar-driven PEC systems can overcome the energy crisis and are highly efficient and economical. Olya et al. (2013) worked on the feasibility of employing solar cells to generate the direct current to provide electrical energy for the PEC process. By optimizing the treatment conditions, the degradation rate of the dye could achieve ~95% in 30 min. The cost analysis was done for this experiment. For this reason, the overall costs of external electrical energy, synthesis of photocatalyst, additional electrolyte and UV lamp were taken into account as major cost items by using the following expression (Eq. (51)), given below (Sun et al., 2014).

$$Operating\ cost\left(USD\ m^{-3}\right) = aC_{photocatalyst} + bC_{electrolyte} + cC_{energy} \quad (51)$$

where $C_{photocatalyst}$ is the amount of photocatalyst consumed (kg m^{-3}), $C_{electrolyte}$ is the amount of electrolyte consumed (kg m^{-3}), and C_{energy} is the amount of energy consumed for electrode operation and UV irradiation (kWh m^{-3}), where the letters *a*, *b* and *c* are the price of each unit. The overall operating cost of Acid Red 88 effluents degradation is about 9.42 USD m^{-3} and associates to saving 17% of the whole cost for the electrode energy supplied via the solar cells (Olya and Pirkarami, 2013). Similarly, Sun et al. (2014) reported a new approach by coating the graphene oxide on the solar cell to convert the infrared light to produce the electricity and this energy utilized during the PEC process with same results. Current combinations of PEC and photoelectric process for the decontamination of organics pollutant, the modern design creates the highest usability of solar energy and likewise conforms to the idea of green chemistry.

However, more fundamental research is needed to develop an efficient PEC system with lower energy consumption, higher degradation efficiency and effluent quality meeting the regulatory standards. Also, the detrimental mass transfer of the reactor configuration and the weak solar light response of the photocatalysts are the obstacles for the technique's industrialization. For the PEC system, the operational stability and the cost concern still want to be evaluated and studied in the near future. Overall, the PEC systems designs occur the cost-effective target and demonstrate a promising potential in the growth of PEC industrialization.

10. Photocatalytic fuel cells driven electrochemical technologies

Photoelectrochemical approaches, as photocatalytic fuel cells, can also be used to produce electricity (photogenerated electrons in photocatalysis via an external circuit to be of use in electrical energy) which will be employed for in-situ driving of electrochemical technologies (Ganiyu et al., 2020; Ganiyu and Martínez-Huitle, 2020; Liu et al., 2011a; Nordin et al., 2017), reducing the energy requirements and costs (section 9) as well as promoting the use of renewable energies sources. Photoelectrochemical cells (PECs) having UV or visible solar light have been specially investigated to split water as a potential alternative for energy conversion and/or wastewater treatment (Liu et al., 2011a; Potter, 1911). The excited holes in the PECs interact with H_2O/OH^- producing ROS (mainly •OH) which promotes the complete oxidation of the organic molecules to CO_2, producing electricity by an external flow of electrons from the photoanodic half-cell to the cathode (Liu et al., 2011a, 2012). This wastewater treatment applicability is frequently denominated as photocatalytic fuel cells (PFCs) (Liu et al, 2011b, 2012). A typical PFC system consisted of a working electrode and a photocathode placed at opposite sides and connected through an external circuit is illustrated in Fig. 6 (Bai et al., 2016; Li et al., 2014a). An external light source was provided for illumination and oxygen/air purging was continuously pumped into the reactor. In 2006, first investigations in PFC cells were reported by Kaneko and co-workers (Kaneko et al., 2006) where a photoanode with TiO_2 as nanoporous film and O_2-reducing cathode was used. Since then, several studies have been performed to produce electricity efficiently by integrating wastewater treatment with PFC technologies with diverse TiO_2-materials or new photoanodes (Li et al, 2014b, 2015b; Liu et al., 2016; Sui et al., 2015; Wu et al., 2015).

The use of TiO_2 photoanodes along with other innovative materials such as n-type Si, GaAs, $BiVO_4$, WO_3, CdSe, Fe_2O_3, ZnS/ZnO and Cu_2O/Cu improves the performance of PFC in organic matter elimination from water and simultaneous electricity generation due to the enhancements on the adsorption of the light, separation of the electron-hole pairs or surface area (Bai et al., 2016; Zhao et al., 2017). In particular case, BiOCl, BiOBr and $BiVO_4$ photoanodes (Bai et al., 2016) have been demonstrated to have a relatively small bandgap which allows higher efficiency for solar energy conversion. Meanwhile, the reduction of electron-hole combination has also been investigated by using $BiVO_4/TiO_2$, $BiVO_4/WO_3$ and WO_3/TiO_2, as dual absorber photoanodes where

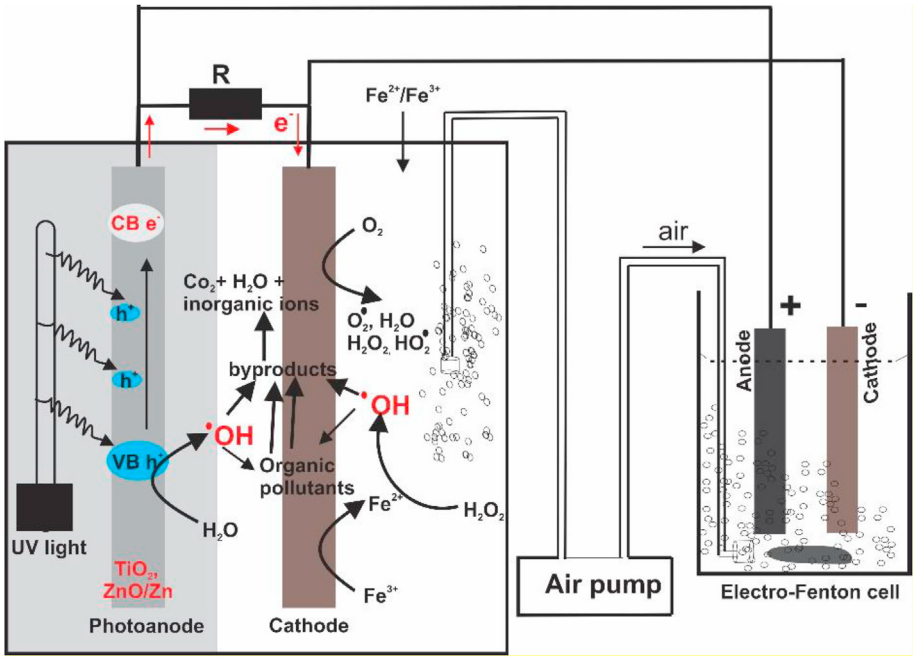

Fig. 6. PFC concept illustrating the mechanisms during electricity production. Reprinted with permission from Ref (Ganiyu et al., 2020). Copyright © 2020 Elsevier B.V.

solid junctions are used to connect two semiconductors (Zhao et al., 2017). The electron-hole recombination is inhibited as well as solar adsorption and interface reactions are improved when bi-absorber with different band gaps and valence/conductive band positions are combined.

The viability of the use of PFCs, which generates electricity in-situ, has been investigated to power the electrooxidation processes, frequently by using the EF approach. However, an important limitation of PFCs in water treatment is that this process is diffusion-controlled because the holes (oxidant) are produced and localized at photoanode/photocathode surface, limiting the radical reactions up to the anode surface vicinity (Zhao et al., 2017). Nevertheless, it could be easily overcome by increasing the photoanode/photocathode surface area or by improving the radical production (i.e. •OH) efficiency and the efficacy of the reactions in bulk. In-situ H_2O_2 production in the effluent with air/O_2 breathing cathode before iron source dosage, favors the production of strong oxidizing species, mainly •OH via Fenton's reaction (Eq. (6)), so called EF-photocatalytic fuel cells (EF-PFCs). The charge transfer process occurring at the cathode by O_2 reduction and the H^+ ions produced through photooxidation generates electricity in the system by electron consumption.

Zhao et al. (2017) investigated the applicability of an EF-PFC system by using a TiO_2-nanotube array photoanode and by adding ferrous ions for degrading an effluent containing with dyestuffs and pharmaceuticals (Zhao et al., 2017). Higher degradation efficiencies were achieved by efficient participation of in-situ generated oxidants by photoexcitation at the photoanode surface and by EF process in the bulk of the solutions. For organic pollutants such as MO, MB, Congo red and tetracycline, the degradation rate was considerably improved by EF-PFC when compared to conventional PFC, producing 2.47 mA cm^{-2} at EF-PFC, being 1.2−2.4 times higher than the current densities produced at PFC. Meanwhile, Nordin et al. (2017) examined the practicability of connecting PFC system driven by EF process during the degradation of Reactive Black 5 as a model pollutant by using ZnO/Zn and carbon plates as photoanode and cathode, respectively. This system generated 11.39 and 15.37 mW cm^{-2}, respectively, and obtaining more than 80% of Reactive Black 5 degradation efficiency by Fenton's reactor when compared to the lower efficacy (<30%) of the hybrid system-PFC reactor.

11. Coupling of soil remediation and photoelectrochemical processes

Soil, an important human resource, is under continuous deterioration because of the several anthropological activities (industrial modernization and agricultural mechanization) (Trellu et al., 2019). Therefore, decontamination approaches have received great attention in the last years, mainly coupled with soil remediation technologies. Then, simultaneous or sequential techniques have been proposed as potential alternatives to eliminate organic/inorganic pollutants from soil. These approaches intensify the removal efficiency or reduce the pollution of wastes produced. In this frame, the integration of photoelectrochemical processes and soil remediation has been considered an interesting challenge. Firstly, the contaminants are eliminated from the soil by using soil decontamination technologies, and subsequently, the PECs are used to treat the effluents generated in the former stage (Carboneras et al., 2019; Nidheesh et al., 2019). This innovative approach and its efficacy depend on the configuration of combined processes, electrodes used and reactor arrangements. Soil remediation techniques predominantly used are soil washing (SW), soil flushing (SF) and electrokinetic and these can be certainly combined with advanced oxidation processes (AOPs) (Rodrigo et al., 2014; Trellu et al., 2016a). Extracting agents (acids, surfactants and chelating agents) are frequently employed in the solutions of SW method, which are denominated, washing solutions (Mao et al., 2015; Rodrigo et al., 2014). With low solubility and strong adhesion towards the soil, pollutants are solubilized in the washing solution via the action of the extracting agents, allowing to mechanically remove these contaminants (Mao et al., 2015). Meanwhile, when SF is used as remediation technology, the extracting agents are directly added to the polluted soil in order to improve the mobility of the contaminants, which is limited by the interfacial pollutants-groundwater tension (Mulligan et al., 2001; Rodrigo et al., 2014; Trellu et al., 2016a). Light-weight polycyclic aromatic hydrocarbons (PAHs), like naphthalene, are preferentially removed from soil by SF, then, contaminant nature, soil heterogeneity, naphthalene saturation and other operating parameters must be evaluated because these can strongly influence the SF efficiency (Atteia et al., 2013).

Comparing SW and SF, the former procedure, an ex-situ process, is more efficient than SF because the washing solution improves the contact between the extracting agents and the soil pollutants (Mousset et al., 2014; Yang et al., 2006). However, in both, significant volumes of contaminated effluents are produced. For this reason, based-hydroxyl radical (•OH) technologies such as AOPs and electrochemical AOPs have been recently proposed to treat the effluents generated after SW or SF treatments, and photocatalytic or photoelectrocatalytic approaches are innovative options (Cheng et al., 2016; Huang et al., 2017; Martínez-Huitle et al., 2015; Martínez-Huitle and Panizza, 2018; Muñoz-Morales et al., 2019; Nidheesh et al., 2019; Rodrigo et al., 2014; Trellu et al., 2016b, 2017, 2019). Among the electrochemical AOPs, PECs has main advantages because it does not require chemical or in a minimal amount for generating strong oxidizing species (reactive species) which are required for degrading organic pollutants (Martínez-Huitle and Panizza, 2018).

dos Santos and co-workers (dos Santos et al., 2017; Vieira Dos Santos et al., 2017) extended their initial research on the management of 100 mg L^{-1} of oxyfluorfen in a soil-washing effluent with sodium dodecyl sulfate (SDS) as surfactant by AO to the photoelectrolysis process with a 15 W UVC irradiation and the sonoelectrolysis one with an US of 24 kHz and 200 W. In the first case, 1000 mL of 100 mg L^{-1} herbicide spiked in a soil washing effluent with SDS surfactant (dosage from 100 to 5000 mg L^{-1}) were treated by using a filter press cell upon a 15 W UVC light (with a BDD and SS electrodes, as anode and cathode, respectively). After 20 Ah L^{-1} at 200 L h^{-1}, oxyfluorfen and SDS were completely removed, releasing 1200 mg L^{-1} SO_4^{2-} in solution. Meanwhile, in the second case when sonoelectrolysis was applied, utilizing a flow electrochemical plant equipped with a BDD and SS as anode and cathode, respectively, and an ultrasounds of 24 kHz and 200 W to treat 1000 mL of 90 mg L^{-1} oxyfluorfen herbicide spiked in a soil washing effluent with SDS surfactant (dosage 400 mg L^{-1}); after consuming a 30−40 Ah L^{-1} in sonoelectrolysis by applying 2.1 A and 200 L h^{-1}, 100% of COD and TOC removal were found and 900 mg L^{-1} SO_4^{2-} were released, also making in evidence the potentiality of this technique for soil remediation.

Photoelectrolysis or sonoelectrolysis are efficient treatments of soil-washing effluents with SDS surfactant contaminated with the dinitroaniline pendimethalin (Almazán-Sánchez et al., 2017) and atrazine (dos Santos et al., 2018) with a flow plant with a filter-press BDD/SS cell with a quartz cover for illumination with a 4 W and 15 W UVC, respectively, and an US of 24 kHz and 200 W, compared to sonolysis, photolysis and AO. The oxidation power of treatments increased as: sonolysis < photolysis ≪ AO < SE < PE, indicating a greater enhancement of the destruction rate of organics by UVC photolysis and oxidation with photogenerated oxidants in PE. In the

case of atrazine, 700 mL of 100 mg L^{-1} herbicide spiked in a soil washing effluent with SDS surfactant (dosage 100 mg L^{-1}) were treated by applying 2.34 A at 160 L h^{-1}, obtaining 100% degradation at 420 min for AO or sonoelectrolysis, at 300 min for photoelectrolysis while 100% of TOC removal for AO after 360 min, for photo after 300 min sonoelectrolysis and for photoelectrolysis after 180 min. When the SDS dosages was compared, the change of atrazine concentration, TOC and COD with time for 100 and 5000 mg L^{-1} of SDS contents by applying 30 mA cm^{-2} is different. While the herbicide decayed more rapidly with the higher SDS content, the opposite behavior was observed for TOC and COD removal due to the presence of higher amounts of organic dissolved matter.

The applicability of SW to remediate Cu and phenanthrene (PHE) contaminated soil was investigated (Tao et al., 2020) where Cu (73.5%) and PHE (68.1%) were simultaneously removed from soil (20 mL g^{-1} of liquid to soil ratio) by using an extraction agent containing 10 g L^{-1} TW80 and 1 mM EDTA. EDTA chelated Cu while a PHE desorption from soil was favored by TW80 micelles. After that, photoelectro-persulfate (PE/PS) process was applied to SW effluent to recover the extracting agent by applying 4 mA cm^{-2} at pH 3.5 with 10 mM PS during 150 min treatment. The results indicated that 36.8% of EDTA and 94.0% of TW80 were recovered while 99.6% of PHE was eliminated and 83.6% of Cu reduced to elemental copper. Thus, SW approach followed by PE/PS treatment can be considered as a cost-effective soil decontamination technology for removing heavy metal and organic pollutants. Quenching experiments allowed to oxidise PHE preferentially by sulfate radical approach and reuse (three washing cycles) could be done with the recovered extracting agent.

A novel photoelectrochemical cell was proposed by Cotillas et al. (2020) for treating SW effluents polluted with 100 mg kg^{-1} of clofibric acid (CA). Direct irradiation to the BDD surface was applied by UV lamp at the bottom of the tank (2 dm^3) which allowed easy scale-up of the photoelectrochemical reactor by multiplication of the electrodes (Fig. 7). The electrodes configuration (two BDD plates and two SS plates as anodes and cathodes, respectively) was determined by the set parallel between them and perpendicular to the UV lamp in order to improve the treatment.

The values obtained after electrolysis and photoelectrolysis treatments of SW effluents polluted with CA (50 mg dm^{-3}) using the new electrochemical cell were 99.35% of CA removal and 96.78% of TOC removal and 99.88% of CA removal and 94.58% of TOC removal, respectively, by applying 10 mA cm^{-2}. The energy requirements were 44.65 and 131.85 kW h m^{-3} for electrolysis and photoelectrolysis, respectively. Although the energy consumption is higher for the photoelectrolysis approach, it was lower than the results obtained by using a conventional electrochemical cell (85.32 and 311.26 kW h m^{-3} for electrolysis and photoelectrolysis, respectively). However, the photoelectrolysis process with conventional electrochemical cell was performed with a lower initial concentration of the pollutant (−90%), resulting in higher energy requirements than those consumed by photoelectrolysis treatment using the new electrochemical cell (311.26 vs. 131.85 kW h m^{-3}). These findings are directly related to the reactor used, confirming that the proposed photoelectrochemical reactor is more efficient compared to other commercial cells, in terms of, CA removal efficiencies from SW effluents and energy requirements.

A clopyralid concentration of 180 mg dm^{-3} was treated by using a set-sup consisted on a single compartment electrochemical flow cell (0.6 dm^{-3} of SW effluent polluted with clopyralid) with carbon felt (CF) anode (Sigracell® GFA6EA) with 100 cm^2 and an AISI 316 steel cathode by applying 5 mA cm^{-2} and by using a UV lamp (254 nm (UV−C)) with a power of 4 W irradiating directly to the reservoir tank (Carboneras et al., 2019). Photoelectrolysis process was also compared with photolysis, sonolysis, electrolysis, sonoelectrolysis and photosonoelectrolysis in which were achieved different removals efficiencies in terms of clopyralid and mineralization (TOC removal). Photoelectrolysis achieved 38% of clopyralid removal and 39% of mineralization, while only 5%, 5%, 31%, 34% and 28% of clopyralid removals and 3%, 3%, 32%, 21% and 0% of TOC removals were accomplished for photolysis, sonolysis, electrolysis, sonoelectrolysis and photosonoelectrolysis, respectively. These results evidenced that, a synergistic effect was achieved in degradation and mineralization of clopyralid photoelectrolysis, improving the kinetic parameters in both cases. For photosonoelectrolysis, an antagonistic effect related to an excessive generation of radicals as well as an improvement on the mass transfer promoted faster radical recombination, affecting the oxidant action and stability of oxidizing species to react with the target pollutant or that the oxidants can be decomposed to oxygen. This implied in an influence on the organic pollutant removal efficiencies. On the other hand, a semi-pilot scale investigation was performed for removing clopyralid (3.87 mg dm^{-3}) from SW wastes with a DiaCell® type 1001, equipped with ten BDD electrodes (0.070 m^2) and five SS (2 faces) electrodes as anodes and cathodes, respectively (Martín de Vidales et al., 2019). Coupling an ultrasound source or an ultraviolet lamp into an auxiliary tank in the irradiated experiments was improved the treatment. Meanwhile, the scale-up of the process using a single cell (1 anode, 70 cm^2) and a stack of cells (10 anodes,

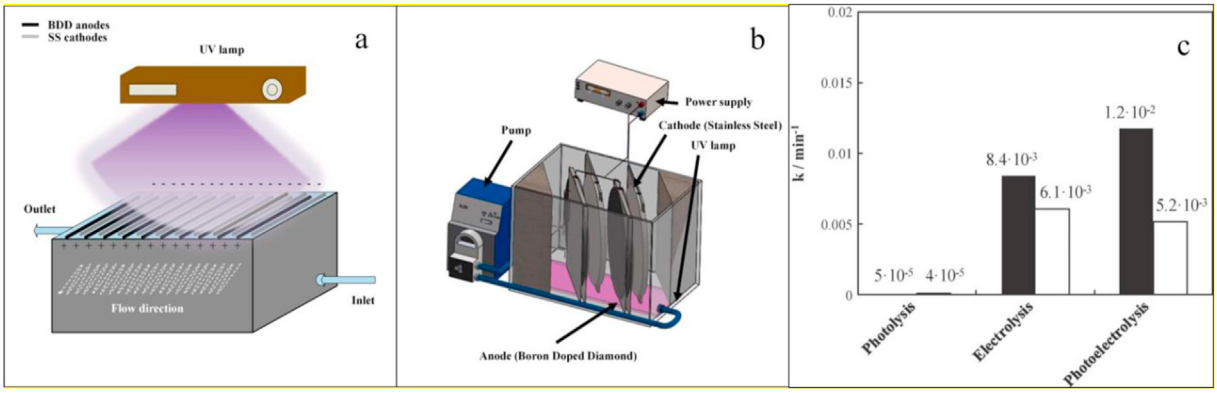

Fig. 7. Photoelectrochemical reactor scheme: (a) Concept; (b) prototype. (c) kinetic constants calculated for the removal of clofibric acid and TOC during the treatment of soil washing effluents polluted with 100 mg kg^{-1} CA. (■) pollutant; (□) TOC; j: 10 mA cm^{-2}; UV254 nm: 15 W. Reprinted with permission from Ref (Cotillas et al., 2020). Copyright © 2019 Elsevier B.V.

700 cm^2) showed that the ratio electrochemical energy/photoelectrochemical energy is more favorable in small devices, achieving higher removal efficiencies. The major part of hybrid processes is focused on the enhancement of the AO treatment of soil-washing effluents by photoelectrochemical with UVC light and surfactant. These methods are more powerful than individual AO and photolysis, where photoelectrolysis treatment yields faster degradation and mineralization of the pollutants and SDS. In chloride medium, the photoelectrolysis process with DSA anodes yields greater mineralization of synthetic clopyralid and glyphosate solutions than using BDD, respectively, due to the high oxidation ability of photogenerated $Cl^{\bullet}$ and Cl_2.

12. Remarks and future perspectives

The mechanisms of the oxidizing species produced at single photochemical, electrochemical and photoelectrochemical processes are relatively well-known and well-investigated, however, it is not the same for the combined approaches. Synergistic effects of integrated photochemical, electrochemical and photoelectrochemical processes:

(i) Increase the hydroxyl radical production site,
(ii) Enhance the mineralization ability through various side reactions such as the production of additional oxidizing species and photodecomposition of complex intermediates such as metal-ligand complexes and carboxylic acid intermediates, and,
(iii) Intensify the advantages and minimizes the disadvantages of the individual processes.

Nevertheless, all of these favorable parameters are dependent on critical operating conditions, such as materials (which are used as anode or cathode, by using single material or by combining both materials to improve the oxidation power of the process), electrochemical systems, wastewater or water matrices characteristics, irradiation intensity and its origin, homogenous and heterogeneous nature of reactive species, the influence of each oxidant on others, the effect of precursors on the reactive species generated, their reactivity and lifetime which are not completely explored yet as well as the fundamental reaction mechanisms. In this frame, more studies are necessary to completely understand the synergic or antagonist effects that can be promoted by using photoelectrochemical methods. In fact, among the integrated photoelectrochemical processes, PEF/PAO/PEC and PEF/PAO/PC could result in the highest amount of $^{\bullet}OH$ radical generation theoretically. However, studies on the integration of triple AOP processes are less and it must be also studied. Meanwhile, thanks to the advances on the analytical and spectroscopic techniques to identify reactive species, the lacks on the mechanisms of formation and their reactivity during oxidation of organic pollutants can be unraveled. At the same time, computational and theoretical chemistry are emerging as interesting tools to comprehend electronic structure of the electrodes, conformational dynamic interactions (which can be attained between the pollutant and oxidizing species, the multipoint interactions between the material and the pollutants as well as the irradiation and the photoanodes), the degradation reactions and the factors that influence them.

The translation of the photoelectrochemical technologies from laboratory to commercial application is necessary to consider a great variety of achievements obtained by employing different photoelectrochemical reactors. Agitated or stirred tanks and flow reactors in divided or undivided setups have been widely adopted in several studies. However, the selection of the electrochemical systems depends on the applicability, irradiation used, geometry of the electrodes, effluent properties and volume treated. Preferentially, undivided electrochemical systems are used (in tank or flow modes), which avoid the use of a membrane or separator that provokes an increase on the potential cell, affecting the production of oxidants, energy requirements and electric costs. This cell option is very common in the laboratories and has many benefits but the use of undivided agitated beaker or undivided stirred tank reactors could offer superficial investigational conditions that are not reproducible and not defined (not completely fixed) and consequently, the reaction environment is difficult to be scaled. For this reason, the most appropriate is to stimulate/motivate to the scientific community to change strategy by using flow photoelectrochemical cells or electrochemical cells exposed to high irradiation sources in discontinuous or continuous modes, allowing the scaling-up of the process. Conversely the batch cells must be used to accurately and quantitatively understand the reaction environment (mathematical descriptions, computational model, theoretical chemistry use and simulations), and to control the surface area/volume ratio to promote an efficient prototype evaluation of the photoelectrochemical method; not more than that.

In undivided photoelectrochemical cells, the electrode material form, size and structure, operation mode as well as the irradiation type, direction, intensity, penetration cover and transparent materials, are factors that must be considered to assemble the internal cell compartment. Therefore, cell compartments are frequently placed in vertical or horizontal positions in order to allow that the effluent flows, favouring well-defined hydrodynamics and rates of mass transfer to/from electrodes together with ease of irradiation supply and penetration. Also, undivided flow cells allow several variants in the electrode arrangements, multi-electrode systems, assembling numerous cell units, as well as by reduced-gaps reactors irradiating the effluent after electrochemical reaction chamber, or by using mass transfer promoters modified/impregnated with photoactive materials. All of these advances have allowed to commercialize few photoelectrochemical applications, but more studies are necessary regarding the reactors used to effectively translate from lab to real applications.

The enhancements on the electrode materials, it has allowed a more efficient degradation of pollutants and production of oxidizing species, which in combination with the hydraulic residence time favored a more effective interaction between the oxidants and the contaminants in the water. Various novel photoanode materials are being studied for the PEC process, especially for the visible light irradiation. However, photoanodes for combining PAO/PEC effects are still being explored. A wide range of electrode sizes and connections are also found, and the operating currents ranging from the mA to the A scale, and these operating conditions vary when scale-up process is attained, then, more investigations must be performed.

Typically, transparent supporting materials are used for preparing photoanodes where TiO_2 was frequently used, but currently, important advances have been done in the elaboration of visible light TiO_2-responsive photoanodes which are modified with other photoactive components. Special attention must be given to the bismuth, quantum dots, graphene, niobium, perovskite and carbon-based nanomaterials, which have shown superb performance and excellent effectiveness for PEC treatment of organic pollutants when are used to modify TiO_2-based materials, or not. The development of micro- and nanostructured materials to provide new substrates and catalysts is also an exciting trend that must be approached.

Higher mineralization of POPs is observed for real wastewater in the coupled processes. However, most of the studies were conducted in lab-scale and the potential for the pilot-scale studies should be explored in real conditions. It is important to indicate

that, no large scales are necessary to achieve efficient commercial application because there are uses where the effluent volume to be treated is reduced and consequently, the design, elaboration and construction of small photoelectrochemical devices is only required. No specific preoccupation with the pollutants concentration should be attained because when the photoelectrochemical methods are capable to treat high concentrate solution/effluents in short time, lower energy requirements and reusable material cycles; the wastewaters with lower contaminant concentrations can be improved from the initial results and technological designs. Therefore, the operational feasibility for the large-scale implementation and the cost/energy consumption of the coupled photoelectrochemical processes are needed to be evaluated and studied in the near future. As a final point, the applicability of photoelectrochemical devices should be tested to drinking water disinfection and water purification in more intense performances in order to expand the horizons of the electrochemistry to other fields. Finally, the use of photoelectrochemical divided reactors to produce hydrogen is a clear challenge to be approached because the utilization of oxidizing species produced at anodic compartment to degrade efficiently organic compounds to obtain an electron flow to be profited in generation of hydrogen is not easy method. Also, the purification of hydrogen is not clear because other gases could be collected reducing the applicability of this technology.

For integrating photocatalysis and electrochemical technologies for soil washing remediation, the treatment depends on the operating conditions; however, the results reported in the existing literature demonstrated that, photoelectrochemical methods can be efficient to treat washing liquids generated from soil remediation treatment. Of course, each effluent contaminated is a particular case because it can contain a specific pollutant or a mixture of pollutants. Therefore, the composition of electrolytes added or other additives can play a essential role in the ex-situ depollution steps for removing organic pollutants from soil, and after that, to promote an efficient decontamination of the washing effluent. Chemical/electrochemical or photochemical phenomena can be attained by pH conditions, dissolved cationic or anionic species, irradiation profiles or modes, temperature, organic concentrations, viscosity, flow directions, and so on. Problems or challenges associated with each one of these factors should be also carefully considered during optimization and scale-up of the association of these technologies.

The photoelectrochemical processes' future is bright. Future developments will rely upon the close collaboration of analytical chemists, engineers and electrochemists to ensure effective application and exploitation of these methods. Nevertheless, great efforts are mandatory. To do this, more real effluents should be treated, more design and construction of optimized photoelectrochemical systems should be done by using stable, cheap and longer service-life electrodes at industrial scale and techno-economic studies must be performed to prove the viability of them respect to commercial technologies.

Declaration of competing interest

The authors declare that they have no known competing financial interests or personal relationships that could have appeared to influence the work reported in this paper.

Acknowledgements

Authors are grateful to the Director, CSIR- NEERI, Nagpur, India, Omvati Devi Degree College, Bhalaswagaj, Haridwar, India; Federal University of Rio Grande do Norte, Brazil; Indian Institute of Technology, Bombay, India, Virginia Tech, USA, United States-India Educational Foundation, India, and Fulbright Program (Fulbright-Nehru Postdoctoral grant: 2471/FNPDR/2019), Institute of International Education, USA for imparting encouragement and support for publicizing the article.

Appendix A. Supplementary data

Supplementary data to this article can be found online at https://doi.org/10.1016/j.chemosphere.2021.130188.

Credit author statement

G. Divyapriya: Data collection, Writing – original draft, Writing – revision. Seema Singh: Data collection, Writing – original draft, Writing – revision. Carlos A. Martínez-Huitle: Data collection, Writing – original draft, Writing – revision, Supervision, Writing – review & editing. Jaimy Scaria: Data collection, Writing – original draft, Writing – revision. Ansaf V Karim: Data collection, Writing – original draft, Writing – revision. P.V. Nidheesh: Conceptualization, Data collection, Supervision, Writing – review & editing.

References

Ahmadi, M., Ghanbari, F., 2018. Degradation of organic pollutants by photoelectro-peroxone/ZVI process: synergistic, kinetic and feasibility studies. J. Environ. Manag. 228, 32–39. https://doi.org/10.1016/j.jenvman.2018.08.102.

Almazán-Sánchez, P.T., Cotillas, S., Sáez, C., Solache-Ríos, M.J., Martínez-Miranda, V., Cañizares, P., Linares-Hernández, I., Rodrigo, M.A., 2017. Removal of pendimethalin from soil washing effluents using electrolytic and electro-irradiated technologies based on diamond anodes. Appl. Catal. B Environ. 213, 190–197. https://doi.org/10.1016/j.apcatb.2017.05.008.

Alves, P.A., Johansen, H.D., Neto, S.A., de Andrade, A.R., de Jesus Motheo, A., Malpass, G.R.P., 2014. Photo-assisted electrochemical degradation of textile effluent to reduce organic halide (AOX) production. Water, air. Soil Pollut 225 (2144). https://doi.org/10.1007/s11270-014-2144-1.

Ama, O.M., Arotiba, O.A., 2017. Exfoliated graphite/titanium dioxide for enhanced photoelectrochemical degradation of methylene blue dye under simulated visible light irradiation. J. Electroanal. Chem. 803, 157–164. https://doi.org/10.1016/j.jelechem.2017.09.015.

Ama, O.M., Kumar, N., Adams, F.V., Ray, S.S., 2018. Efficient and cost-effective photoelectrochemical degradation of dyes in wastewater over an exfoliated graphite-MoO3 nanocomposite electrode. Electrocatalysis 9, 623–631. https://doi.org/10.1007/s12678-018-0471-5.

Antonin, V.S., Garcia-Segura, S., Santos, M.C., Brillas, E., 2015. Degradation of Evans Blue diazo dye by electrochemical processes based on Fenton's reaction chemistry. J. Electroanal. Chem. 747, 1–11. https://doi.org/10.1016/j.jelechem.2015.03.032.

Aquino, J.M., Miwa, D.W., Rodrigo, M.A., Motheo, A.J., 2017. Treatment of actual effluents produced in the manufacturing of atrazine by a photo-electrolytic process. Chemosphere 172, 185–192. https://doi.org/10.1016/j.chemosphere.2016.12.154.

Aravind, P., Subramanyan, V., Ferro, S., Gopalakrishnan, R., 2016. Eco-friendly and facile integrated biological-cum-photo assisted electrooxidation process for degradation of textile wastewater. Water Res. 93, 230–241. https://doi.org/10.1016/j.watres.2016.02.041.

Atteia, O., Del Campo Estrada, E., Bertin, H., 2013. Soil flushing: a review of the origin of efficiency variability. Rev. Environ. Sci. Bio/Technology 12, 379–389. https://doi.org/10.1007/s11157-013-9316-0.

Babu, D.S., Srivastava, V., Nidheesh, P.V., Kumar, M.S., 2019. Detoxification of water and wastewater by advanced oxidation processes. Sci. Total Environ. 696, 133961 https://doi.org/10.1016/j.scitotenv.2019.133961.

Bai, J., Wang, R., Li, Y., Tang, Y., Zeng, Q., Xia, L., Li, X., Li, J., Li, C., Zhou, B., 2016. A solar light driven dual photoelectrode photocatalytic fuel cell (PFC) for simultaneous wastewater treatment and electricity generation. J. Hazard Mater. 311, 51–62. https://doi.org/10.1016/j.jhazmat.2016.02.052.

Baiju, A., Gandhimathi, R., Ramesh, S.T., Nidheesh, P.V., 2018. Combined heterogeneous Electro-Fenton and biological process for the treatment of stabilized landfill leachate. J. Environ. Manag. 210, 328–337. https://doi.org/10.1016/j.jenvman.2018.01.019.

Baltrusaitis, J., Hu, Y., Mcfarland, E.W., Hellman, A., 2014. Photoelectrochemical hydrogen production on a -Fe 2 O 3 (0001): insights from theory and experiments. ChemSusChem 3, 162–171. https://doi.org/10.1002/cssc.201300715.

Bañuelos, J.A., García-Rodríguez, O., El-Ghenymy, A., Rodríguez-Valadez, F.J., Godínez, L.A., Brillas, E., 2016. Advanced oxidation treatment of malachite green dye using a low cost carbon-felt air-diffusion cathode. J. Environ. Chem. Eng 4, 2066–2075. https://doi.org/10.1016/j.jece.2016.03.012.

Başaran Dindaş, G., Çalışkan, Y., Çelebi, E.E., Tekbaş, M., Bektaş, N., Yatmaz, H.C., 2020. Treatment of pharmaceutical wastewater by combination of

electrocoagulation, electro-fenton and photocatalytic oxidation processes. J. Environ. Chem. Eng 8, 103777. https://doi.org/10.1016/j.jece.2020.103777.
Behfar, R., Davarnejad, R., 2019. Pharmaceutical wastewater treatment using UV-enhanced electro-Fenton process: comparative study. Water Environ. Res. 91, 1526–1536. https://doi.org/10.1002/wer.1153.
Bener, S., Atalay, S., Ersöz, G., 2020. The hybrid process with eco-friendly materials for the treatment of the real textile industry wastewater. Ecol. Eng. Times 148, 105789. https://doi.org/10.1016/j.ecoleng.2020.105789.
Bensalah, N., Bedoui, A., 2017. Enhancing the performance of electro-peroxone by incorporation of UV irradiation and BDD anodes. Environ. Technol. (United Kingdom) 38, 2979–2987. https://doi.org/10.1080/09593330.2017.1284271.
Bessegato, G.G., Cardoso, J.C., Silva, B.F., da Zanoni, M.V.B., 2014. Enhanced photo-absorption properties of composites of Ti/TiO2 nanotubes decorated by Sb2S3 and improvement of degradation of hair dye. J. Photochem. Photobiol. Chem. 276, 96–103. https://doi.org/10.1016/j.jphotochem.2013.12.001.
Bessegato, G.G., Guaraldo, T.T., de Brito, J.F., Brugnera, M.F., Zanoni, M.V.B., 2015. Achievements and trends in photoelectrocatalysis: from environmental to energy applications. Electrocatalysis 6, 415–441. https://doi.org/10.1007/s12678-015-0259-9.
Bharagava, R.N., Mishra, S., 2018. Hexavalent chromium reduction potential of Cellulosimicrobium sp. isolated from common effluent treatment plant of tannery industries. Ecotoxicol. Environ. Saf. 147, 102–109. https://doi.org/10.1016/j.ecoenv.2017.08.040.
Borba, F.H., Seibert, D., Pellenz, L., Espinoza-Quiñones, F.R., Borba, C.E., Módenes, A.N., Bergamasco, R., 2018. Desirability function applied to the optimization of the Photoperoxi-Electrocoagulation process conditions in the treatment of tannery industrial wastewater. J. Water Process Eng 23, 207–216. https://doi.org/10.1016/j.jwpe.2018.04.006.
Boye, B., Dieng, M.M., Brillas, E., 2003. Anodic oxidation, electro-Fenton and photoelectro-Fenton treatments of 2,4,5-trichlorophenoxyacetic acid. J. Electroanal. Chem. 557, 135–146. https://doi.org/10.1016/S0022-0728(03)00366-8.
Brillas, E., 2021. Recent development of electrochemical advanced oxidation of herbicides. A review on its application to wastewater treatment and soil remediation. J. Clean. Prod. 290, 125841 https://doi.org/10.1016/j.jclepro.2021.125841.
Brillas, E., 2020. A review on the photoelectro-Fenton process as efficient electrochemical advanced oxidation for wastewater remediation. Treatment with UV light, sunlight, and coupling with conventional and other photo-assisted advanced technologies. Chemosphere 250, 126198. https://doi.org/10.1016/j.chemosphere.2020.126198.
Brillas, E., 2014. A review on the degradation of organic pollutants in waters by UV photoelectro-fenton and solar photoelectro-fenton. J. Braz. Chem. Soc. 25, 393–417. https://doi.org/10.5935/0103-5053.20130257.
Brillas, E., Garcia-Segura, S., 2020. Benchmarking recent advances and innovative technology approaches of Fenton, photo-Fenton, electro-Fenton, and related processes: a review on the relevance of phenol as model molecule. Sep. Purif. Technol. 237, 116337 https://doi.org/10.1016/j.seppur.2019.116337.
Brillas, E., Martínez-Huitle, C.A., 2015. Decontamination of wastewaters containing synthetic organic dyes by electrochemical methods. An updated review. Appl. Catal. B Environ. 166, 603–643. https://doi.org/10.1016/j.apcatb.2014.11.016.
Brillas, E., Sauleda, R., Casado, J., 1998. Degradation of 4-chlorophenol by anodic oxidation, electro-fenton, photoelectro-fenton, and peroxi-coagulation processes. J. Electrochem. Soc. 145, 759–765. https://doi.org/10.1149/1.1838342.
Brillas, E., Sirés, I., Oturan, M.A., 2009. Electro-Fenton process and related electrochemical technologies based on Fenton's reaction chemistry. Chem. Rev. 109, 6570–6631. https://doi.org/10.1021/cr900136g.
Cao, D., Wang, Q., Wu, Y., Zhu, S., Jia, Y., Wang, R., 2020. Solvothermal synthesis and enhanced photocatalytic hydrogen production of Bi/Bi2MoO6 co-sensitized TiO2 nanotube arrays. Sep. Purif. Technol. 250, 117132 https://doi.org/10.1016/j.seppur.2020.117132.
Cao, D., Wang, Y., Qiao, M., Zhao, X., 2018. Enhanced photoelectrocatalytic degradation of norfloxacin by an Ag3PO4/BiVO4 electrode with low bias. J. Catal. 360, 240–249. https://doi.org/10.1016/j.jcat.2018.01.017.
Carboneras, M.B., Rodrigo, M.A., Canizares, P., Villaseñor, J., Fernandez-Morales, F.J., 2019. Electro-irradiated technologies for clopyralid removal from soil washing effluents. Sep. Purif. Technol. 227, 115728 https://doi.org/10.1016/j.seppur.2019.115728.
Cardoso, J.C., Bessegato, G.G., Boldrin Zanoni, M.V., 2016. Efficiency comparison of ozonation, photolysis, photocatalysis and photoelectrocatalysis methods in real textile wastewater decolorization. Water Res. 98, 39–46. https://doi.org/10.1016/j.watres.2016.04.004.
Carraway, E.R., Hoffman, A.J., Hoffmann, M.R., 1994. Photocatalytic oxidation of organic acids on quantum-sized semiconductor colloids. Environ. Sci. Technol. 28, 786–793. https://doi.org/10.1021/es00054a007.
Carreño-Lizcano, M.I., Gualdrón-Reyes, A.F., Rodríguez-González, V., Pedraza-Avella, J.A., Niño-Gómez, M.E., 2020. Photoelectrocatalytic phenol oxidation employing nitrogen doped TiO2-rGO films as photoanodes. Catal. Today 341, 96–103. https://doi.org/10.1016/j.cattod.2019.02.006.
Carvalho, C., Fernandes, A., Lopes, A., Pinheiro, H., Gonçalves, I., 2007. Electrochemical degradation applied to the metabolites of Acid Orange 7 anaerobic biotreatment. Chemosphere 67, 1316–1324. https://doi.org/10.1016/j.chemosphere.2006.10.062.
Chaplin, B.P., 2014. Critical review of electrochemical advanced oxidation processes for water treatment applications. Environ. Sci. Process. Impacts 16, 1182–1203. https://doi.org/10.1039/C3EM00679D.
Chehade, G., Alrawahi, N., Yuzer, B., Dincer, I., 2020. A photoelectrochemical system for hydrogen and chlorine production from industrial waste acids. Sci. Total Environ. 712, 136358 https://doi.org/10.1016/j.scitotenv.2019.136358.
Chen, H., Chen, K.-F., Lai, S.-W., Dang, Z., Peng, Y.-P., 2015a. Photoelectrochemical oxidation of azo dye and generation of hydrogen via CN co-doped TiO2 nanotube arrays. Sep. Purif. Technol. 146, 143–153. https://doi.org/10.1016/j.seppur.2015.03.026.
Chen, H., Chen, K., Lai, S., Dang, Z., Peng, Y., 2015b. Photoelectrochemical oxidation of azo dye and generation of hydrogen via C A N co-doped TiO 2 nanotube arrays. Sep. Purif. Technol. 146, 143–153. https://doi.org/10.1016/j.seppur.2015.03.026.
Chen, Q., Liu, H., Xin, Y., Cheng, X., 2013. TiO2 nanobelts – effect of calcination temperature on optical, photoelectrochemical and photocatalytic properties. Electrochim. Acta 111, 284–291. https://doi.org/10.1016/j.electacta.2013.08.049.
Chen, Z., Jaramillo, T.F., Deutsch, T.G., Kleiman-Shwarsctein, A., Forman, A.J., Gaillard, N., Garland, R., Takanabe, K., Heske, C., Sunkara, M., McFarland, E.W., Domen, K., Milled, E.L., Dinh, H.N., 2010. Accelerating materials development for photoelectrochemical hydrogen production: standards for methods, definitions, and reporting protocols. J. Mater. Res. 25, 3–16. https://doi.org/10.1557/jmr.2010.0020.
Cheng, M., Zeng, G., Huang, D., Lai, C., Xu, P., Zhang, C., Liu, Y., 2016. Hydroxyl radicals based advanced oxidation processes (AOPs) for remediation of soils contaminated with organic compounds: a review. Chem. Eng. J. 284, 582–598. https://doi.org/10.1016/j.cej.2015.09.001.
Coria, G., Pérez, T., Sirés, I., Brillas, E., Nava, J.L., 2018. Abatement of the antibiotic levofloxacin in a solar photoelectro-Fenton flow plant: modeling the dissolved organic carbon concentration-time relationship. Chemosphere 198, 174–181. https://doi.org/10.1016/j.chemosphere.2018.01.112.
Cotillas, S., Lacasa, E., Herraiz-Carboné, M., Sáez, C., Cañizares, P., Rodrigo, M.A., 2020. Innovative photoelectrochemical cell for the removal of CHCs from soil washing wastes. Sep. Purif. Technol. 230, 115876 https://doi.org/10.1016/j.seppur.2019.115876.
Da Silva, L.M., Gonçalves, I.C., Teles, J.J.S., Franco, D.V., 2014. Application of oxide fine-mesh electrodes composed of Sb-SnO 2 for the electrochemical oxidation of Cibacron Marine FG using an SPE filter-press reactor. Electrochim. Acta 146, 714–732. https://doi.org/10.1016/j.electacta.2014.09.070.
Daghrir, R., Drogui, P., El Khakani, M.A., 2013. Photoelectrocatalytic oxidation of chlortetracycline using Ti/TiO2 photo-anode with simultaneous H2O2 production. Electrochim. Acta 87, 18–31. https://doi.org/10.1016/j.electacta.2012.09.020.
de Freitas Araújo, K.C., da Silva, D.R., dos Santos, E.V., Varela, H., Martínez-Huitle, C.A., 2020. Investigation of persulfate production on BDD anode by understanding the impact of water concentration. J. Electroanal. Chem. 860, 113927 https://doi.org/10.1016/j.jelechem.2020.113927.
de Mello Florêncio, T., de Araújo, K.S., Antonelli, R., de Toledo Fornazari, A.L., da Cunha, P.C.R., da Silva Bontempo, L.H., de Jesus Motheo, A., Granato, A.C., Malpass, G.R.P., 2016. Photo-assisted electrochemical degradation of simulated textile effluent coupled with simultaneous chlorine photolysis. Environ. Sci. Pollut. Res. 23, 19292–19301. https://doi.org/10.1007/s11356-016-6912-x.
Demir, M.E., Chehade, G., Dincer, I., Yuzer, B., Selcuk, H., 2019. Synergistic effects of advanced oxidization reactions in a combination of TiO2 photocatalysis for hydrogen production and wastewater treatment applications. Int. J. Hydrogen Energy 44, 23856–23867. https://doi.org/10.1016/j.ijhydene.2019.07.110.
Dincer, I., Acar, C., 2015. Review and evaluation of hydrogen production methods for better sustainability. Int. J. Hydrogen Energy 40, 11094–11111. https://doi.org/10.1016/j.ijhydene.2014.12.035.
Ding, X., Ai, Z., Zhang, L., 2014. A dual-cell wastewater treatment system with combining anodic visible light driven photoelectro-catalytic oxidation and cathodic electro-Fenton oxidation. Sep. Purif. Technol. 125, 103–110. https://doi.org/10.1016/j.seppur.2014.01.046.
Ding, X., Ai, Z., Zhang, L., 2012. Design of a visible light driven photo-electrochemical/electro-Fenton coupling oxidation system for wastewater treatment. J. Hazard Mater. 239–240, 233–240. https://doi.org/10.1016/j.jhazmat.2012.08.070.
Divyapriya, G., Nambi, I., Senthilnathan, J., 2018. Ferrocene functionalized graphene based electrode for the electro À Fenton oxidation of cipro fl oxacin. Chemosphere 209, 113–123. https://doi.org/10.1016/j.chemosphere.2018.05.148.
Divyapriya, G., Nidheesh, P.V., 2020. Importance of graphene in the electro-fenton process. ACS Omega 5, 4725–4732. https://doi.org/10.1021/acsomega.9b04201.
Dos Santos, A.J., De Lima, M.D., Da Silva, D.R., Garcia-Segura, S., Martínez-Huitle, C.A., 2016. Influence of the water hardness on the performance of electro-Fenton approach: decolorization and mineralization of Eriochrome Black T. Electrochim. Acta 208, 156–163. https://doi.org/10.1016/j.electacta.2016.05.015.
dos Santos, E.V., Sáez, C., Cañizares, P., Rodrigo, M.A., Martínez-Huitle, C.A., 2018. Coupling photo and sono technologies with BDD anodic oxidation for treating soil-washing effluent polluted with atrazine. J. Electrochem. Soc. E262–E267. https://doi.org/10.1149/2.1281805jes, 165.
dos Santos, E.V., Sáez, C., Martínez-Huitle, C.A., Cañizares, P., Rodrigo, M.A., 2015. Combined soil washing and CDEO for the removal of atrazine from soils. J. Hazard Mater. 300, 129–134. https://doi.org/10.1016/j.jhazmat.2015.06.064.
dos Santos, E.V., Sáez, C., Cañizares, P., Martínez-Huitle, C.A., Rodrigo, M.A., 2017. UV assisted electrochemical technologies for the removal of oxyfluorfen from soil washing wastes. Chem. Eng. J. 318, 2–9. https://doi.org/10.1016/

j.cej.2016.03.015.
El-Desoky, H.S., Ghoneim, M.M., El-Sheikh, R., Zidan, N.M., 2010. Oxidation of Levafix CA reactive azo-dyes in industrial wastewater of textile dyeing by electro-generated Fenton's reagent. J. Hazard Mater. 175, 858–865. https://doi.org/10.1016/j.jhazmat.2009.10.089.
El-Ghenymy, A., Centellas, F., Rodríguez, R.M., Cabot, P.L., Garrido, J.A., Sirés, I., Brillas, E., 2015. Comparative use of anodic oxidation, electro-Fenton and photoelectro-Fenton with Pt or boron-doped diamond anode to decolorize and mineralize Malachite Green oxalate dye. Electrochim. Acta 182, 247–256. https://doi.org/10.1016/j.electacta.2015.09.078.
Ensaldo-Rentería, M.K., Ramírez-Robledo, G., Sandoval-González, A., Pineda-Arellano, C.A., Álvarez-Gallegos, A.A., Zamudio-Lara, Á., Silva-Martínez, S., 2018. Photoelectrocatalytic oxidation of acid green 50 dye in aqueous solution using Ti/TiO2-NT electrode. J. Environ. Chem. Eng 6, 1182–1188. https://doi.org/10.1016/j.jece.2018.01.034.
Esbenshade, J.L., Cardoso, J.C., Zanoni, M.V.B., 2010. Removal of sunscreen compounds from swimming pool water using self-organized TiO2 nanotubular array electrodes. J. Photochem. Photobiol. Chem. 214, 257–263. https://doi.org/10.1016/j.jphotochem.2010.07.005.
Escalona-Durán, F., Ribeiro da Silva, D., Martínez-Huitle, C.A., Villegas-Guzman, P., 2020. The synergic persulfate-sodium dodecyl sulfate effect during the electro-oxidation of caffeine using active and non-active anodes. Chemosphere 253, 126599. https://doi.org/10.1016/j.chemosphere.2020.126599.
Esquivel, K., Arriaga, L.G., Rodríguez, F.J., Martínez, L., Godínez, L.A., 2009. Development of a TiO2 modified optical fiber electrode and its incorporation into a photoelectrochemical reactor for wastewater treatment. Water Res. 43, 3593–3603. https://doi.org/10.1016/j.watres.2009.05.035.
Fan, S., Li, X., Tan, J., Zeng, L., Yin, Z., Tadé, M.O., Liu, S., 2018. Enhanced photoeletrocatalytic reduction dechlorinations of PCP by Ru-Pd BQDs anchored Titania NAEs composites with double Schottky junctions: first-principles evidence and experimental verifications. Appl. Catal. B Environ. 227, 499–511. https://doi.org/10.1016/j.apcatb.2018.01.043.
Fang, T., Liao, L., Xu, X., Peng, J., Jing, Y., 2013. Removal of COD and colour in real pharmaceutical wastewater by photoelectrocatalytic oxidation method. Environ. Technol. (United Kingdom) 34, 779–786. https://doi.org/10.1080/09593330.2012.715760.
Fernández-Domene, R.M., Roselló-Márquez, G., Sánchez-Tovar, R., Lucas-Granados, B., García-Antón, J., 2019. Photoelectrochemical removal of chlorfenvinphos by using WO3 nanorods: influence of annealing temperature and operation pH. Sep. Purif. Technol. 212, 458–464. https://doi.org/10.1016/j.seppur.2018.11.049.
Flores, N., Brillas, E., Centellas, F., Rodríguez, R.M., Cabot, P.L., Garrido, J.A., Sirés, I., 2018. Treatment of olive oil mill wastewater by single electrocoagulation with different electrodes and sequential electrocoagulation/electrochemical Fenton-based processes. J. Hazard Mater. 347, 58–66. https://doi.org/10.1016/j.jhazmat.2017.12.059.
Flores, N., Cabot, P.L., Centellas, F., Garrido, J.A., Rodríguez, R.M., Brillas, E., Sirés, I., 2017. 4-Hydroxyphenylacetic acid oxidation in sulfate and real olive oil mill wastewater by electrochemical advanced processes with a boron-doped diamond anode. J. Hazard Mater. 321, 566–575. https://doi.org/10.1016/j.jhazmat.2016.09.057.
Flox, C., Cabot, P.-L., Centellas, F., Garrido, J.A., Rodríguez, R.M., Arias, C., Brillas, E., 2007. Solar photoelectro-Fenton degradation of cresols using a flow reactor with a boron-doped diamond anode. Appl. Catal. B Environ. 75, 17–28. https://doi.org/10.1016/J.APCATB.2007.03.010.
Frangos, P., Wang, H., Shen, W., Yu, G., Deng, S., Huang, J., Wang, B., Wang, Y., 2016. A novel photoelectro-peroxone process for the degradation and mineralization of substituted benzenes in water. Chem. Eng. J. 286, 239–248. https://doi.org/10.1016/j.cej.2015.10.096.
Fu, J.F., Zhao, Y.Q., Xue, X.D., Li, W.C., Babatunde, A.O., 2009. Multivariate-parameter optimization of acid blue-7 wastewater treatment by Ti/TiO2 photoelectrocatalysis via the Box–Behnken design. Desalination 243, 42–51. https://doi.org/10.1016/j.desal.2008.03.038.
Ganiyu, S.O., de Araújo, M.J.G., de Araújo Costa, E.C.T., Santos, J.E.L., dos Santos, E.V., Martínez-Huitle, C.A., Pergher, S.B.C., 2021a. Design of highly efficient porous carbon foam cathode for electro-Fenton degradation of antimicrobial sulfanilamide. Appl. Catal. B Environ. 283, 119652 https://doi.org/10.1016/j.apcatb.2020.119652.
Ganiyu, S.O., Martínez-Huitle, C.A., 2020. The use of renewable energies driving electrochemical technologies for environmental applications. Curr. Opin. Electrochemistry 22, 211–220. https://doi.org/10.1016/j.coelec.2020.07.007.
Ganiyu, S.O., Martínez-Huitle, C.A., Oturan, M.A., 2021b. Electrochemical advanced oxidation processes for wastewater treatment: advances in formation and detection of reactive species and mechanisms. Curr. Opin. Electrochem 27, 100678. https://doi.org/10.1016/j.coelec.2020.100678.
Ganiyu, S.O., Martínez-Huitle, C.A., Rodrigo, M.A., 2020. Renewable energies driven electrochemical wastewater/soil decontamination technologies: a critical review of fundamental concepts and applications. Appl. Catal. B Environ. 270, 118857 https://doi.org/10.1016/j.apcatb.2020.118857.
Ganiyu, S.O., Zhou, M., Martínez-Huitle, C.A., 2018. Heterogeneous electro-Fenton and photoelectro-Fenton processes: a critical review of fundamental principles and application for water/wastewater treatment. Appl. Catal. B Environ. 235, 103–129. https://doi.org/10.1016/j.apcatb.2018.04.044.
Garcia-Segura, S., Almeida, L.C., Bocchi, N., Brillas, E., 2011. Solar photoelectro-Fenton degradation of the herbicide 4-chloro-2-methylphenoxyacetic acid optimized by response surface methodology. J. Hazard Mater. 194, 109–118. https://doi.org/10.1016/j.jhazmat.2011.07.089.
Garcia-Segura, S., Brillas, E., 2017. Applied photoelectrocatalysis on the degradation of organic pollutants in wastewaters. J. Photochem. Photobiol. C Photochem. Rev. 31, 1–35. https://doi.org/10.1016/j.jphotochemrev.2017.01.005.
Garcia-Segura, S., Brillas, E., 2014. Advances in solar photoelectro-Fenton: decolorization and mineralization of the Direct Yellow 4 diazo dye using an autonomous solar pre-pilot plant. Electrochim. Acta 140, 384–395. https://doi.org/10.1016/j.electacta.2014.04.009.
Garcia-Segura, S., Dosta, S., Guilemany, J.M., Brillas, E., 2013. Solar photoelectrocatalytic degradation of Acid Orange 7 azo dye using a highly stable TiO2 photoanode synthesized by atmospheric plasma spray. Appl. Catal. B Environ. 132–133, 142–150. https://doi.org/10.1016/j.apcatb.2012.11.037.
Garcia-Segura, S., Ocon, J.D., Chong, M.N., 2018. Electrochemical oxidation remediation of real wastewater effluents — a review. Process Saf. Environ. Prot 113, 48–67. https://doi.org/10.1016/j.psep.2017.09.014.
Garza-Campos, B., Brillas, E., Hernández-Ramírez, A., El-Ghenymy, A., Guzmán-Mar, J.L., Ruiz-Ruiz, E.J., 2016. Salicylic acid degradation by advanced oxidation processes. Coupling of solar photoelectro-Fenton and solar heterogeneous photocatalysis. J. Hazard Mater. 319, 34–42. https://doi.org/10.1016/j.jhazmat.2016.02.050.
Garza-Campos, B.R., Guzmán-Mar, J.L., Reyes, L.H., Brillas, E., Hernández-Ramírez, A., Ruiz-Ruiz, E.J., 2014. Coupling of solar photoelectro-Fenton with a BDD anode and solar heterogeneous photocatalysis for the mineralization of the herbicide atrazine. Chemosphere 97, 26–33. https://doi.org/10.1016/j.chemosphere.2013.10.044.
George, S.J., Gandhimathi, R., Nidheesh, P.V., Ramesh, S.T., 2014. Electro-fenton oxidation of salicylic acid from aqueous solution: batch studies and degradation pathway. Clean - soil, Air. Water 42, 1701–1711. https://doi.org/10.1002/clen.201300453.
Georgieva, J., Valova, E., Armyanov, S., Philippidis, N., Poulios, I., Sotiropoulos, S., 2012. Bi-component semiconductor oxide photoanodes for the photo-electrocatalytic oxidation of organic solutes and vapours: a short review with emphasis to TiO 2-WO 3 photoanodes. J. Hazard Mater. 211–212, 30–46. https://doi.org/10.1016/j.jhazmat.2011.11.069.
Ghanbari, F., Wu, J., Khatebasreh, M., Ding, D., Lin, K.Y.A., 2020. Efficient treatment for landfill leachate through sequential electrocoagulation, electrooxidation and PMS/UV/CuFe2O4 process. Sep. Purif. Technol. 242 https://doi.org/10.1016/j.seppur.2020.116828.
Ghasemian, S., Omanovic, S., 2017. Fabrication and characterization of photoelectrochemically-active Sb-doped Sn x -W (100-x)% -oxide anodes: towards the removal of organic pollutants from wastewater. Appl. Surf. Sci. 416, 318–328. https://doi.org/10.1016/j.apsusc.2017.04.138.
GilPavas, E., Correa-Sánchez, S., 2019. Optimization of the heterogeneous electro-Fenton process assisted by scrap zero-valent iron for treating textile wastewater: assessment of toxicity and biodegradability. J. Water Process Eng 32, 100924. https://doi.org/10.1016/j.jwpe.2019.100924.
GilPavas, E., Dobrosz-Gómez, I., Gómez-García, M.Á., 2018. Optimization of solar-driven photo-electro-Fenton process for the treatment of textile industrial wastewater. J. Water Process Eng 24, 49–55. https://doi.org/10.1016/j.jwpe.2018.05.007.
Gong, J., Pu, W., Yang, C., Zhang, J., 2013. Novel one-step preparation of tungsten loaded TiO2 nanotube arrays with enhanced photoelectrocatalytic activity for pollutant degradation and hydrogen production. Catal. Commun. 36, 89–93. https://doi.org/10.1016/j.catcom.2013.03.009.
Goulart, L.A., Alves, S.A., Mascaro, L.H., 2019. Photoelectrochemical degradation of bisphenol A using Cu doped WO 3 electrodes. J. Electroanal. Chem. 839, 123–133. https://doi.org/10.1016/j.jelechem.2019.03.027.
Guaraldo, T.T., Gonçales, V.R., Silva, B.F., De Torresi, S.I.C., Zanoni, M.V.B.B., Torresi, S.I.C. De, Zanoni, M.V.B.B., 2016. Hydrogen production and simultaneous photoelectrocatalytic pollutant oxidation using a TiO 2/WO 3 nanostructured photoanode under visible light irradiation. J. Electroanal. Chem. 765, 188–196. https://doi.org/10.1016/j.jelechem.2015.07.034.
Gui, L., Peng, J., Li, P., Peng, R., Yu, P., Luo, Y., 2019. Electrochemical degradation of dye on TiO2 nanotube array constructed anode. Chemosphere 235, 1189–1196. https://doi.org/10.1016/j.chemosphere.2019.06.170.
Guo, R., Zhu, G., Gao, Y., Li, B., Gou, J., Cheng, X., 2019. Synthesis of 3D Bi2S3/TiO2 NTAs photocatalytic system and its high visible light driven photocatalytic performance for organic compound degradation. Sep. Purif. Technol. 226, 315–322. https://doi.org/10.1016/j.seppur.2019.05.067.
Guo, X., Lu, G., Chen, J., 2015. Graphene-based materials for photoanodes in dye-sensitized solar cells. Front. Energy Res. 3, 1–15. https://doi.org/10.3389/fenrg.2015.00050.
Gutierrez, M.I.J., Revero, E.P., Diaz, M.R.C., Gomez, M.E.N., Avella, J.A.P., 2016. Photoelectrocatalytic hydrogen production from oilfield-produced wastewater in a filter-press reactor using TiO2-based photoanodes. Catal. Today 266, 17–26. https://doi.org/10.1016/j.cattod.2015.12.008.
Hasanzadeh, A., Khataee, A., Zarei, M., Joo, S.W., 2018. Photo-assisted electrochemical abatement of trifluralin using a cathode containing a C60-carbon nanotubes composite. Chemosphere 199, 510–523. https://doi.org/10.1016/j.chemosphere.2018.02.061.
He, X., Chen, M., Chen, R., Zhu, X., Liao, Q., Ye, D., Zhang, B., Zhang, W., Yu, Y., 2018. A solar responsive photocatalytic fuel cell with the membrane electrode assembly design for simultaneous wastewater treatment and electricity generation. J. Hazard Mater. 358, 346–354. https://doi.org/10.1016/

j.jhazmat.2018.07.031.
Hernández, R., Olvera-Rodríguez, I., Guzmán, C., Medel, A., Escobar-Alarcón, L., Brillas, E., Sirés, I., Esquivel, K., 2018. Microwave-assisted sol-gel synthesis of an Au-TiO2 photoanode for the advanced oxidation of paracetamol as model pharmaceutical pollutant. Electrochem. Commun. 96, 42–46. https://doi.org/10.1016/j.elecom.2018.09.009.
Hirakawa, T., Koga, C., Negishi, N., Takeuchi, K., Matsuzawa, S., 2009. An approach to elucidating photocatalytic reaction mechanisms by monitoring dissolved oxygen: effect of H2O2 on photocatalysis. Appl. Catal. B Environ. 87, 46–55. https://doi.org/10.1016/j.apcatb.2008.08.027.
Hoffmann, M.R., Martin, S., Choi, W., Bahnemann, D.W., 1995. Environmental applications of semiconductor photocatalysis. Chem. Rev. 95, 69–96. https://doi.org/10.1021/cr00033a004.
Hosseini, M., Esrafili, A., Farzadkia, M., Kermani, M., Gholami, M., 2020. Degradation of ciprofloxacin antibiotic using photo-electrocatalyst process of Ni-doped ZnO deposited by RF sputtering on FTO as an anode electrode from aquatic environments: synthesis, kinetics, and ecotoxicity study. Microchem. J. 154, 104663 https://doi.org/10.1016/j.microc.2020.104663.
Hou, Y., Yuan, G., Wang, S., Yu, Z., Qin, S., Tu, L., Yan, Y., Chen, X., Zhu, H., Tang, Y., 2020. Nitrofurazone degradation in the self-biased bio-photoelectrochemical system: g-C3N4/CdS photocathode characterization, degradation performance, mechanism and pathways. J. Hazard Mater. 384, 121438 https://doi.org/10.1016/j.jhazmat.2019.121438.
Hu, X., Yang, J., Zhang, J., 2011. Magnetic loading of TiO2/SiO2/Fe3O4 nanoparticles on electrode surface for photoelectrocatalytic degradation of diclofenac. J. Hazard Mater. 196, 220–227. https://doi.org/10.1016/j.jhazmat.2011.09.009.
Huang, D., Hu, C., Zeng, G., Cheng, M., Xu, P., Gong, X., Wang, R., Xue, W., 2017. Combination of Fenton processes and biotreatment for wastewater treatment and soil remediation. Sci. Total Environ. 574, 1599–1610. https://doi.org/10.1016/j.scitotenv.2016.08.199.
Hunge, Y.M., Yadav, A.A., Mahadik, M.A., Bulakhe, R.N., Shim, J.J., Mathe, V.L., Bhosale, C.H., 2018. Degradation of organic dyes using spray deposited nanocrystalline stratified WO 3/TiO 2 photoelectrodes under sunlight illumination. Opt. Mater. (Amst) 76, 260–270. https://doi.org/10.1016/j.optmat.2017.12.044.
Iervolino, G., Tantis, I., Sygellou, L., Vaiano, V., Sannino, D., Lianos, P., 2017. Photocurrent increase by metal modification of Fe 2 O 3 photoanodes and its effect on photoelectrocatalytic hydrogen production by degradation of organic substances. Appl. Surf. Sci. 400, 176–183. https://doi.org/10.1016/j.apsusc.2016.12.173.
Iranifam, M., Zarei, M., Khataee, A.R., 2011. Decolorization of C.I. Basic Yellow 28 solution using supported ZnO nanoparticles coupled with photoelectro-Fenton process. J. Electroanal. Chem. 659, 107–112. https://doi.org/10.1016/j.jelechem.2011.05.010.
Isarain-Chávez, E., De La Rosa, C., Godínez, L.A., Brillas, E., Peralta-Hernández, J.M., 2014. Comparative study of electrochemical water treatment processes for a tannery wastewater effluent. J. Electroanal. Chem. 713, 62–69. https://doi.org/10.1016/j.jelechem.2013.11.016.
Isarain-Chávez, E., Rodríguez, R.M., Cabot, P.L., Centellas, F., Arias, C., Garrido, J.A., Brillas, E., 2011. Degradation of pharmaceutical beta-blockers by electrochemical advanced oxidation processes using a flow plant with a solar compound parabolic collector. Water Res. 45, 4119–4130. https://doi.org/10.1016/j.watres.2011.05.026.
Ishihara, H., Bock, J.P., Sharma, R., Hardcastle, F., Kannarpady, G.K., Mazumder, M.K., Biris, A.S., 2010. Electrochemical synthesis of titania nanostructural arrays and their surface modification for enhanced photoelectrochemical hydrogen production. Chem. Phys. Lett. 489, 81–85. https://doi.org/10.1016/j.cplett.2010.02.038.
Jaafarzadeh, N., Barzegar, G., Ghanbari, F., 2017. Photo assisted electro-peroxone to degrade 2,4-D herbicide: the effects of supporting electrolytes and determining mechanism. Process Saf. Environ. Prot 111, 520–528. https://doi.org/10.1016/j.psep.2017.08.012.
Jaafarzadeh, N., Omidinasab, M., Ghanbari, F., 2016. Combined electrocoagulation and UV-based sulfate radical oxidation processes for treatment of pulp and paper wastewater. Process Saf. Environ. Prot 102, 462–472. https://doi.org/10.1016/j.psep.2016.04.019.
Jacqueline George, S., Gandhimathi, R., Nidheesh, P.V., Ramesh, S.T., 2016. Optimization of salicylic acid removal by electro Fenton process in a continuous stirred tank reactor using response surface methodology. Desalin. Water Treat 57, 4234–4244. https://doi.org/10.1080/19443994.2014.992970.
Jaramillo-Gutiérrez, M.I., Carreño-Lizcano, M.I., Ruiz–Lizarazo, J.O., Pedraza–Avella, J.A., Rivero, E.P., Cruz-Díaz, M.R., 2020. Design, mathematical modelling, and numerical simulation of a novel tubular photoelectrochemical reactor and experimental validation by residence time distribution and mass transfer coefficients. Chem. Eng. J. 386, 123895 https://doi.org/10.1016/j.cej.2019.123895.
Jiao, Y., Ma, L., Tian, Y., Zhou, M., 2020. A flow-through electro-Fenton process using modified activated carbon fiber cathode for orange II removal. Chemosphere 252, 126483. https://doi.org/10.1016/j.chemosphere.2020.126483.
José Martín de Vidales, M., Mais, L., Sáez, C., Cañizares, P., Walsh, F.C., Rodrigo, M.A., Rodrigues, C. de A., Ponce de León, C., 2016. Photoelectrocatalytic oxidation of Methyl orange on a TiO 2 nanotubular anode using a flow cell. Chem. Eng. Technol. 39, 135–141. https://doi.org/10.1002/ceat.201500085.
Joy, A.C., Gandhimathi, R., Niveditha, S.V., Ramesh, S.T., Nidheesh, P.V., 2020. Photoelectro-peroxone process for the degradation of reactive azo dye in aqueous solution. Separ. Sci. Technol. 55, 2550–2559. https://doi.org/10.1080/01496395.2019.1634732.
Juang, Y., Nurhayati, E., Huang, C., Pan, J.R., Huang, S., 2013. A hybrid electrochemical advanced oxidation/microfiltration system using BDD/Ti anode for acid yellow 36 dye wastewater treatment. Sep. Purif. Technol. 120, 289–295. https://doi.org/10.1016/j.seppur.2013.09.042.
Kaneko, M., Nemoto, J., Ueno, H., Gokan, N., Ohnuki, K., Horikawa, M., Saito, R., Shibata, T., 2006. Photoelectrochemical reaction of biomass and bio-related compounds with nanoporous TiO2 film photoanode and O2-reducing cathode. Electrochem. Commun. 8, 336–340. https://doi.org/10.1016/j.elecom.2005.12.004.
Khataee, A.R., Safarpour, M., Zarei, M., Aber, S., 2012. Combined heterogeneous and homogeneous photodegradation of a dye using immobilized TiO 2 nanophotocatalyst and modified graphite electrode with carbon nanotubes. J. Mol. Catal. Chem. 363–364, 58–68. https://doi.org/10.1016/j.molcata.2012.05.016.
Khataee, A.R., Vahid, B., Behjati, B., Safarpour, M., 2013. Treatment of a dye solution using photoelectro-fenton process on the cathode containing carbon nanotubes under recirculation mode: investigation of operational parameters and artificial neural network modeling. Environ. Prog. Sustain. Energy 32, 557–563. https://doi.org/10.1002/ep.11657.
Klauck, C.R., Giacobbo, A., de Oliveira, E.D.L., da Silva, L.B., Rodrigues, M.A.S., 2017. Evaluation of acute toxicity, cytotoxicity and genotoxicity of landfill leachate treated by biological lagoon and advanced oxidation processes. J. Environ. Chem. Eng 5, 6188–6193. https://doi.org/10.1016/j.jece.2017.11.058.
Koiki, B.A., Orimolade, B.O., Zwane, B.N., Nkosi, D., Mabuba, N., Arotiba, O.A., 2020. Cu2O on anodised TiO2 nanotube arrays: a heterojunction photoanode for visible light assisted electrochemical degradation of pharmaceuticals in water. Electrochim. Acta 340, 135944. https://doi.org/10.1016/j.electacta.2020.135944.
Koo, M.S., Cho, K., Yoon, J., Choi, W., 2017. Photoelectrochemical degradation of organic compounds coupled with molecular hydrogen generation using electrochromic TiO2 nanotube Arrays. Environ. Sci. Technol. 51, 6590–6598. https://doi.org/10.1021/acs.est.7b00774.
Kushwaha, H.S., Halder, A., Thomas, P., Vaish, R., 2017. CaCu3Ti4O12: a bifunctional perovskite electrocatalyst for oxygen evolution and reduction reaction in alkaline medium. Electrochim. Acta 252, 532–540. https://doi.org/10.1016/j.electacta.2017.09.030.
Lalwani, J., Gupta, A., Thatikonda, S., Subrahmanyam, C., 2020. An industrial insight on treatment strategies of the pharmaceutical industry effluent with varying qualitative characteristics. J. Environ. Chem. Eng 8, 104190. https://doi.org/10.1016/j.jece.2020.104190.
Lee, S.L., Ho, L.N., Ong, S.A., Wong, Y.S., Voon, C.H., Khalik, W.F., Yusoff, N.A., Nordin, N., 2016. Enhanced electricity generation and degradation of the azo dye Reactive Green 19 in a photocatalytic fuel cell using ZnO/Zn as the photoanode. J. Clean. Prod. 127, 579–584. https://doi.org/10.1016/j.jclepro.2016.03.169.
Li, D., Xing, Z., Yu, X., Cheng, X., 2015a. One-step hydrothermal synthesis of C-N-S-tridoped TiO2-based nanosheets photoelectrode for enhanced photoelectrocatalytic performance and mechanism. Electrochim. Acta 170, 182–190. https://doi.org/10.1016/j.electacta.2015.04.148.
Li, G., Qu, J., Zhang, X., Ge, J., 2006. Electrochemically assisted photocatalytic degradation of Acid Orange 7 with β-PbO2 electrodes modified by TiO2. Water Res. 40, 213–220. https://doi.org/10.1016/j.watres.2005.10.039.
Li, K., Zhang, H., Tang, T., Xu, Y., Ying, D., Wang, Y., Jia, J., 2014a. Optimization and application of TiO2/Ti-Pt photo fuel cell (PFC) to effectively generate electricity and degrade organic pollutants simultaneously. Water Res. 62, 1–10. https://doi.org/10.1016/j.watres.2014.05.044.
Li, L., Wang, G., Chen, R., Zhu, X., Wang, H., Liao, Q., Yu, Y., 2014b. Optofluidics based micro-photocatalytic fuel cell for efficient wastewater treatment and electricity generation. Lab Chip 14, 3368–3375. https://doi.org/10.1039/c4lc00595c.
Li, L., Xue, S., Chen, R., Liao, Q., Zhu, X., Wang, Z., He, X., Feng, H., Cheng, X., 2015b. Performance characteristics of a membraneless solar responsive photocatalytic fuel cell with an air-breathing cathode under different fuels and electrolytes and air conditions. Electrochim. Acta 182, 280–288. https://doi.org/10.1016/j.electacta.2015.09.090.
Li, X.Z., Zhao, B.X., Wang, P., 2007. Degradation of 2, 4-dichlorophenol in aqueous solution by a hybrid oxidation process. J. Hazard Mater. 147, 281–287. https://doi.org/10.1016/j.jhazmat.2006.12.077.
Li, Z., Li, S., Tang, Y., Li, X., Wang, J., Li, L., 2020. Highly efficient degradation of perfluorooctanoic acid: an integrated photo-electrocatalytic ozonation and mechanism study. Chem. Eng. J. 391 https://doi.org/10.1016/j.cej.2019.123533.
Liao, W., Yang, J., Zhou, H., Murugananthan, M., Zhang, Y., 2014. Electrochemically self-doped TiO2 nanotube Arrays for efficient visible light photoelectrocatalytic degradation of contaminants. Electrochim. Acta 136, 310–317. https://doi.org/10.1016/j.electacta.2014.05.091.
Liu, C.F., Huang, C.P., Hu, C.C., Huang, C., 2019. A dual TiO2/Ti-stainless steel anode for the degradation of orange G in a coupling photoelectrochemical and photoelectro-Fenton system. Sci. Total Environ. 659, 221–229. https://doi.org/10.1016/j.scitotenv.2018.12.224.
Liu, J., Li, J., Li, Y., Guo, J., Xu, S.-M., Zhang, R., Shao, M., 2020. Photoelectrochemical water splitting coupled with degradation of organic pollutants enhanced by surface and interface engineering of BiVO4 photoanode. Appl. Catal. B Environ. 278, 119268 https://doi.org/10.1016/j.apcatb.2020.119268.
Liu, C., Li, J., Sun, L., Zhou, Y., Liu, C., Wang, H., Huo, P., Ma, C., Yan, Y., 2018. Visible-light driven photocatalyst of CdTe/CdS homologous heterojunction on N-rGO photocatalyst for efficient degradation of 2,4-dichlorophenol. J. Taiwan Inst. Chem. Eng. 93, 603–615. https://doi.org/10.1016/j.jtice.2018.09.005.

Liu, Y., Li, J., Zhou, B., Chen, H., Wang, Z., Cai, W., 2011a. A TiO2-nanotube-array-based photocatalytic fuel cell using refractory organic compounds as substrates for electricity generation. Chem. Commun. 47, 10314–10316. https://doi.org/10.1039/c1cc13388h.

Liu, Y., Li, J., Zhou, B., Li, X., Chen, H., Chen, Q., Wang, Z., Li, L., Wang, J., Cai, W., 2011b. Efficient electricity production and simultaneously wastewater treatment via a high-performance photocatalytic fuel cell. Water Res. 45, 3991–3998. https://doi.org/10.1016/j.watres.2011.05.004.

Liu, Y., Li, J., Zhou, B., Lv, S., Li, X., Chen, H., Chen, Q., Cai, W., 2012. Photo-electrocatalytic degradation of refractory organic compounds enhanced by a photocatalytic fuel cell. Appl. Catal. B Environ. 111–112, 485–491. https://doi.org/10.1016/j.apcatb.2011.10.038.

Liu, Y., Liu, L., Yang, F., 2016. Energy-efficient degradation of rhodamine B in a LED illuminated photocatalytic fuel cell with anodic Ag/AgCl/GO and cathodic ZnIn2S4 catalysts. RSC Adv. 6, 12068–12075. https://doi.org/10.1039/c5ra25557k.

Lofrano, G., Meriç, S., Zengin, G.E., Orhon, D., 2013. Chemical and biological treatment technologies for leather tannery chemicals and wastewaters: a review. Sci. Total Environ. 461–462, 265–281. https://doi.org/10.1016/j.scitotenv.2013.05.004.

Longobucco, G., Pasti, L., Molinari, A., Marchetti, N., Caramori, S., Cristino, V., Boaretto, R., Bignozzi, C.A., 2017. Photoelectrochemical mineralization of emerging contaminants at porous WO3 interfaces. Appl. Catal. B Environ. 204, 273–282. https://doi.org/10.1016/j.apcatb.2016.11.007.

Lu, X., Xie, S., Yang, H., Tong, Y., Ji, H., 2014. Photoelectrochemical hydrogen production from biomass derivatives and water. Chem. Soc. Rev. 43, 7581–7593. https://doi.org/10.1039/c3cs60392j.

Lui, G., Jiang, G., Fowler, M., Yu, A., Chen, Z., 2019. A high performance wastewater-fed flow-photocatalytic fuel cell. J. Power Sources 425, 69–75. https://doi.org/10.1016/j.jpowsour.2019.03.091.

Ma, X., Zhang, J., Wang, B., Li, Q., Chu, S., 2018. Hierarchical Cu 2 O foam/g-C 3 N 4 photocathode for photoelectrochemical hydrogen production. Appl. Surf. Sci. 427, 907–916. https://doi.org/10.1016/j.apsusc.2017.09.075.

Macías-Sánchez, J., Hinojosa-Reyes, L., Guzmán-Mar, J.L., Peralta-Hernández, J.M., Hernández-Ramírez, A., 2011. Performance of the photo-Fenton process in the degradation of a model azo dye mixture. Photochem. Photobiol. Sci. 10, 332–337. https://doi.org/10.1039/C0PP00158A.

Mais, L., Mascia, M., Palmas, S., Vacca, A., 2019. Photoelectrochemical oxidation of phenol with nanostructured TiO2-PANI electrodes under solar light irradiation. Sep. Purif. Technol. 208, 153–159. https://doi.org/10.1016/j.seppur.2018.03.074.

Manenti, D.R., Módenes, A.N., Soares, P.A., Espinoza-Quiñones, F.R., Boaventura, R.A.R., Bergamasco, R., Vilar, V.J.P., 2014. Assessment of a multistage system based on electrocoagulation, solar photo-Fenton and biological oxidation processes for real textile wastewater treatment. Chem. Eng. J. 252, 120–130. https://doi.org/10.1016/j.cej.2014.04.096.

Mao, X., Jiang, R., Xiao, W., Yu, J., 2015. Use of Surfactants for the Remediation of Contaminated Soils: A Review. J. Hazard. Mater. https://doi.org/10.1016/j.jhazmat.2014.12.009.

Martín de Vidales, M.J., Castro, M.P., Sáez, C., Cañizares, P., Rodrigo, M.A., 2019. Radiation-assisted electrochemical processes in semi-pilot scale for the removal of clopyralid from soil washing wastes. Sep. Purif. Technol. 208, 100–109. https://doi.org/10.1016/j.seppur.2018.04.074.

Martín de Vidales, M.J., Millán, M., Sáez, C., Cañizares, P., Rodrigo, M.A., 2017. Irradiated-assisted electrochemical processes for the removal of persistent pollutants from real wastewater. Sep. Purif. Technol. 175, 428–434. https://doi.org/10.1016/j.seppur.2016.11.014.

Martínez-Huitle, C.A., Ferro, S., 2006. Electrochemical oxidation of organic pollutants for the wastewater treatment: direct and indirect processes. Chem. Soc. Rev. 35, 1324–1340. https://doi.org/10.1039/b517632h.

Martínez-Huitle, C.A., Ferro, S., De Battisti, A., 2005. Electrochemical incineration of oxalic acid: reactivity and engineering parameters. J. Appl. Electrochem. 35, 1087–1093. https://doi.org/10.1007/s10800-005-9003-0.

Martínez-Huitle, C.A., Ferro, S., Reyna, S., Cerro-López, M., De Battisti, A., Quiroz, M.A., 2008. Electrochemical oxidation of oxalic acid in the presence of halides at boron doped diamond electrode. J. Braz. Chem. Soc. 19, 150–156. https://doi.org/10.1590/S0103-50532008000100021.

Martínez-Huitle, C.A., Panizza, M., 2018. Electrochemical oxidation of organic pollutants for wastewater treatment. Curr. Opin. Electrochem 11, 62–71. https://doi.org/10.1016/j.coelec.2018.07.010.

Martínez-Huitle, C.A., Rodrigo, M.A., Sirés, I., Scialdone, O., 2015. Single and Coupled Electrochemical Processes and Reactors for the Abatement of Organic Water Pollutants: A Critical Review. Chem. Rev. 115, 13362–13407. https://doi.org/10.1021/acs.chemrev.5b00361.

Masudy-Panah, S., Siavash Moakhar, R., Chua, C.S., Tan, H.R., Wong, T.I., Chi, D., Dalapati, G.K., 2016. Nanocrystal engineering of sputter-grown CuO photocathode for visible-light-driven electrochemical water splitting. ACS Appl. Mater. Interfaces 8, 1206–1213. https://doi.org/10.1021/acsami.5b09613.

Merényi, G., Lind, J., Naumov, S., Sonntag, C. Von, 2010. Reaction of ozone with hydrogen peroxide (peroxone process): a revision of current mechanistic concepts based on thermokinetic and quantum-chemical considerations. Environ. Sci. Technol. 44, 3505–3507. https://doi.org/10.1021/es100277d.

Meshram, N., Mahadik, M.A., Jeong, I.-K., Seo, Y.S., Cho, M., Jang, J.S., 2019. Effect of tetravalent ions dopants and CoO surface modification on hematite nanorod array for photoelectrochemical degradation of Orange-II dye. J. Taiwan Inst. Chem. Eng 97, 305–315. https://doi.org/10.1016/j.jtice.2019.02.025.

Módenes, A.N., Espinoza-Quiñones, F.R., Borba, F.H., Manenti, D.R., 2012. Performance evaluation of an integrated photo-Fenton – electrocoagulation process applied to pollutant removal from tannery effluent in batch system. Chem. Eng. J. 197, 1–9. https://doi.org/10.1016/j.cej.2012.05.015.

Mohammad, A., Khan, M.E., Karim, M.R., Cho, M.H., 2019. Synergistically effective and highly visible light responsive SnO2-g-C3N4 nanostructures for improved photocatalytic and photoelectrochemical performance. Appl. Surf. Sci. 495, 143432 https://doi.org/10.1016/j.apsusc.2019.07.174.

Mohite, S.V., Ganbavle, V.V., Rajpure, K.Y., 2016. Solar photoelectrocatalytic activities of rhodamine-B using sprayed WO3 photoelectrode. J. Alloys Compd. https://doi.org/10.1016/j.jallcom.2015.09.154, 655-106-113.

Moradi, M., Moussavi, G., 2019. Enhanced treatment of tannery wastewater using the electrocoagulation process combined with UVC/VUV photoreactor: parametric and mechanistic evaluation. Chem. Eng. J. 358, 1038–1046. https://doi.org/10.1016/j.cej.2018.10.069.

Moraes, P.B., Pelegrino, R.R.L., Bertazzoli, R., 2007. Degradation of Acid Blue 40 dye solution and dye house wastewater from textile industry by photo-assisted electrochemical process. J. Environ. Sci. Heal. - Part A Toxic/Hazardous Subst. Environ. Eng 42, 2131–2138. https://doi.org/10.1080/10934520701629591.

Moreira, F.C., Boaventura, R.A.R., Brillas, E., Vilar, V.J.P., 2017. Electrochemical advanced oxidation processes : a review on their application to synthetic and real wastewaters. "Applied Catal. B,. Environ. Times 202, 217–261. https://doi.org/10.1016/j.apcatb.2016.08.037.

Moreira, F.C., Garcia-Segura, S., Vilar, V.J.P., Boaventura, R.A.R., Brillas, E., 2013. Decolorization and mineralization of Sunset Yellow FCF azo dye by anodic oxidation, electro-Fenton, UVA photoelectro-Fenton and solar photoelectro-Fenton processes. Appl. Catal. B Environ. 142–143, 877–890. https://doi.org/10.1016/j.apcatb.2013.03.023.

Moreira, F.C., Soler, J., Alpendurada, M.F., Boaventura, R.A.R., Brillas, E., Vilar, V.J.P., 2016. Tertiary treatment of a municipal wastewater toward pharmaceuticals removal by chemical and electrochemical advanced oxidation processes. Water Res. 105, 251–263. https://doi.org/10.1016/j.watres.2016.08.036.

Mousset, E., Dionysiou, D.D., 2020. Photoelectrochemical reactors for treatment of water and wastewater: a review. Environ. Chem. Lett. 18, 1301–1318. https://doi.org/10.1007/s10311-020-01014-9.

Mousset, E., Huang Weiqi, V., Foong Yang Kai, B., Koh, J.S., Tng, J.W., Wang, Z., Lefebvre, O., 2017. A new 3D-printed photoelectrocatalytic reactor combining the benefits of a transparent electrode and the Fenton reaction for advanced wastewater treatment. J. Mater. Chem. 5, 24951–24964. https://doi.org/10.1039/c7ta08182k.

Mousset, E., Oturan, M.A., Van Hullebusch, E.D., Guibaud, G., Esposito, G., 2014. Soil washing/flushing treatments of organic pollutants enhanced by cyclodextrins and integrated treatments: state of the art. Crit. Rev. Environ. Sci. Technol. 44, 705–795. https://doi.org/10.1080/10643389.2012.741307.

Mulligan, C.N., Yong, R.N., Gibbs, B.F., 2001. Surfactant-enhanced remediation of contaminated soil: a review. Eng. Geol. 60, 371–380. https://doi.org/10.1016/S0013-7952(00)00117-4.

Muñoz-Morales, M., Sáez, C., Cañizares, P., Rodrigo, M.A., 2019. Anodic oxidation for the remediation of soils polluted with perchloroethylene. J. Chem. Technol. Biotechnol. 94, 288–294. https://doi.org/10.1002/jctb.5774.

Nava, J., Quiroz, M., Martinez-Huitle, C.A., 2008. Electrochemical treatment of synthetic wastewaters containing alphazurine A dye: role of electrode material in the colour and COD removal. J. Mex. Chem. Soc. 52, 249–255. https://doi.org/10.29356/jmcs.v52i4.1076.

Nava, J.L., Sirés, I., Brillas, E., 2014. Electrochemical incineration of indigo. A comparative study between 2D (plate) and 3D (mesh) BDD anodes fitted into a filter-press reactor. Environ. Sci. Pollut. Res. 21, 8485–8492. https://doi.org/10.1007/s11356-014-2781-3.

Nidheesh, P.V., 2017. Graphene-based materials supported advanced oxidation processes for water and wastewater treatment: a review. Environ. Sci. Pollut. Res. 24, 27047–27069. https://doi.org/10.1007/s11356-017-0481-5.

Nidheesh, P.V., Gandhimathi, R., 2014. Effect of solution pH on the performance of three electrolytic advanced oxidation processes for the treatment of textile wastewater and sludge characteristics. RSC Adv. 4, 27946–27954. https://doi.org/10.1039/c4ra02958e.

Nidheesh, P.V., Gandhimathi, R., Ramesh, S.T., 2013. Degradation of dyes from aqueous solution by Fenton processes: a review. Environ. Sci. Pollut. Res. 20, 2099–2132. https://doi.org/10.1007/s11356-012-1385-z.

Nidheesh, P.V., Zhou, M., Oturan, M.A., 2018a. An overview on the removal of synthetic dyes from water by electrochemical advanced oxidation processes. Chemosphere 197, 210–227. https://doi.org/10.1016/j.chemosphere.2017.12.195.

Nidheesh, P.V., Gandhimathi, R., 2012. Trends in electro-Fenton process for water and wastewater treatment: an overview. Desalination 299, 1–15. https://doi.org/10.1016/j.desal.2012.05.011.

Nidheesh, P.V., Gandhimathi, R., Velmathi, S., Sanjini, N.S., 2014. Magnetite as a heterogeneous electro Fenton catalyst for the removal of Rhodamine B from aqueous solution. RSC Adv. 4 (5698) https://doi.org/10.1039/c3ra46969g.

Nidheesh, P.V., Syam Babu, D., Dasgupta, B., Behara, P., Ramasamy, B., Suresh Kumar, M., 2020. Treatment of arsenite-contaminated water by electrochemical advanced oxidation processes. ChemElectroChem 7, 2418–2423. https://doi.org/10.1002/celc.202000549.

Nidheesh, P.V., Divyapriya, G., Oturan, N., Trellu, C., Oturan, M.A., 2019. Environmental applications of boron-doped diamond electrodes: 1. Applications in water and wastewater treatment. ChemElectroChem 6, 2124–2142. https://doi.org/10.1002/celc.201801876.

Nidheesh, P.V.V., Olvera-Vargas, H., Oturan, N., Oturan, M.A.A., 2018b. Heterogeneous electro-fenton process: principles and applications. In: Zhou, M., Oturan, M.A., Sirés, I. (Eds.), Electro-Fenton Process: New Trends and Scale-Up. Springer Singapore, Singapore, pp. 85–110. https://doi.org/10.1007/698_2017_72.

Nordin, N., Ho, L.N., Ong, S.A., Ibrahim, A.H., Wong, Y.S., Lee, S.L., Oon, Y.S., Oon, Y.L., 2017. Hybrid system of photocatalytic fuel cell and Fenton process for electricity generation and degradation of Reactive Black 5. Sep. Purif. Technol. 177, 135–141. https://doi.org/10.1016/j.seppur.2016.12.030.

Oliveira, H.G., Ferreira, L.H., Bertazzoli, R., Longo, C., 2015. Remediation of 17-α-ethinylestradiol aqueous solution by photocatalysis and electrochemically-assisted photocatalysis using TiO2 and TiO2/WO3 electrodes irradiated by a solar simulator. Water Res. 72, 305–314. https://doi.org/10.1016/j.watres.2014.08.042.

Olvera-Rodríguez, I., Hernández, R., Medel, A., Guzmán, C., Escobar-Alarcón, L., Brillas, E., Sirés, I., Esquivel, K., 2019. TiO2/Au/TiO2 multilayer thin-film photoanodes synthesized by pulsed laser deposition for photoelectrochemical degradation of organic pollutants. Sep. Purif. Technol. 224, 189–198. https://doi.org/10.1016/j.seppur.2019.05.020.

Olvera-Vargas, H., Gore-Datar, N., Garcia-Rodriguez, O., Mutnuri, S., Lefebvre, O., 2021. Electro-Fenton treatment of real pharmaceutical wastewater paired with a BDD anode: reaction mechanisms and respective contribution of homogeneous and heterogenous [rad]OH. Chem. Eng. J. 404, 126524 https://doi.org/10.1016/j.cej.2020.126524.

Olya, M.E., Pirkarami, A., 2013. Cost-effective photoelectrocatalytic treatment of dyes in a batch reactor equipped with solar cells. Sep. Purif. Technol. 118, 557–566. https://doi.org/10.1016/j.seppur.2013.07.038.

Olya, M.E., Pirkarami, A., Soleimani, M., Bahmaei, M., 2013. Photoelectrocatalytic degradation of acid dye using Ni–TiO2 with the energy supplied by solar cell: mechanism and economical studies. J. Environ. Manag. 121, 210–219. https://doi.org/10.1016/j.jenvman.2013.01.041.

Orimolade, B.O., Zwane, B.N., Koiki, B.A., Rivallin, M., Bechelany, M., Mabuba, N., Lesage, G., Cretin, M., Arotiba, O.A., 2020. Coupling cathodic Electro-Fenton with anodic photo-electrochemical oxidation: a feasibility study on the mineralization of paracetamol. J. Environ. Chem. Eng 8, 104394. https://doi.org/10.1016/j.jece.2020.104394.

Oturan, M.A., Aaron, J.-J., 2014. Advanced oxidation processes in water/wastewater treatment: principles and applications. A review. Crit. Rev. Environ. Sci. Technol. 44, 2577–2641. https://doi.org/10.1080/10643389.2013.829765.

Oturan, M.A., Nidheesh, P.V., Zhou, M., 2018. Electrochemical advanced oxidation processes for the abatement of persistent organic pollutants. Chemosphere 209, 17–19. https://doi.org/10.1016/j.chemosphere.2018.06.049.

Ou, B., Wang, J., Wu, Y., Zhao, S., Wang, Z., 2019. Treatment of polyaniline wastewater by coupling of photoelectro-fenton and heterogeneous photocatalysis with black TiO2 nanotubes. ACS Omega 4, 9664–9672. https://doi.org/10.1021/acsomega.9b00352.

Pandey, R.A., Sanyal, P.B., Chattopadhyay, N., Kaul, S.N., 2003. Treatment and reuse of wastes of a vegetable oil refinery. Resour. Conserv. Recycl. 37, 101–117. https://doi.org/10.1016/S0921-3449(02)00071-X.

Pang, Y., Li, Y., Xu, G., Hu, Y., Kou, Z., Feng, Q., Lv, J., Zhang, Y., Wang, J., Wu, Y., 2019. Z-scheme carbon-bridged Bi2O3/TiO2 nanotube arrays to boost photoelectrochemical detection performance. Appl. Catal. B Environ. 248, 255–263. https://doi.org/10.1016/j.apcatb.2019.01.077.

Panizza, M., 2018. Fine chemical industry, pulp and paper industry, petrochemical industry and pharmaceutical industry. In: Electrochemical Water and Wastewater Treatment. Elsevier Inc., pp. 335–364. https://doi.org/10.1016/B978-0-12-813160-2.00013-4

Panizza, M., Delucchi, M., Sirés, I., 2010. Electrochemical process for the treatment of landfill leachate. J. Appl. Electrochem. 40, 1721–1727. https://doi.org/10.1007/s10800-010-0109-7.

Paracchino, A., Laporte, V., Sivula, K., Grätzel, M., Thimsen, E., 2011. Highly active oxide photocathode for photoelectrochemical water reduction. Nat. Mater. 10, 456–461. https://doi.org/10.1038/nmat3017.

Parmar, J., Jang, S., Soler, L., Kim, D.P., Sánchez, S., 2015. Nano-photocatalysts in microfluidics, energy conversion and environmental applications. Lab Chip 15, 2352–2356. https://doi.org/10.1039/c5lc90047f.

Patel, M., Kim, H.S., Patel, D.B., Kim, J., 2016. CuO photocathode-embedded semi-transparent photoelectrochemical cell. J. Mater. Res. 31, 3205–3213. https://doi.org/10.1557/jmr.2016.364.

Peerakiatkhajohn, P., Yun, J.H., Butburee, T., Chen, H., Thaweesak, S., Lyu, M., Wang, S., Wang, L., 2021. Bifunctional photoelectrochemical process for humic acid degradation and hydrogen production using multi-layered p-type Cu2O photoelectrodes with plasmonic Au@TiO2. J. Hazard Mater. 402, 123533 https://doi.org/10.1016/j.jhazmat.2020.123533.

Peleyeju, M.G., Arotiba, O.A., 2018. Recent trend in visible-light photoelectrocatalytic systems for degradation of organic contaminants in water/wastewater. Environ. Sci. Water Res. Technol 4, 1389–1411. https://doi.org/10.1039/c8ew00276b.

Pellenz, L., Borba, F.H., Daroit, D.J., Lassen, M.F.M., Baroni, S., Zorzo, C.F., Guimarães, R.E., Espinoza-Quiñones, F.R., Seibert, D., 2020. Landfill leachate treatment by a boron-doped diamond-based photo-electro-Fenton system integrated with biological oxidation: a toxicity, genotoxicity and by products assessment. J. Environ. Manag. 264 https://doi.org/10.1016/j.jenvman.2020.110473, 0–11.

Peralta-Hernández, J.M., Meas-Vong, Y., Rodríguez, F.J., Chapman, T.W., Maldonado, M.I., Godínez, L.A., 2008. Comparison of hydrogen peroxide-based processes for treating dye-containing wastewater: decolorization and destruction of Orange II azo dye in dilute solution. Dyes Pigments 76, 656–662. https://doi.org/10.1016/j.dyepig.2007.01.001.

Pereira De Sousa, D.D., Pinto, C.F., Tonhela, M.A., Granato, A.C., De Jesus Motheo, A., De Faria Lima, A., Ferreira, D.C., Fernandes, D.M., De Toledo Fornazari, A.L., Malpass, G.R.P., 2019. Treatment of real dairy wastewater by electrolysis and photo-assisted electrolysis in presence of chlorides. Water Sci. Technol. 80, 961–969. https://doi.org/10.2166/wst.2019.339.

Pipi, A.R.F., Sirés, I., De Andrade, A.R., Brillas, E., 2014. Application of electrochemical advanced oxidation processes to the mineralization of the herbicide diuron. Chemosphere 109, 49–55. https://doi.org/10.1016/j.chemosphere.2014.03.006.

Popat, A., Nidheesh, P.V., Singh, T.S.A., Kumar, M.S., 2019. Mixed industrial wastewater treatment by combined electrochemical advanced oxidation and biological processes. Chemosphere 237, 124419. https://doi.org/10.1016/j.chemosphere.2019.124419.

Potter, M.C., 1911. Electrical effects accompanying the decomposition of organic compounds. Proc. R. Soc. London. Ser. B. Contain. Pap. a Biol. Character 84, 260–276. https://doi.org/10.1098/rspb.1911.0073.

Qi, J., Li, X., Zheng, H., Li, P., Wang, H., 2015. Simultaneous removal of methylene blue and copper(II) ions by photoelectron catalytic oxidation using stannic oxide modified iron(III) oxide composite electrodes. J. Hazard Mater. 293, 105–111. https://doi.org/10.1016/j.jhazmat.2015.03.059.

Rajput, H., Kwon, E.E., Younis, S.A., Weon, S., Jeon, T.H., Choi, W., Kim, K., 2021. Photoelectrocatalysis as a high-efficiency platform for pulping wastewater treatment and energy production. Chem. Eng. J. 128612 https://doi.org/10.1016/j.cej.2021.128612.

Ramírez, R.J., Arellano, C.A.P., Gallegos, A.A.Á., González, A.E.J., Martínez, S.S., 2015. H2O2-assisted TiO2 generation during the photoelectrocatalytic process to decompose the acid green textile dye by Fenton reaction. J. Photochem. Photobiol. Chem. 305, 51–59. https://doi.org/10.1016/j.jphotochem.2015.03.004.

Raptis, D., Dracopoulos, V., Lianos, P., 2017. Renewable energy production by photoelectrochemical oxidation of organic wastes using WO3 photoanodes. J. Hazard Mater. 333, 259–264. https://doi.org/10.1016/j.jhazmat.2017.03.044.

Rather, R.A., Lo, I.M.C., 2020. Photoelectrochemical sewage treatment by a multifunctional g-C3N4/Ag/AgCl/BiVO4 photoanode for the simultaneous degradation of emerging pollutants and hydrogen production, and the disinfection of E. coli. Water Res. 168, 115166 https://doi.org/10.1016/j.watres.2019.115166.

Ray, A.K., 1998. Development of a new photocatalytic reactor for water purification. Dev.. A new photocatalytic react. water purićation 40, 73–83.

Renou, S., Givaudan, J.G., Poulain, S., Dirassouyan, F., Moulin, P., 2008. Landfill leachate treatment: review and opportunity. J. Hazard Mater. 150, 468–493. https://doi.org/10.1016/j.jhazmat.2007.09.077.

Rezaei, B., Soleimany, R., Ensafi, A.A., Irannejad, N., 2018. Photocatalytic degradation enhancements of dyes with bi-functionalized zones of modified nanoflower like TiO2 with Pt-C3N4 under sunlight irradiation. J. Environ. Chem. Eng 6, 7010–7020. https://doi.org/10.1016/j.jece.2018.11.008.

Rodrigo, M.A., Oturan, N., Oturan, M.A., 2014. Electrochemically Assisted Remediation of Pesticides in Soils and Water: A Review. Chem. Rev. 114, 8720–8745. https://doi.org/10.1021/cr500077e.

Ruiz, E.J., Arias, C., Brillas, E., Hernández-Ramírez, A., Peralta-Hernández, J.M., 2011. Mineralization of Acid Yellow 36azo dye by electro-Fenton and solar photoelectro-Fenton processes with a boron-doped diamond anode. Chemosphere 82, 495–501. https://doi.org/10.1016/j.chemosphere.2010.11.013.

Salazar, R., Brillas, E., Sirés, I., 2012. Finding the best Fe 2+/Cu 2+ combination for the solar photoelectro-Fenton treatment of simulated wastewater containing the industrial textile dye Disperse Blue 3. Appl. Catal. B Environ. 115–116, 107–116. https://doi.org/10.1016/j.apcatb.2011.12.026.

Salazar, R., Garcia-Segura, S., Ureta-Zañartu, M.S., Brillas, E., 2011a. Degradation of disperse azo dyes from waters by solar photoelectro-Fenton. Electrochim. Acta 56, 6371–6379. https://doi.org/10.1016/j.electacta.2011.05.021.

Salazar, R., Garcia-Segura, S., Ureta-Zañartu, M.S., Brillas, E., 2011b. Degradation of disperse azo dyes from waters by solar photoelectro-Fenton. Electrochim. Acta 56, 6371–6379. https://doi.org/10.1016/j.electacta.2011.05.021.

Santos, E.V. Dos, Sáez, C., Martínez-Huitle, C.A., Cañizares, P., Rodrigo, M.A., 2015. The role of particle size on the conductive diamond electrochemical oxidation of soil-washing effluent polluted with atrazine. Electrochem. Commun. Now. 55, 26–29. https://doi.org/10.1016/j.elecom.2015.03.003.

Santos, J.E.L., Antonio Quiroz, M., Cerro-Lopez, M., De Moura, D.C., Martínez-Huitle, C.A., 2018. Evidence for the electrochemical production of persulfate at TiO2 nanotubes decorated with PbO2. New J. Inside Chem. 42, 5523–5531. https://doi.org/10.1039/c7nj02604h.

Saraswat, S.K., Rodene, D.D., Gupta, R.B., 2018. Recent advancements in semiconductor materials for photoelectrochemical water splitting for hydrogen production using visible light. Renew. Sustain. Energy Rev. 89, 228–248. https://doi.org/10.1016/j.rser.2018.03.063.

Sathre, R., Scown, C.D., Morrow, W.R., Stevens, J.C., Sharp, I.D., Ager, J.W., Walczak, K., Houle, F.A., Greenblatt, J.B., 2014. Life-cycle net energy assessment of large-scale hydrogen production via photoelectrochemical water splitting. Energy Environ. Sci. 7, 3264–3278. https://doi.org/10.1039/c4ee01019a.

Seibert, D., Borba, F.H., Bueno, F., Inticher, J.J., Módenes, A.N., Espinoza-Quiñones, F.R., Bergamasco, R., 2019. Two-stage integrated system photo-electro-Fenton and biological oxidation process assessment of sanitary landfill leachate treatment: an intermediate products study. Chem. Eng. J. 372, 471–482. https://doi.org/10.1016/j.cej.2019.04.162.

Selvaraj, H., Aravind, P., George, H.S., Sundaram, M., 2020. Removal of sulfide and recycling of recovered product from tannery lime wastewater using photoassisted-electrochemical oxidation process. J. Ind. Eng. Chem. 83, 164–172. https://doi.org/10.1016/j.jiec.2019.11.024.

Shang, J., Zhang, Y., Zhu, T., Wang, Q., Song, H., 2011. The promoted photo-electrocatalytic degradation of rhodamine B over TiO2 thin film under the half-wave pulsed direct current. Appl. Catal. B Environ. 102, 464–469. https://doi.org/10.1016/j.apcatb.2010.12.027.

Sharma, S., Simsek, H., 2019. Treatment of canola-oil refinery effluent using electrochemical methods: a comparison between combined electrocoagulation + electrooxidation and electrochemical peroxidation methods. Chemosphere 221, 630–639. https://doi.org/10.1016/j.chemosphere.2019.01.066.

Shen, W., Wang, Y., Zhan, J., Wang, B., Huang, J., Deng, S., Yu, G., 2017. Kinetics and operational parameters for 1,4-dioxane degradation by the photoelectro-peroxone process. Chem. Eng. J. 310, 249–258. https://doi.org/10.1016/j.cej.2016.10.111.

Shi, H., Wang, Y., Tang, C., Wang, W., Liu, M., Zhao, G., 2019. Mechanisim investigation on the enhanced and selective photoelectrochemical oxidation of atrazine on molecular imprinted mesoporous TiO2. Appl. Catal. B Environ. 246, 50–60. https://doi.org/10.1016/j.apcatb.2019.01.018.

Sirés, I., Brillas, E., 2021. Upgrading and expanding the electro-Fenton and related processes. Curr. Opin. Electrochem 27, 100686. https://doi.org/10.1016/j.coelec.2020.100686.

Sirés, I., Brillas, E., Oturan, M.A., Rodrigo, M.A., Panizza, M., 2014. Electrochemical advanced oxidation processes: today and tomorrow. A review. Environ. Sci. Pollut. Res. 21, 8336–8367. https://doi.org/10.1007/s11356-014-2783-1.

Solano, A.M.S., Martínez-Huitle, C.A., Garcia-Segura, S., El-Ghenymy, A., Brillas, E., 2016. Application of electrochemical advanced oxidation processes with a boron-doped diamond anode to degrade acidic solutions of Reactive Blue 15 (Turqueoise Blue) dye. Electrochim. Acta 197, 210–220. https://doi.org/10.1016/j.electacta.2015.08.052.

Souza, F.L., Saéz, C., Lanza, M.R.V., Cañizares, P., Rodrigo, M.A., 2016. Removal of pesticide 2,4-D by conductive-diamond photoelectrochemical oxidation. Appl. Catal. B Environ. 180, 733–739. https://doi.org/10.1016/j.apcatb.2015.07.038.

Sruthi, T., Gandhimathi, R., Ramesh, S.T., Nidheesh, P.V., 2018. Stabilized landfill leachate treatment using heterogeneous Fenton and electro-Fenton processes. Chemosphere 210, 38–43. https://doi.org/10.1016/j.chemosphere.2018.06.172.

Su, Y., Han, S., Zhang, X., Chen, X., Lei, L., 2008. Preparation and visible-light-driven photoelectrocatalytic properties of boron-doped TiO2 nanotubes. Mater. Chem. Phys. 110, 239–246. https://doi.org/10.1016/j.matchemphys.2008.01.036.

Su, Y., Liu, G., Zeng, C., Lu, Y., Luo, H., Zhang, R., 2020. Carbon quantum dots-decorated TiO2/g-C3N4 film electrode as a photoanode with improved photo-electrocatalytic performance for 1,4-dioxane degradation. Chemosphere 251, 126381. https://doi.org/10.1016/j.chemosphere.2020.126381.

Subba Rao, A.N., Venkatarangaiah, V.T., Nagarajappa, G.B., Nataraj, S.H., Krishnegowda, P.M., 2017. Enhancement in the photo-electrocatalytic activity of SnO 2 -Sb 2 O 4 mixed metal oxide anode by nano-WO 3 modification: application to trypan blue dye degradation. J. Environ. Chem. Eng 5, 4969–4979. https://doi.org/10.1016/j.jece.2017.09.033.

Sui, M., Dong, Y., You, H., 2015. Enhanced photocatalytic activity for the degradation of rhodamine B by integrating salinity gradient power into a photocatalytic fuel cell. RSC Adv. 5, 94184–94190. https://doi.org/10.1039/c5ra20093h.

Sun, B., Li, Q., Zheng, M., Su, G., Lin, S., Wu, M., Li, C., Wang, Q., Tao, Y., Dai, L., Qin, Y., Meng, B., 2020. Recent advances in the removal of persistent organic pollutants (POPs) using multifunctional materials:a review. Environ. Pollut. 265, 114908 https://doi.org/10.1016/j.envpol.2020.114908.

Sun, S., Wang, W., Jiang, D., Zhang, L., Zhou, J., 2014. Infrared light induced photo-electrocatalytic application via graphene oxide coated thermoelectric device. Appl. Catal. B Environ. 158–159, 136–139. https://doi.org/10.1016/j.apcatb.2014.04.009.

Tao, Y., Huang, H., Zhang, H., 2020. Remediation of Cu-phenanthrene co-contaminated soil by soil washing and subsequent photoelectrochemical process in presence of persulfate. J. Hazard Mater. 400, 123111 https://doi.org/10.1016/j.jhazmat.2020.123111.

Tauchert, E., Schneider, S., de Morais, J.L., Peralta-Zamora, P., 2006. Photochemically-assisted electrochemical degradation of landfill leachate. Chemosphere 64, 1458–1463. https://doi.org/10.1016/j.chemosphere.2005.12.064.

Tayebi, M., Kolaei, M., Tayyebi, A., Masoumi, Z., Belbasi, Z., Lee, B.-K., 2019. Reduced graphene oxide (RGO) on TiO2 for an improved photoelectrochemical (PEC) and photocatalytic activity. Sol. Energy 190, 185–194. https://doi.org/10.1016/j.solener.2019.08.020.

Thiam, A., Salazar, R., 2019. Fenton-based electrochemical degradation of metolachlor in aqueous solution by means of BDD and Pt electrodes: influencing factors and reaction pathways. Environ. Sci. Pollut. Res. 26, 2580–2591. https://doi.org/10.1007/s11356-018-3768-2.

Thiam, A., Sirés, I., Brillas, E., 2015. Treatment of a mixture of food color additives (E122, E124 and E129) in different water matrices by UVA and solar photo-electro-Fenton. Water Res. 81, 178–187. https://doi.org/10.1016/j.watres.2015.05.057.

Tolod, K.R., Hernández, S., Russo, N., 2017. Recent advances in the BiVO4 photocatalyst for sun-driven water oxidation: top-performing photoanodes and scale-up challenges. Catalysts 7. https://doi.org/10.3390/catal7010013.

Trellu, C., Chakraborty, S., Nidheesh, P.V., Oturan, M.A., 2019. Environmental applications of boron-doped diamond electrodes: 2. Soil remediation and sensing applications. ChemElectroChem 6, 2143–2156. https://doi.org/10.1002/celc.201801877.

Trellu, C., Ganzenko, O., Papirio, S., Pechaud, Y., Oturan, N., Huguenot, D., van Hullebusch, E.D., Esposito, G., Oturan, M.A., 2016b. Combination of anodic oxidation and biological treatment for the removal of phenanthrene and Tween 80 from soil washing solution. Chem. Eng. J. 306, 588–596. https://doi.org/10.1016/j.cej.2016.07.108.

Trellu, C., Mousset, E., Pechaud, Y., Huguenot, D., van Hullebusch, E.D., Esposito, G., Oturan, M.A., 2016a. Removal of hydrophobic organic pollutants from soil washing/flushing solutions: a critical review. J. Hazard Mater. 306, 149–174. https://doi.org/10.1016/j.jhazmat.2015.12.008.

Trellu, C., Oturan, N., Pechaud, Y., van Hullebusch, E.D., Esposito, G., Oturan, M.A., 2017. Anodic oxidation of surfactants and organic compounds entrapped in micelles – selective degradation mechanisms and soil washing solution reuse. Water Res. 118, 1–11. https://doi.org/10.1016/j.watres.2017.04.013.

Turolla, A., Bestetti, M., Antonelli, M., 2018. Optimization of heterogeneous photo-electrocatalysis on nanotubular TiO2 electrodes: reactor configuration and kinetic modelling. Chem. Eng. Sci. 182, 171–179. https://doi.org/10.1016/j.ces.2018.02.041.

Vacca, A., Mais, L., Mascia, M., Usai, E.M., Palmas, S., 2020. Design of experiment for the optimization of pesticide removal from wastewater by photo-electrochemical oxidation with TiO2 nanotubes. Catalysts 10 (512). https://doi.org/10.3390/catal10050512.

Valim, R.B., Reis, R.M., Castro, P.S., Lima, A.S., Rocha, R.S., Bertotti, M., Lanza, M.R.V., 2013. Electrogeneration of hydrogen peroxide in gas diffusion electrodes modified with tert-butyl-anthraquinone on carbon black support. Carbon N. Y. 61, 236–244. https://doi.org/10.1016/j.carbon.2013.04.100.

Venu, D., Gandhimathi, R., Nidheesh, P.V., Ramesh, S.T., 2016. Effect of solution pH on leachate treatment mechanism of peroxicoagulation process. J. Hazardous, toxic, radioact. Waste 20, 4–7. https://doi.org/10.1061/(ASCE)HZ.2153-5515.0000315.

Verla, A.W., Verla, E.N., Adowei, P., Briggs, A., Horsfall, M., 2014. Quality assessment of vegetable oil industry effluents in port harcourt, rivers state, Nigeria. Int. Lett. Chem. Phys. Astron. 33, 179–189. https://dx.doi.org/10.18052/www.scipress.com/ilcpa.33.179.

Vidal, J., Carvajal, A., Huiliñir, C., Salazar, R., 2019. Slaughterhouse wastewater treatment by a combined anaerobic digestion/solar photoelectro-Fenton process performed in semicontinuous operation. Chem. Eng. J. 378, 122097 https://doi.org/10.1016/j.cej.2019.122097.

Vidal, J., Huiliñir, C., Salazar, R., 2016. Removal of organic matter contained in slaughterhouse wastewater using a combination of anaerobic digestion and solar photoelectro-Fenton processes. Electrochim. Acta 210, 163–170. https://doi.org/10.1016/j.electacta.2016.05.064.

Vieira Dos Santos, E., Sáez, C., Cañizares, P., Martínez-Huitle, C.A., Rodrigo, M.A., 2017. Treating soil-washing fluids polluted with oxyfluorfen by sono-electrolysis with diamond anodes. Ultrason. Sonochem. 34, 115–122. https://doi.org/10.1016/j.ultsonch.2016.05.029.

Wang, T.H., Lin, C.A., Xu, S., Wang, C.F., Chen, C.W., DongDi, C., Huang, C.P., 2019. Toward concurrent organics removal and potential hydrogen production in wastewater treatment: Photoelectrochemical decolorization of methylene blue over hematite electrode in the presence of Mn(II). Appl. Catal. B Environ. 244, 140–149. https://doi.org/10.1016/j.apcatb.2018.11.048.

Wang, A., Zhang, Y., Zhong, H., Chen, Y., Tian, X., Li, D., Li, J., 2018. Efficient mineralization of antibiotic ciprofloxacin in acid aqueous medium by a novel photoelectro-Fenton process using a microwave discharge electrodeless lamp irradiation. J. Hazard Mater. 342, 364–374. https://doi.org/10.1016/j.jhazmat.2017.08.050.

Wang, C.-T., Hu, J.-L., Chou, W.-L., Kuo, Y.-M., 2008. Removal of color from real dyeing wastewater by Electro-Fenton technology using a three-dimensional graphite cathode. J. Hazard Mater. 152, 601–606. https://doi.org/10.1016/j.jhazmat.2007.07.023.

Wang, D., Li, X., Chen, J., Tao, X., 2012. Enhanced visible-light photoelectrocatalytic degradation of organic contaminants at iodine-doped titanium dioxide film electrode. Ind. Eng. Chem. Res. 51, 218–224. https://doi.org/10.1021/ie202009a.

Wang, D., Li, Y., Li Puma, G., Lianos, P., Wang, C., Wang, P., 2017. Photo-electrochemical cell for simultaneous electricity generation and heavy metals recovery from wastewater. J. Hazard Mater. 323, 681–689. https://doi.org/10.1016/j.jhazmat.2016.10.037.

Wang, D., Li, Y., Li Puma, G., Wang, C., Wang, P., Zhang, W., Wang, Q., 2015. Dye-sensitized photoelectrochemical cell on plasmonic Ag/AgCl @ chiral TiO2 nanofibers for treatment of urban wastewater effluents, with simultaneous production of hydrogen and electricity. Appl. Catal. B Environ. 168–169, 25–32. https://doi.org/10.1016/j.apcatb.2014.11.012.

Wu, Z., Zhao, G., Zhang, Y., Liu, J., Zhang, Y.N., Shi, H., 2015. A solar-driven photocatalytic fuel cell with dual photoelectrode for simultaneous wastewater treatment and hydrogen production. J. Mater. Chem. 3, 3416–3424. https://doi.org/10.1039/c4ta06604a.

Wu, Z., Zhou, Z., Zhang, Y., Wang, J., Shi, H., Shen, Q., Wei, G., Zhao, G., 2017. Simultaneous photoelectrocatalytic aromatic organic pollutants oxidation for hydrogen production promotion with a self-biasing photoelectrochemical cell. Electrochim. Acta 254, 140–147. https://doi.org/10.1016/j.electacta.2017.09.130.

Xia, L., Bai, J., Li, J., Zeng, Q., Li, L., Zhou, B., 2017. High-performance BiVO4 photoanodes cocatalyzed with an ultrathin α-Fe2O3 layer for photoelectrochemical application. Appl. Catal. B Environ. 204, 127–133. https://doi.org/10.1016/j.apcatb.2016.11.015.

Xia, M., Chen, R., Zhu, X., Liao, Q., An, L., Wang, Z., He, X., Jiao, L., 2016. A micro

photocatalytic fuel cell with an air-breathing, membraneless and monolithic design. Sci. Bull. 61, 1699–1710. https://doi.org/10.1007/s11434-016-1178-8.
Xie, G., Chang, X., Adhikari, B.R., Thind, S.S., Chen, A., 2016. Photoelectrochemical degradation of acetaminophen and valacyclovir using nanoporous titanium dioxide. Cuihua Xuebao/Chinese J. Catal 37, 1062–1069. https://doi.org/10.1016/S1872-2067(15)61101-9.
Xie, Y.B., Li, X.Z., 2006. Interactive oxidation of photoelectrocatalysis and electro-Fenton for azo dye degradation using TiO2-Ti mesh and reticulated vitreous carbon electrodes. Mater. Chem. Phys. 95, 39–50. https://doi.org/10.1016/j.matchemphys.2005.05.048.
Xu, D., Xiao, Y., Pan, H., Mei, Y., 2019b. Toxic effects of tetracycline and its degradation products on freshwater green algae. Ecotoxicol. Environ. Saf. 174, 43–47. https://doi.org/10.1016/j.ecoenv.2019.02.063.
Xu, J., Olvera-vargas, H., Jian, B., Loh, H., Lefebvre, O., 2020. Applied Catalysis B : environmental FTO-TiO2 photoelectrocatalytic degradation of triphenyltin chloride coupled to photoelectro-Fenton : a mechanistic study. Appl. Catal. B Environ. 271, 118923 https://doi.org/10.1016/j.apcatb.2020.118923.
Xu, P., Xu, H., Zheng, D., 2019a. Simultaneous electricity generation and wastewater treatment in a photocatalytic fuel cell integrating electro-Fenton process. J. Power Sources 421, 156–161. https://doi.org/10.1016/j.jpowsour.2019.03.033.
Xu, Y.L., Zhong, D.J., Jia, J.P., Chen, S., Li, K., 2008. Enhanced dye wastewater degradation efficiency using a flowing aqueous film photoelectrocatalytic reactor. J. Environ. Sci. Heal. - Part A Toxic/Hazardous Subst. Environ. Eng 43, 1215–1222. https://doi.org/10.1080/10934520802171790.
Yang, J.-S., Lai, W.W.-P., Panchangam, S.C., Lin, A.Y.-C., 2020. Photoelectrochemical degradation of perfluorooctanoic acid (PFOA) with GOP25/FTO anodes: intermediates and reaction pathways. J. Hazard Mater. 391, 122247 https://doi.org/10.1016/j.jhazmat.2020.122247.
Yang, K., Zhu, L., Xing, B., 2006. Enhanced soil washing of phenanthrene by mixed solutions of TX100 and SDBS. Environ. Sci. Technol. 40, 4274–4280. https://doi.org/10.1021/es060122c.
Yao, L., Wang, W., Liang, Y., Fu, J., Shi, H., 2019. Plasmon-enhanced visible light photoelectrochemical and photocatalytic activity of gold nanoparticle-decorated hierarchical TiO2/Bi2WO6 nanorod arrays. Appl. Surf. Sci. 469, 829–840. https://doi.org/10.1016/j.apsusc.2018.11.031.
Ye, Z., Zhang, H., Zhang, X., Zhou, D., 2016. Treatment of landfill leachate using electrochemically assisted UV/chlorine process: effect of operating conditions, molecular weight distribution and fluorescence EEM-PARAFAC analysis. Chem. Eng. J. 286, 508–516. https://doi.org/10.1016/j.cej.2015.10.017.
Yu, S., Xi, M., Han, K., Wang, Z., Yang, W., Zhu, H., 2010. Preparation and photoelectrocatalytic properties of polyaniline/layered manganese oxide self-assembled film. Thin Solid Films 519, 357–361. https://doi.org/10.1016/j.tsf.2010.07.105.
Zeng, Q., Bai, J., Li, J., Li, L., Xia, L., Zhou, B., Sun, Y., 2018. Highly-stable and efficient photocatalytic fuel cell based on an epitaxial TiO2/WO3/W nanothorn photoanode and enhanced radical reactions for simultaneous electricity production and wastewater treatment. Appl. Energy 220, 127–137. https://doi.org/10.1016/j.apenergy.2018.03.042.
Zhang, H., Li, Y., Wu, X., 2012b. Statistical experiment design approach for the treatment of landfill leachate by photoelectro-fenton process. J. Environ. Eng. 138, 278–285. https://doi.org/10.1061/(ASCE)EE.1943-7870.0000448.
Zhang, O., Lin, B.-Z., Chen, Y.-L., Gao, B.-F., Fu, L.-M., Li, B., 2012a. Electrochemical and photoelectrochemical characteristics of TiNbO5 nanosheet electrode. Electrochim. Acta 81, 74–82. https://doi.org/10.1016/j.electacta.2012.07.085.
Zhang, X., Nengzi, L., Li, B., Liu, L., Cheng, X., 2020a. Design and construction of a highly efficient photoelectrocatalytic system based on dual-Pd/TNAs photoelectrodes for elimination of triclosan. Sep. Purif. Technol. 235, 116232 https://doi.org/10.1016/j.seppur.2019.116232.
Zhang, X., Sun, P., Wei, K., Huang, X., Zhang, Xiaoyuan, 2020b. Enhanced H2O2 activation and sulfamethoxazole degradation by Fe-impregnated biochar. Chem. Eng. J. 385, 123921 https://doi.org/10.1016/j.cej.2019.123921.
Zhang, Y., Wang, A., Tian, X., Wen, Z., Lv, H., Li, D., Li, J., 2016. Efficient mineralization of the antibiotic trimethoprim by solar assisted photoelectro-Fenton process driven by a photovoltaic cell. J. Hazard Mater. 318, 319–328. https://doi.org/10.1016/j.jhazmat.2016.07.021.
Zhao, K., Zeng, Q., Bai, J., Li, J., Xia, L., Chen, S., Zhou, B., 2017. Enhanced organic pollutants degradation and electricity production simultaneously via strengthening the radicals reaction in a novel Fenton-photocatalytic fuel cell system. Water Res. 108, 293–300. https://doi.org/10.1016/j.watres.2016.11.002.
Zhao, X., Pan, D., Chen, X., Li, R., Jiang, T., Wang, W., Li, G., Leung, D.Y.C., 2019. g-C 3 N 4 photoanode for photoelectrocatalytic synergistic pollutant degradation and hydrogen evolution. Appl. Surf. Sci. 467–468, 658–665. https://doi.org/10.1016/j.apsusc.2018.10.090.
Zhao, X., Qu, J., Liu, H., Wang, C., Xiao, S., Liu, R., Liu, P., Lan, H., Hu, C., 2010. Photoelectrochemical treatment of landfill leachate in a continuous flow reactor. Bioresour. Technol. 101, 865–869. https://doi.org/10.1016/j.biortech.2009.08.098.
Zhou, Z., Wu, Z., Xu, Q., Zhao, G., 2017. A solar-charged photoelectrochemical wastewater fuel cell for efficient and sustainable hydrogen production. J. Mater. Chem. 5, 25450–25459. https://doi.org/10.1039/c7ta08112j.
Zhu, L., Xie, J., Cui, X., Shen, J., Yang, X., Zhang, Z., 2010. Photoelectrochemical and optical properties of N-doped TiO2 thin films prepared by oxidation of sputtered TiNx films. Vacuum 84, 797–802. https://doi.org/10.1016/j.vacuum.2009.10.040.